Spring 5-20-2023

Synthesis, Characterization and Biological Evaluation of Polyarginine Derived Bone-Targeting Peptides

Gina L. Antuono
Seton Hall University, gina.antuono@shu.edu

Synthesis, Characterization and Biological Evaluation of Polyarginine Derived Bone-Targeting Peptides

By

Gina L. Antuono

Advisors: Dr. Sabatino, Dr. Wiedman, Dr. Cottrell, PhD

A thesis submitted to the Department of Chemistry and Biochemistry at Seton Hall University in partial fulfillment of the requirements for the degree of Doctor of Philosophy

Department of Chemistry and Biochemistry

Seton Hall University

South Orange, New Jersey, USA

2023

College of Arts and Sciences

Department of Chemistry and Biochemistry

APPROVAL FOR SUCCESSFUL DEFENSE

Gina Antuono has successfully defended and made the required modifications to the text of the doctoral dissertation for the Ph.D.
during the spring 2023 semester.

DISSERTATION COMMITTEE

_____

Mentor: Gregory Wiedman, Ph.D. Date

_____

Reader: Jessica Cottrell, Ph.D. Date

_____

Reader: Cosimo Antonacci, Ph.D. Date

My thesis is warmly dedicated to my loving family who have supported me through every up and down in life.

Thank you endlessly for instilling in me the importance of a strong education, the power of intrinsic motivation, and the belief and confidence to achieve my goals and dreams.

"Being a family means you are a part of something very wonderful. It means you will love and be loved for the rest of your life." -Lisa Weed

"Everyone needs a house to live in, but a supportive family is what builds a home." -Anthony Liccione

"My family is my life, and everything else comes second as far as what's important to me." - Michael Imperioli

Synthesis, Characterization and Biological Evaluation of Polyarginine Derived Bone-Targeting Peptides

Osteoblast-targeting peptides in the treatment of bone disease is a new and novel approach to offering effective treatment of various cancers and can be used in bio-medical, medicinal chemistry and biotechnology applications. By targeting adhesion proteins produced by osteoblast cells, certain cancers which migrate and metastasize to the bone may be more effectively treated. An osteoblast-targeting peptide composed of Ser-Asp-Ser-Ser-Asp (SDSSD) which selectively binds to osteoblast cells via periostin has recently been identified. This peptide was functionalized with polyurethane, generating nanomicelles which encapsulated RNA for the therapeutic treatment of osteoporosis. This study has served as the basis for the research presented in this thesis, where the SDSSD peptide was synthesized and functionalized with polyarginine tails of either 9 or 12 Arginine residues long. These synthesized peptides served to allow the selective osteoblast cell uptake of siRNA encoding for the cell surface adhesion protein, N-cadherin.

Chapter 2 of this thesis highlights the successful synthesis as well as characterization of the SDSSD peptide. Using Solid-Phase peptide synthesis as well as reverse phase high performance liquid chromatography and mass spectroscopy, the identity of each peptide was confirmed to have been made. UV-visible spectroscopy was used to quantify the peptide concentration in solution after the fluorescent tagging of each completed sequence. The synthesized peptide binds specifically to periostin, and this was tested and confirmed by incubating the peptide with osteoblast cell line MC3T3.E1 and testing against a negative control cell line (ATDC5). When incubated with the ATDC5 cells, no peptide binding was observed via flow cytometry, but when the MC3T3.E1 cells were incubated with the peptides binding was

confirmed. On average about 30% of the MC3T3.E1 cells in a given cell population were shown to be expressing periostin on their surface. The cells were also run on flow cytometry after incubation with a periostin binding antibody, and similar results were found as compared to the cell populations incubated with peptide, confirming the expression of periostin on the cell surface as well as the success of the peptide in binding to its intended target. Finally, to examine uptake of the peptide into the cells, flow cytometry was once again performed after incubating cells with peptide, and splitting this population to incubate half with Trypan Blue and half without. The Trypan blue would quench any external FITC signal, while not affecting anything internalized by the MC3T3.E1 cells. The results showed obvious shifts between both samples, where the majority of FITC labeled peptides appeared to have been taken into the cells. These results indicated that the peptides should serve as suitable delivery vehicles for the siRNA.

In Chapter 3 of this thesis the synthesis of the siRNA sequence is examined as well as the success of peptide:siRNA complexation and stability. the N-cadherin siRNA was successfully synthesized as well as purified, but yields were unreliable, and the process was inefficient. As a result, the siRNA was purchased to ensure consistent yield and to save time, as there was no way to purify the siRNA on a large scale in-house. The proper ratio to successfully complex the peptide to the siRNA was tested and found to be a 1:1 mole ratio of peptide to RNA. This was tested by combing peptides in various amounts to siRNA held constant, running a gel and staining to detect the presence of free RNA. A 1:1 ratio was the lowest ratio where no free RNA was detected. This was then used moving forward for all other gels as well as complexations. The gel results to test stability and displacement of the siRNA from the complex showed that the peptide:siRNA complexes were very stable, even in the presence of FBS at various time points, and the results showed that the peptide bound very tightly to the siRNA. Furthermore, heparin

displacement assays did indicate that the release of the RNA from the peptide was possible, sometimes at very low concentrations of 0.1:1 (heparin:complex), and consistently at ratios of 5:1 and 10:1. These results suggested that the complexes perhaps would release RNA into the cell as desired and remain stable long enough to do so. In addition, TEM and DLS results showed that the complexes formed aggregates and exhibited particle sizes slightly larger than desirable for cell entry for the RNA duplex as well as the FITC-Ahx-R_9:siRNA samples but formed less aggregates and more defined particles for both FITC-Ahx-R_{12}:siRNA and FITC-Ahx-SDSSD-Ahx-R_9:siRNA samples. This was promising as the less aggregation with the addition of the periostin targeting portion (SDSSD) indicated that the peptide:siRNA complxes would have a good chance of being taken into the cells to induce RNAi.

In Chapter 4 the effectiveness of the complexes at silencing the expression of N-cadherin was examined. The results indicated that N-cadherin expression was being silenced as expected, when cells were incubated with the peptide:siRNA complexes. These results were confirmed by qPCR. In addition, the peptides exhibited low cytotoxicity when incubated with cells for 1 hour and examined by flow cytometry and Annexin V eFluor450/7-AAD.

Finally, Chapter 5 of this thesis will briefly conclude and summarize the results obtained and examine the option for future work pertaining to the experiments performed.

Keywords: siRNA, osteoblast, cancer-targeting, peptide, polyarginine, therapeutic, cancer, bone, periostin, cell surface adhesion proteins, solid-phase peptide synthesis, RNA synthesis, RNA interference

Acknowledgments

Most children dream of becoming astronauts or firefighters, but I dreamt of becoming a scientist. Since the third grade I knew my passion resided in the sciences, specifically chemistry, after learning about the periodic table and the states of matter. Throughout my educational career I was slowly able to refine my interest specifically in Biochemistry thanks to the guidance and direction of my high school AP Biology teacher. After discovering the field, I wasted no time in apply to colleges which offered the major. I always aspired to have a PhD, am overwhelmed with endless gratitude for the having the chance to achieve this dream.

I would like to thank my advisor, Dr. David Sabatino for allowing me to be a part of his lab and providing me with the knowledge and training to refine my skills as a biochemist. He helped expand my knowledge base in priceless ways and taught my lab mates and I to become better scientists. Thank you for showing us the value of meticulousness in the lab.

I would also like to especially thank Dr. Jessica Cottrell as well as Dr. Wiedman for helping me complete the remainder of my project, being there to help act as stand-in mentors and advisors and making me feel immediately welcome in their labs. Their encouragement helped me through some of the hardest moments of my PhD career, and without their guidance and support I believe completing my project would have proven even more difficult. Thank you so much for the kindness you have both shown me, welcoming attitudes and constant willingness to help, teach and be available no matter the circumstances.

I want to also thank the rest of my thesis committee: Dr. Murphy, and Dr. Kelty. You have all been very helpful whether it be through useful suggestions, helpful advice, or guidance that has aided me in my success. I appreciate all the help I have received from you. A specific thank you to Dr. Wiedman who also agreed to act as a stand-in advisor where applicable and always aimed to provide help and support when asked.

I would also like to thank all my colleagues here at Seton Hall: Nelson, Allyson, Sunil, Chris, Katherine, Pooja, Isabella, Alex, Cristina and Akilah. You have all made my time here so much better in so many ways. Some of you have become my good friends and I hope that will continue throughout our life journeys. You have all been invaluable to bounce ideas off of or chat with or to teach me things or lend a helping hand. Thank you all so very much, from the bottom of my heart.

Finally, I would like to especially thank my family once again for always standing by me through all the ups and downs and through the good and bad during this journey. They have always encouraged me and made sure to support me in any way, shape, or form. Thank you so much for always pushing me, encouraging me, and giving me hope when times were tough. This journey could have never happened without you all. I dedicate this work to you all.

Table of Contents

Chapter 1: Introduction to Common siRNA applications and RNAi Theory and Gene Based Therapy

Chapter 2: Targeting Osteoblast Cell Surface Receptor Periostin as A Viable Option for Peptide Binding to Bone Tissue

Chapter 3: Cell Surface Adhesion Proteins: Viable Therapeutic Targets Which Play an Indirect Role in Cancer Cell Migration and Metastasis in Bone Tissue

Chapter 4: Osteoblast Cells Expression of Adhesion Proteins Makes Them Viable Therapeutic Targets to Help Potentially Prevent Cancer Spread and Metastasis

Chapter 5: Conclusions, Contributions to Knowledge and Future Work

List of Figures

List of Tables

List of Schemes

Abbreviations and Symbols

°C	Degrees Celsius
®	Registered
©	copyright
λ	wavelength
β	Beta
α	alpha
α-MEM	Alpha Minimum Essential Medium
Å	Angstroms
µg	micrograms
µL	microliters
µM	micromolar
µm	micrometers
1° ab	primary antibody
2° ab	secondary antibody
7-AAD	7-amino-actinomycin D
A	Adenine
AHX	Amino-hexanoic acid
APC	Antigen-presenting cells
BCA	Bicinchoninic acid assay
BM	Bone microenvironment
bp	base pair
BSA	Bovine serum albumin

C	cytosine
Ca^{2+}	Calcium
CAFs	Cancer associated fibroblasts
CAM-DR	Cell Adhesion-mediated drug resistance
CD40	Cluster of differentiation 40
CPG	Controlled pore glass
CTT	Cancer-targeted Technology
D	Aspartic Acid
ddH_2O	double-distilled water
DICER	Endoribonuclease Dicer
DI H_2O	Deionized water
dNTP	deoxynucleotide triphosphate
dT	deoxythymine
cDNA	Complimentary DNA
C_t	Fold Change
CTP	Cell Targeting Peptide
DCM	Dichloromethane
DLS	Dynamic Light Scattering
DMF	Dimethylformamide
DNA	Deoxyribonucleic acid
dsRNA	Double-stranded RNA
EC1	First Extracellular domain
E-cad.	E-cadherin

ECL	Enhanced chemiluminescence
ECM	Extracellular Matrix
EDTA	Ethylenediaminetetraacetic acid
EMT	Epithelial to Mesenchymal Transition
EtOH	Ethanol
ETT	5-ethylthiotetrazole
FA	Formic Acid
FACS	Fluorescence Assisted Cell Sorting
FBS	Fetal Bovine Serum
FGFR	Fibroblast growth factor receptor
FITC	Fluorescein Isothiocyanate
FMOC	Fluorenylmethyloxycarbonyl protecting group
FN	Fibronectin
G	Guanosine
g	Grams
GAPDH	Glyceraldehyde 3-phosphate dehydrogenase
GTPase	GTP-binding proteins
H_2O	Water
HCTU	O-(1H-6-Chlorobenzotriazole-1-yl)-1,1,3,3-tetramethyluronium hexafluorophosphate
HPLC	High Performance Liquid chromatography
hr	Hour
HRP	Horseradish peroxidase

HSC	Hematopoietic stem cell
IGF	Insulin-like growth factor
IgG	Immunoglobulin G
LC/MS	Liquid Chromatography/Mass spectroscopy
M	Molar
MM	Mastermix
MMI	Mastermix I
MMII	Mastermix II
mAB	Monoclonal antibody
mAmps	milliamps
MC3T3	Mus musculus (mouse) calvaria
MeCN	Acetonitrile
MeOH	Methanol
miRNA	microRNA
mg	milligrams
mL	milliliters
mM	millimolar
mmol	millimoles
MM	Multiple Myeloma
mRNA	Messenger RNA
MS	Mass Spectroscopy
MW	Molecular weight
m/z	mass to charge ratio

N-cad.	N-cadherin
NaCl	Sodium Chloride
ncRNA	non-coding RNA
NH_4OH	Ammonium Hydroxide
nm	nanometers
NMM	N-Methylmorpholine
O.D.	Optical Density
OSB	Osteoblast
PAGE	Polyacrylamide Gel Electrophoresis
PBS	Phosphate-buffered saline
PCR	Polymerase Chain Reaction
P/S	Penicillin/Streptomycin
Q	Glutamine
R	Arginine
RANKL	Receptor activator of nuclear factor kappa-B ligand
RISC	RNA-Induced Silencing Complex
RNA	Ribonucleic Acid
RNAi	Ribonucleic Acid Interference
RPMI	Roswell Park Memorial Institute Medium
rt-PCR	Reverse transcription polymerase chain reaction
S	Serine
SDS	Sodium dodecyl-sulfate
SDS-PAGE	Sodium dodecyl-sulfate polyacrylamide gel electrophoresis

siRNA	Short-interfering RNA
SPPS	Solid-Phase Peptide Synthesis
T	Thymine
TAE	Tris/Acetic Acid/EDTA
TBDMS	Tert-Butyldimethylsilyl
TBE	Tris/Borate/EDTA
TBS	Tris/NaCl/ddH_2O
TBST	Tris-Buffered Saline/Tween-20
TEAA	Triethylamine Acetate
TEMED	Tetramethylethylenediamine
TEM	Transmission Electron Microscopy
TES	Triethylsilane
TFA	Trifluoroacetic acid
TGFB	Transforming growth factor beta
THF	Tetrahydrofuran
TRIS	Tris(hydroxymethyl)aminomethane
U	Uracil
UV-vis	Ultraviolet Visible Spectroscopy
vs	versus
Wnt	Wingless-related integration site
Z	Charge State

Chapter 1: Introduction to Common siRNA applications and RNAi Theory and Gene Based Therapy

1.1 The Discovery of RNAi

The process, commonly referred to as RNAi, known as RNA interference, is a regulatory process endogenous to the cellular environment. Most Eukaryotic cells utilize RNAi through the processing and recognition of small double-stranded RNA molecules as a form of gene expression regulation.[1] Small interfering RNAs are much shorter than most other forms of RNA, and are typically around 21 base pairs long, and are double stranded.[1] They also contain overhang ends around 3 base pairs long, which serve the function of allowing for enhanced recognition by the RISC complex, an essential enzyme in the RNAi process. The RISC complex, or the RNA-induced silencing complex, is a multiprotein complex which is responsible for incorporating a single strand of siRNA as a template for recognition of complementary strands of mRNA already present within the cell.[2]

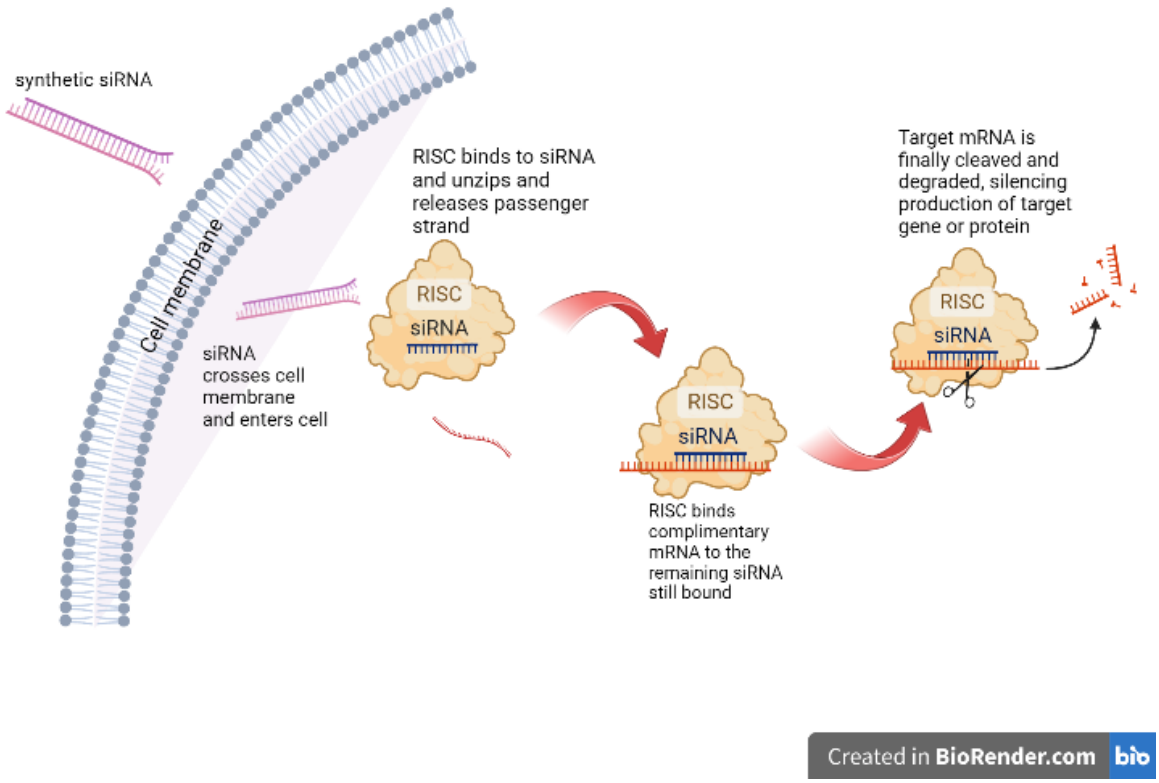

Figure 1.1: Mechanistic view of the RNAi pathway adapted from *Alnylam Therapeutics*[3]

Typically, within mammalian cells, these shorter RNAs are produced from longer, double-stranded RNA molecules by the RNase III endonuclease Dicer.[4] As shown in Figure 1, the RNAs which bind to the RISC complex are double-stranded and are then processed and snipped which results in a single-stranded RNA still bound to the RISC complex, the antisense strand. The enzyme responsible for the cleavage of the dsRNA bound to RISC is the Apo-2 enzyme which releases the "passenger" strand of RNA.[5] The result ultimately achieves the downregulation of a specific gene through the cleavage of complementary messenger RNAs to the antisense strand bound to the RISC complex.

One of the earliest applications of RNAi was performed by Andrew Fire, where effective inhibition and production of the unc-22 and unc-54 genes were observed in *C. elegans*.[6] In the aforementioned study, DNA fragments encoding for both the unc-22 and unc-54 genes were isolated and placed in reverse orientation within vectors to subsequently produce RNA within body wall muscles.[6] After injection of the resultant plasmids within oocytes, results consistent with reduction or elimination of the gene encoded for the RNA were produced.[6] Further testing revealed that the "antisense" RNA strands were responsible for the reduction or elimination of certain genes and resulted in specific loss of muscle function.[6]

Further work was done in the early stages of the discovery of RNAi, such as the experimental work by Guo and Kemphues. Guo and Kemphues studied the *par-1* gene in *C. elegans*, which is an essential protein involved in the embryonic development of these worms.[7] In order to study the effect of this protein, they performed an inhibitory experiment, which involved directly injecting antisense RNA into the gonads of worms.[7] Upon injection of antisense RNA, nearly all worms exhibited cell-division patterns characteristic with the loss of *par-1* gene function, as well as near 100% fatality.[7] Their results further corroborated the findings of Andrew Fire in that antisense RNA played an inhibitory role in gene expression in cells. Building upon this discovery, Fire completed more novel work in the realm of RNA. He specifically set out to study the mechanism by which RNA had inhibitory effects upon gene expression. He did this through examining the effects of both single-stranded antisense RNA, which had previously been shown to be an effective molecule for the disruption of endogenous gene expression within cells, and the introduction of double-stranded RNAs in cells.[8] He found that the double-stranded RNA was much more effective at gene silencing than the single stranded antisense strands.[8] When compared, the antisense strands had modest effects on gene

expression, whereas the double-stranded RNAs had very specific and very strong effects upon gene xpression.[8] Ultimately, this study led to three major claims regarding the role and function of RNA in gene expression: mRNA was the target molecule for the RNAi pathway, it was essential to target exon regions of the intended gene (promotor or intronic regions had little to no effect), and double-stranded RNA was able to easily cross cell boundaries.[8] Based on these findings, they also concluded that the RNAi pathway was endogenous to most cellular environments as a form of gene regulation, and that vertebrates and invertebrates alike relied on it.[8]

1.2 The RNAi Pathway: siRNA Structure and Function

RNA interference, the process of gene regulation within cells is governed by small interfering RNAs, or siRNAs. These siRNAs are the results of double-stranded RNA which has been spliced into shorter duplex sequences, ~21 base pairs long.[9] These short sequences also contain small overhangs on each 3' end and are eventually incorporated into a multimeric protein known as RISC, which further processes them, eventually remaining bound to the antisense strand.[9] This bound antisense strand then functions to guide the RISC complex to complementary RNA sequences present within the cell. Once found, these complementary sequences are cleaved and the resultant gene or protein is no longer expressed, resulting in knockdown of gene expression.[9]

In order to increase efficiency of siRNA, the selected target sites should be present within the coding region and at least 50 nucleotides downstream of the start codon.[9, 10] Furthermore, it is recommended that there be at least a 50% GC base pair content as well as a sequence motive of either AA N_{19} or TT.[9] Furthermore, functional duplexes of siRNA have been found to be less thermodynamically stable than nonfunctional duplexes, and the stability of the terminal base

pairs on both siRNAs are the determinants to the degree each strand participates in the RNAi pathway.[11] Because of this, it has been hypothesized that siRNA incorporation into the RISC complex is governed by an RNA helicase which initiates the dissociation of the siRNA duplex at the least thermodynamically stable end.[11]

While siRNA is typically the main focus of the RNAi pathway, there are also RNAs which serve important functions, and are also important precursors to the various siRNAs encoding for specific genes. Namely, ncRNAs, which are known as non-coding RNAs have been found to serve important functions as well in gene expression.[12] Among these functions, the regulation of the epithelial to mesenchymal transition is included, and this process serves as an important process in the development of cancers.[12] In addition to ncRNAs, microRNAs also possess the ability to activate the RNAi pathway. MicroRNAs(miRNAs) are a class of noncoding RNAs which are typically transcribed from DNA gene sequences, which are processed into primary miRNAs and processed into precursor miRNAs, and finally mature miRNAs (Figure 1.2).[13] Generally, miRNAs interact with the 3′ untranslated region of target mRNAs to induce mRNA degradation and translational repression, which is the same overall outcome duplex RNAs achieve in the RNAi pathway.[13] Furthermore, under certain conditions, miRNAs also have the ability to activate translation or regulate transcription.[13] The aforementioned classes of RNA are typically endogenous to the cell, meaning they are natural to a cellular environment.

The RNAi pathway can also be induced through the introduction of exogenously produced RNA, such as siRNA. This class of RNA, also commonly known as small-interfering RNAs are typically double-stranded and around 20 to 25 nucleotide base pairs long.[14] siRNA's are processed from double-stranded RNA which is somehow introduced into the cellular environment.[15] These double-stranded RNAs are formed through complementary base pairing on

each strand of RNA. Dicer, a key enzyme in the RNAi pathway then cleaves dsRNA into siRNA which allows for downstream degradation of complementary strands to the antisense strand. This ultimately leads to the regulation or silencing of the production of specific target genes of interest. A unique characteristic of siRNA is the 3'-OH overhang on both the sense and antisense strand.[14] The main function of siRNA is to protect the cell from exogenous mRNA attacks, such as from infectious agents like viruses which function through the introduction of their genetic material into an existing cell.[14, 16-17]

In order for siRNA to trigger the RNAi pathway, it must be introduced to the cell within the cytoplasm. Once present, it is processed, and leads to gene knockdown as previously stated. Because of its ability to bind very specifically to the RISC complex and allow for degradation of all complementary mRNA within the cell, siRNAs serve important roles in being used as therapeutics for treatments of various diseases originating from mutations within proteins necessary for function, disease related to protein expression, or diseases which can be controlled through reducing or silencing proteins or genes of interest.

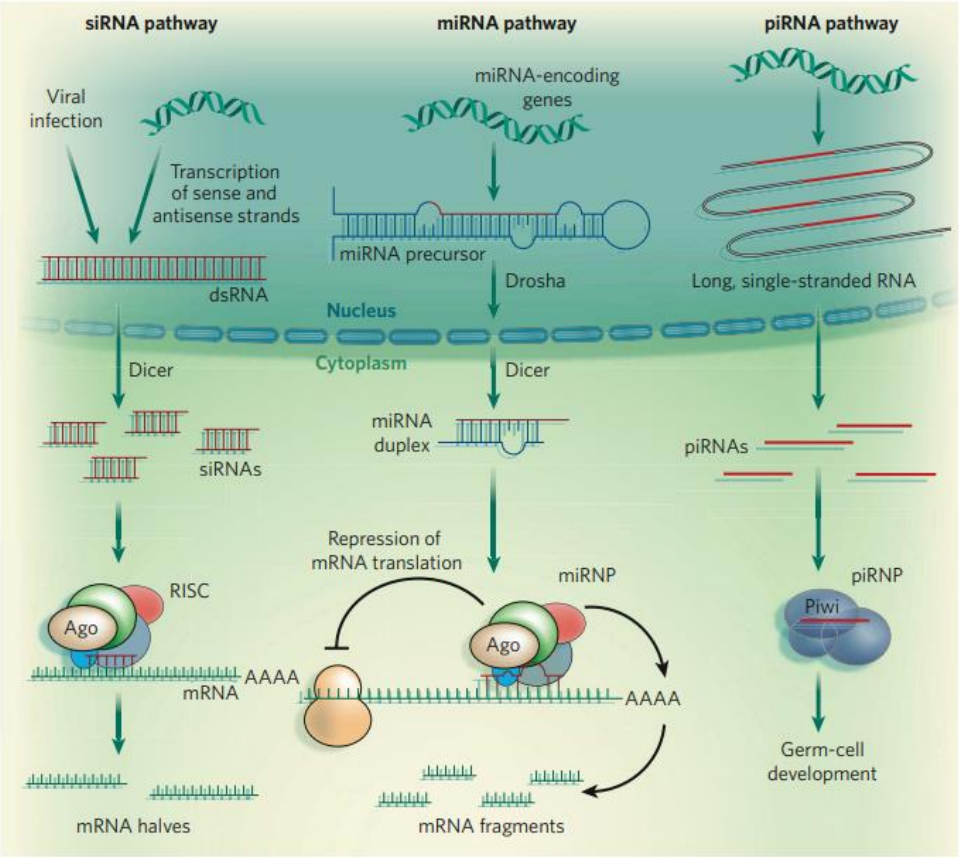

Figure 1.2: Formation and Function of small RNAs. Reprinted with permission from Reference 15. Copyright 2008 Nature.

1.3 Cancer Gene Therapy: siRNA's Applications and Role

Due to the highly specific nature of siRNAs for their target genes, they have become very popular therapeutic agents in the treatment of genetic disorders. Namely, they are a promising therapy option in the treatment of cancers. Existing cancer treatments often produce unwanted side effects for the recipients of such therapies. Many common cancer drugs produce toxic or unwanted side effects and lack the specificity to target cancerous cells while sparing healthy cells. Because of this, the desire to find more effective and specific treatment options, which spare negative or unpleasant side effects has become a popular pursuit in the field of biochemistry.[18]

In order to address the concern for therapies which produce unwanted side effects, the field of gene therapy has been heavily explored, often with much success. Preclinical and *in vitro* animal models have proven to be highly efficacious, such as in the case with lung cancer models.[18,19] More specifically, cancer vaccines have been created using gene therapy methods, cancer cells have been targeted to induce cell death and lysis, reduce blood flow and supply to tumors, and to introduce genes to either restore normal cellular phenotypes or that will cause cell death within the cancer cells.[19] Aside from the numerous benefits which gene therapy has the potential and ability to provide, it has also been shown to spare the recipient from numerous cytotoxic effects common to cancer treatments, such as damage to immune cells as well as other healthy cells.[20] The most common side effects experienced from various types of gene therapy are typically fever like symptoms or localized swelling at the injection site, if the treatment is administered as an injection.[18] These side effects are typically short lived making gene therapy a novel and promising field of alternative medicine to explore.

Cancer is one of the diseases siRNAs can effectively be used to treat. This is because cancer is characterized by a series of genetic mutations which lead to uncontrolled cell proliferation. These mutations can be used to silence as well as target tumors since the genetic mutations are unique to the cancerous cells over their lifespan.[21] These genes are known as oncogenes and play a critical role in regulating cell proliferation, survival, and differentiation.[22] Gene amplification is the distinct mechanism which activates oncogenes within human tumors, resulting in elevated levels of gene expression and gene amplification is a common occurrence in tumors.[22] Because siRNAs are used to target and recognize

specific key sequences in genes, they can be engineered to treat cancers. On such set of genes are known as “drivers” which aid in tumor progression and these sets of genetic mutations can act as ideal therapeutic targets for siRNAs.[23]

Oncogene	Tumor/Cancer Type	Process of Activation
HER2/Neu	Ovarian, breast, gastric	Amplification
EGFR/HER1	Lung, breast, glioblastoma	Amplification & mutations
Myc	Various tumor types	Mutations & amplifications
PRAD1/Cyclin D1	Lymphoma, esophageal, breast, parathyroid adenoma	Amplification & translocation
Myb	Leukemia	Overexpression & amplification
Int2/FGF3	Head, neck, esophageal, gastric	Amplification

Table 1.1: Representative oncogenes activated by amplification in human tumors and cancer types. Table adapted from *Pathophysiology of Disease: An Introduction to Clinical Medicine (Lange Medical Books), 7th Ed. CHAPTER 5*.[24]

1.4 siRNA Modifications and Their clinical Applications

The field of gene therapy relies on the application and modification of siRNA to target and perform its desired role upon delivery within the cell’s cytoplasm. siRNA’s have proven to be superior to other forms of gene therapy due to the way it executes its function: Watson-Crick base pairing with mRNA.[25] This highly specific interaction is what avoids off-targeting binding, effects or reactions from taking place consequently ensuring that only target genes or protein production is focused on. Although siRNA treatments have various pros, one of its main barriers to successful application is how quickly siRNA degrades. Aside from this, unmodified siRNA is unstable, exhibits poor pharmacokinetic behavior, and can potentially have off-target effects.[25]

This makes crossing the cellular membrane difficult and requires key modifications to the siRNA to ensure that it can cross the cell membrane intact.

The most common modification to siRNA is the substitution of the 2'-OH with a 2'-O-methyl (2'-OMe) or a 2'-methoxyethyl (2'-MOE) along with the substitution of certain nucleotides for unlocked nucleic acids (UNA), locked nucleic acids (LNA), or glycol nucleic acids (GNA) to suppress immunostimulatory siRNA-driven innate immune activation.[25,26,27,28,29,30] Many siRNA modifications are introduced simultaneously at the phosphate backbone, the base or the ribose moiety.[25]

Gene therapy and siRNA modifications have allowed for a broader approach to cancer treatments and have become one of the main clinical applications of siRNA therapeutics. "Rational chemical designs have allowed siRNA passenger strands to be more likely to modification than siRNA guide strands. These synthetic strategies have enabled to replace either non-bridging oxygen on the phosphate linkage with a sulfur atom, the 2′-hydroxyl group modification of the sugar ring with a methyl group (2′-OCH_3) and ethyl group (2′-OCH_2CH_3), among others."[31] Immunotherapy has gained attention as a promising strategy for treating cancer by activating the host's immune system in several ways. These include introducing cell signaling molecules such as cytokines, using cancer vaccines or monoclonal antibodies, or through the use of antigen-presenting cells (APC) through Toll-like receptors.[31] Dendritic cells (immune cells found in skin and bone tissue) are the strongest antigen-exhibiting cells and show the strongest stimulation to naïve T cells (type of white blood cell) and stimulate the differentiation and growth of B cells (white blood cell that creates antibodies) and include a system of leukocytes found in all tissues. [31] DC therapy may offer a novel and promising immunotherapeutic method for prevention and treatment of advanced cancer as well as autoimmune disorders."[31] These

novel approaches have been implemented in immunotherapies involving dendritic cell-based therapies as well as RNAi therapies. For example, Qian et al reported that "siRNA may be combined to DC-based therapy in order to manipulate CD40 expression levels"[31] CD40 is a transmembrane protein found on antigen-presenting cells and is necessary for their activation.

1.5 RNAi Activity: Cell Uptake, Trafficking, and Release

While the use of siRNA as a form of gene therapy has proven to be promising, there are various barriers to overcome to ensure its success. Most of these barriers center around efficient cellular uptake, long-term stability, and off-target effects.[31] For example, mammalian cells express Toll-like receptors (TLRs) which serve to recognize pathogens and molecules derived from microbes, and some synthetic siRNAs have been shown to stimulate the immune response, even when they are not derived from viral particles, and still induce the production of inflammatory cytokines.[31] In addition to immune responses, miRNA off-target silencing has also been reported as well as the saturation of RNAi machinery mediated by synthetic siRNAs is another source of off-target binding.[31] "Some data have shown that synthetic siRNAs when entered the RNAi pathway tend to compete with endogenous miRNAs for RISC. This process has been observed in certain model studies in which both transcript upregulation and target script downregulation have been observed."[31, 32]

In order to mediate and bypass many of these limitations, effective delivery methods have been established to deliver siRNAs into the cytoplasm of cells, where they can induce the RNAi pathway. Some delivery methods typically used to deliver siRNAs include antibody conjugates, natural polysaccharides, micelles, synthetic cationic polymers, peptides, and microparticles.[31] Some of the more successful delivery options have involved the use of lipids or cationic lipids.[33]

Another method used to bypass the body's response to siRNAs as foreign has been to slightly modify the sequence used. These modifications must be minimal to ensure binding to the RISC complex as well as to maintain sequence identity. As a result, most of these modifications are placed at either end of the strand.[31] These modifications enable three key features to maintaining siRNA efficacy by avoiding exonuclease degradation, increased affinity to RISC, a lower immunostimulatory response, and the avoidance of miRNA-like effects.[31, 34, 35-38] Furthermore, introducing double stranded RNA has also been shown to increase stability within saline buffer.[31-38]

Finally, delivering siRNA as a therapy must be done effectively and must eliminate unwanted side effects while still being effective. Intravenous administration is one of the more popular routes explored but has still posed some drawbacks. This is due to the complex route the siRNA must take to reach its desired target when introduced into the bloodstream first. For example, "After intravenous injection, siRNA is distributed to organs via the blood circulation and at the same time undergoes elimination. Within an organ, siRNA leaves the intravascular space within a blood vessel to enter the interstitium (i.e., extravasation). After entering the tissue interstitium, siRNA is transported across the interstitial space to the target cells. After reaching the target cell, siRNA undergoes internalization *via* endocytosis, a process that involves siRNA being encapsulated in endocytic vesicles that fuse with endosomes. After entering the cell, siRNA must escape from the endosomes and be released from its carrier to the cytosol in order to be loaded onto RISC."[39] Because of this it has been found that local regional delivery may prove to be a more effective method for the introduction of siRNA therapeutically.[39]

1.6 Delivery Systems of siRNA-Cell Targeting Peptides

Cell-targeting peptides (CPPs) are small peptides which exhibit a high specificity and affinity for their target receptors. Because of their high specificity they have gained popularity as therapeutic delivery agents for other molecules or drugs. Furthermore, research has shown that they are easy to synthesize, small in size (helpful for crossing the cell membrane) and have lower toxicity and immunogenicity than antibodies.[40] In addition to these positive characteristics, CPPs have shown promise and ability in overcoming cellular entry obstacles, overcoming the blood-brain barrier, and easily distributing into organs.[40,41]

The ability to use CPPs to treat various diseases has also extended to the treatment of various cancers. This is done by utilizing the CPP as the delivery method for the anti-cancer therapy (CTT)…and numerous reports have demonstrated the potential of CTTs to treat leukemia, lung, breast, ovarian, pancreatic, and colon cancers.[42] "The mechanism of inhibition is similar in most of the cases: a target interaction is determined and a portion or the whole interacting protein is attached to a CPP. The CTT is then transduced across the plasma membrane and delivered into the cytosol or nucleus to block the endogenous pro-cancerous interactions from occurring."[42] Because CTPs can be designed synthetically, virtually any desired receptor or cell type can be targeted and the desired drug or therapy can be delivered directly to the desired system, cell type, or organ.

1.7 Cell Surface Adhesion Proteins- An Indirect Target for Cancer Therapy

Some of the most important proteins responsible for keeping the skeletal matrix intact are cell surface adhesion proteins. These adhesion molecules mediate the interactions between cells or between cells and the extracellular matrix (ECM).[43] There are four families of adhesion molecules: cadherins, integrins, selectins, and immunoglobulin-like adhesion molecules.[43] Of

particular interest is the cadherin superfamily. These adhesion proteins are a family of glycoproteins involved in the Ca^{2+} dependent cell-cell adhesion mechanism.[43] The cadherins are further divided into subclasses of n-cadherins, E-cadherins, and P-cadherins. These subclasses have key similarities such as molecular weight, calcium and protease sensitivity, but each subclass exhibits unique tissue distribution as well as immunological specificity.[44]

Molecule	Animal	Tissue distribution	References
E-cadherin	mouse	*early embryo (at preimplantation)*	Yoshida & Takeichi, 1982
uvomorulin	mouse	blastomeres	Hyafil *et al.* 1980
Cell CAM120/80	human/mouse	inner cell mass	Damsky *et al.* 1983
Arc-1	dog	trophectoderm	Behrens *et al.* 1985
L-CAM	chicken	*early embryo (at postimplantation)*	Gallin *et al.* 1983
		ectoderm	
		endoderm	
		late embryo	
		most epithelial tissues	
N-cadherin	mouse/chicken	*early embryo*	Hatta & Takeichi, 1986
A-CAM	chicken	mesoderm	Volk & Geiger, 1984
N-Cal-CAM	chicken	notochord	Bixby *et al.* 1987
		late embryo	
		neural tissues	
		lens & some other epithelial tissues	
		cardiac & skeletal muscles	
		nephric primordia	
		some mesenchymal tissues	
		mesothelium	
		primordial germ cells	
P-cadherin	mouse	*early embryo*	Nose & Takeichi, 1986
		extraembryonic ectoderm	
		visceral endoderm	
		lateral plate mesoderm	
		notochord	
		late embryo	
		placenta	
		epidermis & some other epithelial tissues	
		pigmented retina	
		mesothelium	
gp140K	*Xenopus*	epithelial lines	Nomura *et al.* 1988

Molecules that have been shown or believed to be identical or the interspecies homologue are grouped. *Early and late embryo* roughly define embryos at the stage before and after neurulation, respectively. This table does not cover all tissues, especially those expressing N- and P-cadherin. As the tissue distribution pattern of each cadherin subclass changes during development, some of the tissues listed here express them only transiently.

Table 1.2: *Cadherin subclasses and the related molecules.* Reprinted with permission from reference 44. Copyright 1988 The Company of Biologists.

One type of previously mentioned cadherin binding protein E-cadherin has been the most widely studied binding protein. It plays a role in cell adhesion, transmits chemical signals within

cells, and controls cell maturation and movement.[45] In addition, E-cadherin is a tumor-suppressor protein which prevents cells from proliferating in an uncontrolled way.[45] Thus, maintain proper levels of such adhesion proteins along the cell surface is crucial in conserving the healthy monolayers of cells. The downregulation of E-cadherin "is regarded as one of the main molecular events responsible for dysfunction in cell-cell adhesion. Most tumors have abnormal cellular architecture, and loss of tissue integrity can lead to local invasion. Thus, loss of function of E-cadherin tumor suppressor protein correlates with increased invasiveness and metastasis of tumors, resulting in it being referred to as the "suppressor of invasion" gene."[46,47] Structurally, E-cadherin is made up of an extracellular domain which contains five tandem repeats of a 100-residue amino acid motif which accounts for the largest portion of its N-terminus, responsible for adhesive activity.[46] E-cadherin is a calcium binding protein and E-cadherin proteins interact with one another through homotypic interactions of their extracellular domains in what is known as lateral dimerization.[46]

Although it has typically been accepted that E-cadherin has played a role in the transition of cells from healthy to malignant, it has emerged more recently that another adhesion protein, N-cadherin plays a much larger role than previously believed. N-cadherin is a classical type I cadherin which is made up of five extracellular domains linked to one intracellular domain.[48]. N-cadherin proteins interact with one another due to a tryptophan residue on its first extracellular domain (EC1) with the hydrophobic pocket of another n-cadherin's EC1.[48] This is known as trans adhesion and is illustrated below in Figure 1.3.[48]. This adhesion protein also plays an important role in morphogenetic processes during the formation of cardiac and neural tissues, is involved in osteogenesis and myogenesis, and maturation of vasculature.[48,44,49-52]

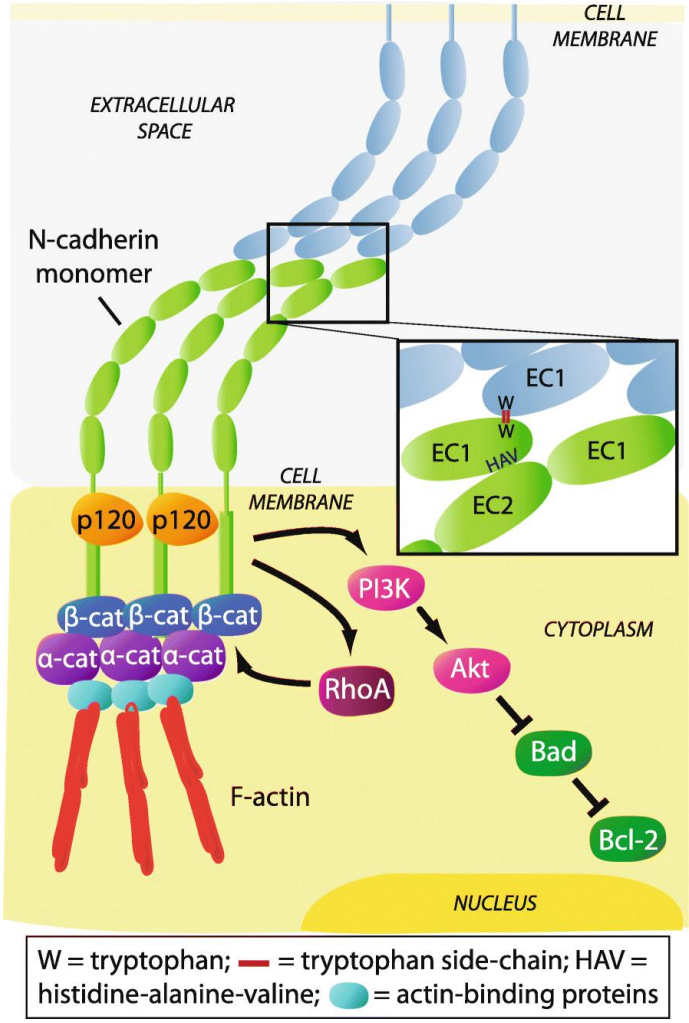

Figure 1.3: *N-cadherin-catenin adhesive complex.*[48] Image free for use under the *Creative Commons Attribution-NonCommercial-No Derivatives License (CC BY NC ND)*

N-cadherin also plays a role in localized actin filament assembly. These assemblies stimulate membrane protrusions at points of cell to cell contact, helping to bind cells to one another.[48,53] The formation of actin filaments is crucial to proper early cell adhesion and recognition.[53] Furthermore, n-cadherin is responsible for activating the Rho GTPase family member Rac which in turn facilitates the maturation of n-cadherin and eventually suppresses actin branching thought he sequestration of β-catenin to the cadherin intracellular domain.[48]

Because of the crucial role cadherins play in maintaining proper cell proliferation homeostasis, healthy monolayers of cells, cell communication and epithelial cell properties, the dysregulation of these adhesion proteins often coincides with genetic mutations present in cancers. These mutations often present as an overexpression of n-cadherin in cancerous cells, and a downregulation of E-cadherin. When this occurs, cancers lose their epithelial-like properties and consequently gain more stem cell-like properties. This includes increased migration and as a result, metastasis of said cancers. This transition from epithelial to stem cell-like is known as the epithelial to mesenchymal transition, or the EMT transition. The EMT transition "is a biologic process that allows a polarized epithelial cell, which normally interacts with basement membrane via its basal surface, to undergo multiple biochemical changes that enable it to assume a mesenchymal cell phenotype, which includes enhanced migratory capacity, invasiveness, elevated resistance to apoptosis, and greatly increased production of ECM components… The completion of an EMT is signaled by the degradation of underlying basement membrane and the formation of a mesenchymal cell that can migrate away from the epithelial layer in which it originated… A number of distinct molecular processes are engaged in order to initiate an EMT and enable it to reach completion. These include activation of transcription factors, expression of specific cell-surface proteins, reorganization and expression of cytoskeletal proteins, production of ECM-degrading enzymes, and changes in the expression of specific microRNAs."[54] There are three types of EMT transitions contributing to various stages of disease in the body. Specifically Type 3 EMTs occur in neoplastic cells which have previously undergone epigenetic and genetic changes which specifically favor the growth of localized tumors or in genes that favor clonal outgrowth.[54]

Cancers such as prostate, breast, pancreatic and urothelial cancers show a marked increased in the production of n-cadherin, whereas normal healthy cells express this protein in much lower levels.[48] These upregulate levels of n-cadherin are associated with increased tumor aggressiveness, adding to the increased rate of cancer metastasis within bone tissues.[48] Examples of increased N-cadherin expression in cancers are illustrated below in Table 1.3.

Table 1 Association of increased N-cadherin expression in cancer with clinicopathologic features and survival

Cancer type	Cohort information & treatment details	No. of patients	N-cadherin detection method	Association with clinicopathologic features	Association with survival	Reference
Epithelial cancers						
Breast cancer	Pre-metastatic; resected	574	IHC	High grade & LN metastasis	Shorter PFS (U)	[47]
	Early-stage invasive	1902	IHC	Earlier development of distant metastasis	n/a	[48]
	Primary inoperable and LN negative	275	IHC	n.s.	Shorter OS (U)	[49]
	Invasive; no prior therapy	94	IHC	High grade, late stage & LN metastasis	n/a	[50]
Prostate cancer	Clinically localised; radical prostatectomy	104	IHC	Poor differentiation, seminal vesicle invasion & pelvic LN metastasis	Shorter time to biochemical failure (U), clinical recurrence (M) & skeletal metastasis (U)	[8]
	Castration-resistant; transurethral resection	26	IHC	Higher Gleason score & metastasis	n/a	[51]
	Localised; no therapy prior to radical prostatectomy	157	IHC	Later stage, higher PSA & Gleason score, seminal vesicle invasion and LN metastasis	n/a	[52]
	Blood from cancer follow-up patients	179	Serum ELISA (sN-cad)	Higher PSA	n/a	[53]
	Radical prostatectomy, metformin-treated	49	IHC	n/a	Increased recurrence	[54]
Lung cancer	Adenocarcinoma & squamous cell carcinoma; no therapy prior to surgery	68	IHC	Higher TNM stage & poor differentiation	Shorter OS (M)	[55]
	Primary adenocarcinoma; no therapy prior to surgery	147	IHC	n/a	Shorter OS (M)	[56]
	Surgical resection of adenocarcinoma; no prior therapy	57	qPCR	LN metastasis	n/a	[57]
	No post-operative surgery	186	IHC	Higher TNM stage & metastasis	n/a	[58]
	Adenocarcinoma & squamous cell carcinoma; blood collected prior to or up to 3 weeks after platinum-based therapy	43	IF (on CTCs)	n/a	Shorter PFS	[59]
Urothelial cancers	Radical cystecomy with pelvic LN dissection, clinically nonmetastatic bladder cancer	433	IHC	Higher clinical & pathologic tumour stage, LN metastasis & LN stage, lymphovascular invasion	Shorter RFS (M), OS (U) & cancer-specific survival (U)	[60]
	Invasive bladder cancer undergoing radical cystectomy; no prior treatment	30	qPCR	n/a	Shorter OS	[61]
	Transurethral resection of non-muscle-invasive bladder cancer	115	IHC	Higher incidence of intravesical recurrence	Shorter intravesical RFS (M)	[62]
	Clinically-localised upper urinary tract carcinoma undergoing nephroureterectomy; cisplatin- based therapy in late-stage patients	59	IHC	n/a	Intravesical and extravesical RFS (M)	[63]
Liver cancer	Resection of hepatocellular carcinoma	100	IHC	Higher histologic grade, multifocal tumours & vascular invasion	Shorter disease-free and OS	[64]
	Surgical resection of hepatocellular carcinoma	57	IHC	n.s.	Increased recurrence-rate within 2 years of resection	[65]

Table 1.3: "*Association of increased N-cadherin expression in cancer with clinicopathologic features and survival*".[48] Image free for use under the *Creative Commons Attribution-NonCommercial-No Derivatives License (CC BY NC ND)*

The ability of n-cadherin to promote the migratory properties of cancerous epithelial cells has been well documented. One such study conducted by Rachel Hazan, which demonstrated that n-cadherin expression in cell tumor lines under expressing E-cadherin enhanced the aggressive phenotypes of breast cancer.[55] Hazan and associates transfected a weakly metastatic, E-cadherin expressing breast cancer line of cells (MCF-7) with n-cadherin to examine the effects n-cadherin would have on the cancerous cell line's properties.[55] From this work, Hazan found that "n-cadherin expressing cells migrated more efficiently, showed an increased invasion of Matrigel, and adhered more efficiently to monolayers of endothelial cells… When injected into the mammary fat pad of nude mice, N-cadherin–expressing cells, but not control MCF-7 cells, metastasized widely to the liver, pancreas, salivary gland, omentum, lung, lymph nodes, and lumbar spinal muscle. The expression of both E- and N-cadherin was maintained both in the primary tumors and metastatic lesions. These results demonstrate that N-cadherin promotes motility, invasion, and metastasis even in the presence of the normally suppressive E-cadherin."[55] N-cadherin mainly promotes the migratory capacity of cancerous or tumor cells through three key mechanisms. These mechanisms are through the signaling and modulation of canonical Wnt signaling, through the facilitation of collective cell migration, and through the augmentation of fibroblast growth factor-receptor (FGFR).[48] Because of the complex and crucial role n-cadherin plays in maintaining healthy epithelial cell monolayers, it is a promising potential therapeutic target for treating cancers and potentially decreasing malignant cell migration and metastasis. Furthermore, n-cadherin is of particular interest as a therapeutic target due to its unique ability to shield certain cancers from anti-cancer drugs, imparting cell surface adhesion protein mediated drug resistance.[56] Finally, the EMT transition is a reversible process which has been characterized by an increase in the expression of N-cadherin and a decrease in the

expression of E-cadherin, further solidifying the importance of N-cadherin as a potential therapeutic target.[57]

1.8 The Skeletal Matrix and its Relationship to Cancers

The bone microenvironment provides an ideal place for cancers to metastasize. Many processes contribute to this vicious cycle and also to the difficulty in treating myelomas. The prognosis for patients diagnosed with a multiple myeloma is less than 20% after five years of being diagnosed.[57] One of the main events which drives cancer cell metastasis within bone tissue is the detachment of cancer cells from their site of origin and migration to the bone tissue.[57] "cancer metastases, once established in bone, modify their immediate environment to support their own survival and growth. Thus, tumour-derived factors such as parathyroid hormone-related protein (PTHrP) up-regulate the expression of Receptor Activator of Nuclear Factor KB Ligand (RANKL) by cells of the osteoblast lineage (i.e., osteoblast precursors, osteoblasts and osteocytes). RANKL then binds to the Receptor Activator of Nuclear Factor KB (RANK) on osteoclasts and osteoclast precursors to increase osteoclast recruitment and formation, and to activate bone resorption. Accelerated bone resorption then triggers the release of growth factors embedded in the bone matrix, which in turn act on cancer cells to promote their further growth."[58] Furthermore, "Finally, the bone matrix contains numerous non-collagenous proteins (e.g., osteopontin, vitronectin) which are able to interact directly with adhesion molecules on cancer cells, commonly via RGD sequences, and thus alter cancer cell behaviour."[58] Finally, in conjunction with the bone microenvironment (BM) behaving as a fertile breeding ground for cancers, it has also been observed that during an EMT transition, there is a remodeling of the extracellular matrix which takes place which specifically facilitates the migration and movement of cells into the bone tissue.[57] "Recent studies have shown that cancer-associated fibroblasts

(CAFs) can remodel the matrix and create tracks, which can then be used by migrating cancer cells (72). Moreover, by generating heterotypic junctions between N-cadherin on the CAF membranes and E-cadherin on the cancer cell membrane, CAFs can generate intercellular physical force and drive collective invasion of cancer cells."[57] "The proliferation of myeloma cancer cells and the acquisition of an invasive profile is related to integrin clustering. This is mediated by the rearrangement of cytoskeletal proteins and the recruitment of molecules involved in the signaling cascade, as well as the phosphorylation of pp60 Src and focal adhesion kinase [19]. The role of CAMs in MM The role of CAMs in MM pathophysiology is primarily related to the homing of tumor cells in the BM, which in turn aids in the recirculation of the malignant plasma cells (PC) and stimulates growth factor production, as illustrated below in Figure 1.4."[59]

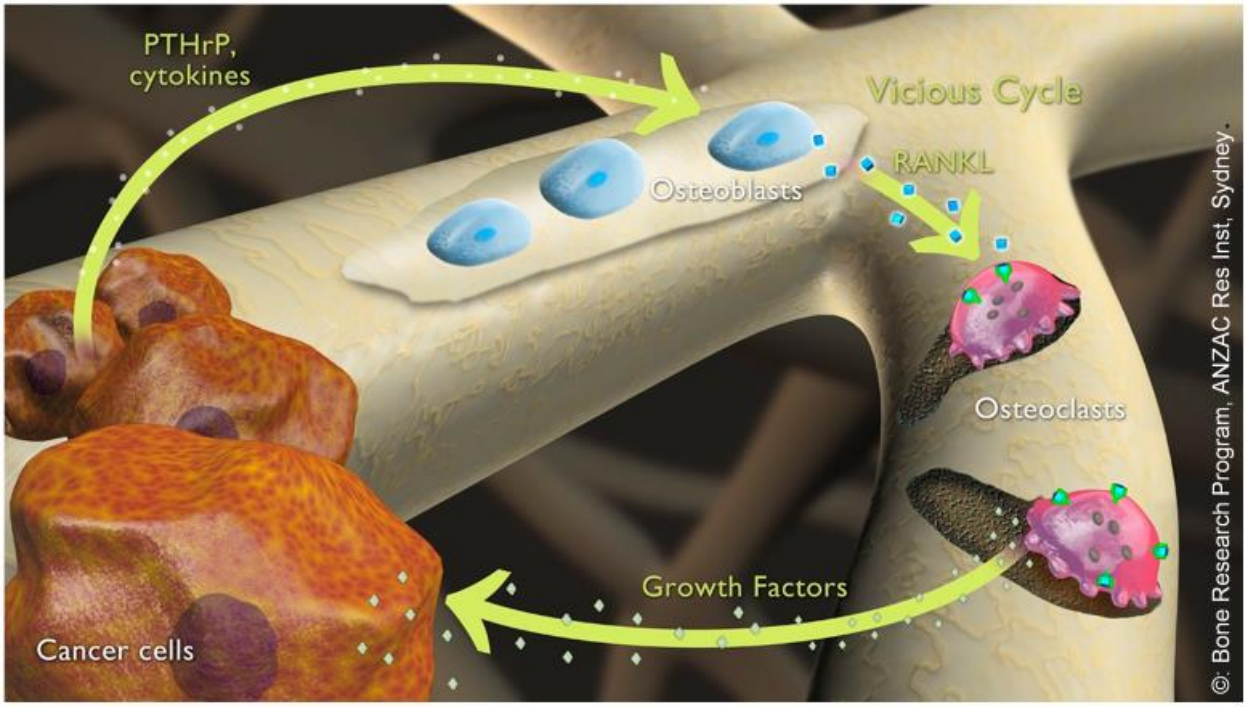

Figure 1.4: Cancer cell stimulation by bone cell growth factor release[58]. Image free for use under the *Creative Commons Attribution-NonCommercial-No Derivatives License (CC BY NC ND)*

1.9 Thesis Objectives

The basis of the completed research project will be highlighted in Chapter 1 of this thesis. The established principles of RNAi as well as peptide delivery systems within cells have served as the origin of the completed research and will be explored and further explained in Chapter 1. Cell-targeting peptides have been found to serve as highly specific targets for receptors of interest, allowing them to be more highly successful in drug delivery systems, while minimizing unwanted off-target effects commonly seen in most established drug treatments. Furthermore, cell-surface adhesion proteins play many roles in maintaining proper cell growth, function, and a healthy equilibrium in cell division. Adhesion proteins have also been found to play a role in cancer cell migration and metastasis within bone tissues because of their ability to interact with adhesion proteins along the surface of some cancer cells. Because of their crucial role in maintaining healthy cell monolayers, when cancer cells have begun to metastasize within bone tissue, the production and balance of adhesion proteins is disrupted. Consequently, these proteins are involved in the EMT transition, or the Epithelial to Mesenchymal Transition, which grants epithelial cells more stem-like properties. This has a direct role on the ability of cancers within the bone to migrate and metastasize within the body as a whole.

The first research objective completed was the synthesis and characterization of the OSB-targeting peptides and siRNAs targeting cell-surface adhesion proteins. This thesis revolves around and focuses on the ability to successfully utilize the already established properties and functions of siRNA within the cell to achieve the eventual downregulation of cell-surface adhesion proteins. This work is centered on the already successful synthesis of periostin targeting peptides as a therapeutic target in the treatment of osteoporosis in bone tissues. The

OSB peptides proved to selectively bind to periostn, making them viable options to functionalize with various polyarginine tails. The polyarginine tails on these peptides range from 9-12 arginine residues in length and consist of ‘spacers’. The spacer used is 6-(Fmoc-amino)hexanoic acid, and has been placed between the polyarginine tails and the periostin targeting portion of the peptide. It has also been placed before the addition of the fluorophore, Fluorescein isothiocyanate, or FITC. The placement of the spacers in both these locations was chosen to 1) prevent degradation of the fluorophore after addition to the peptide, and 2) to maintain symmetry of the peptide sequence with spacers on both ends. The fluorophore, FITC was chosen to be added to the final peptide sequences so that quantitative analysis of the sequences would be made simpler. This was done using the basic principle of the Beer-Lambert equation, where concentration of a substance is directly correlated to the absorbance of the substance. This will be highlighted in Chapter 2 of the thesis.

Chapter 3 of the thesis will highlight the synthesis of various siRNA sequences encoding for cell-surface adhesion proteins, which are present on the surface of osteoblast cells. This chapter will focus on the selection as well as synthesis of the siRNA sequences. The sequences chosen are all sequences encoding for key cell-surface adhesion proteins. Each protein chosen plays a crucial role in the EMT transition and is necessary for maintain healthy cell monolayers, regulating cell signaling to maintain appropriate levels of cell division and maintain the proper interaction between osteoblast cells to form the skeletal network. Each sequence has been successfully synthesized to show proof of concept. All sequences made were confirmed to be homologous between mouse and human lines.

Chapter 4 of this thesis aims to examine the effectiveness of the complexes in achieving silencing of the n-cadherin protein in the osteoblast cells. This will be done by examining and

confirming expression of n-cadherin in the osteoblast cells, and determining if the peptide:siRNA complexes are successful in silencing the expression of n-cadherin in the cells. Furthermore, the cells will be exposed to the peptides and their cytotoxicity will be examined via flow cytometry.

Finally, chapter 5 of this thesis will discuss the potential future work which can be performed using the data gathered in this thesis, pertaining to this project. It will also serve as the concluding chapter, summarizing the work performed, results obtained and will examine the success of the project as well as any areas where improvements could be made.

1.10 References

1. Kim, D. H.; Rossi, J. J. RNAi Mechanisms and Applications. BioTechniques 2008, 44 (5), 613–616. https://doi.org/10.2144/000112792.
2. Zhang, Y. RNA-Induced Silencing Complex (RISC). In Encyclopedia of Systems Biology; Dubitzky, W., Wolkenhauer, O., Cho, K.-H., Yokota, H., Eds.; Springer New York: New York, NY, 2013; pp 1876–1876. https://doi.org/10.1007/978-1-4419-9863-7_329.
3. RNAi Therapeutics | How RNA Interference Works | Alnylam® Pharmaceuticals. RNAi Therapeutics | How RNA Interference Works | Alnylam® Pharmaceuticals. https://www.alnylam.com/our-science/the-science-of-rnai (accessed 2023-05-22).
4. Zhang, H.; Kolb, F. A.; Jaskiewicz, L.; Westhof, E.; Filipowicz, W. Single Processing Center Models for Human Dicer and Bacterial RNase III. Cell 2004, 118 (1), 57–68. https://doi.org/10.1016/j.cell.2004.06.017.
5. Tang, G. SiRNA and MiRNA: An Insight into RISCs. Trends in Biochemical Sciences 2005, 30 (2), 106–114. https://doi.org/10.1016/j.tibs.2004.12.007.
6. Fire, A.; Albertson, D.; Harrison, S. W.; Moerman, D. G. Production of Antisense RNA Leads to Effective and Specific Inhibition of Gene Expression in C. Elegans Muscle. Development 1991, 113 (2), 503–514. https://doi.org/10.1242/dev.113.2.503.
7. Guo, S.; Kemphues, K. J. Par-1, a Gene Required for Establishing Polarity in C. Elegans Embryos, Encodes a Putative Ser/Thr Kinase That Is Asymmetrically Distributed. Cell 1995, 81 (4), 611–620. https://doi.org/10.1016/0092-8674(95)90082-9.
8. Fire, A.; Xu, S.; Montgomery, M. K.; Kostas, S. A.; Driver, S. E.; Mello, C. C. Potent and Specific Genetic Interference by Double-Stranded RNA in Caenorhabditis Elegans. Nature 1998, 391 (6669), 806–811. https://doi.org/10.1038/35888.
9. Kurreck, J. SiRNA Efficiency: Structure or Sequence—That Is the Question. Journal of Biomedicine and Biotechnology 2006, 2006, 1–7. https://doi.org/10.1155/JBB/2006/83757.
10. Elbashir, S. Analysis of Gene Function in Somatic Mammalian Cells Using Small Interfering RNAs. Methods 2002, 26 (2), 199–213. https://doi.org/10.1016/S1046-2023(02)00023-3.
11. Schwarz, D. S.; Hutvágner, G.; Du, T.; Xu, Z.; Aronin, N.; Zamore, P. D. Asymmetry in the Assembly of the RNAi Enzyme Complex. Cell 2003, 115 (2), 199–208. https://doi.org/10.1016/S0092-8674(03)00759-1.
12. Mattick, J. S. The Genetic Signatures of Noncoding RNAs. PLoS Genet 2009, 5 (4), e1000459. https://doi.org/10.1371/journal.pgen.1000459.
13. O'Brien, J.; Hayder, H.; Zayed, Y.; Peng, C. Overview of MicroRNA Biogenesis, Mechanisms of Actions, and Circulation. Front. Endocrinol. 2018, 9, 402. https://doi.org/10.3389/fendo.2018.00402.
14. Chauhan, D. T. siRNA (Small Interfering RNA): Structure And Function. Genetic Education. https://geneticeducation.co.in/sirna-small-interfering-rna-structure-and-function/ (accessed 2023-05-22).
15. Großhans, H.; Filipowicz, W. The Expanding World of Small RNAs. Nature 2008, 451 (7177), 414–416. https://doi.org/10.1038/451414a.
16. Dana, H.; Chalbatani, G. M.; Mahmoodzadeh, H.; Karimloo, R.; Rezaiean, O.; Moradzadeh, A.; Mehmandoost, N.; Moazzen, F.; Mazraeh, A.; Marmari, V.; Ebrahimi,

M.; Rashno, M. M.; Abadi, S. J.; Gharagouzlo, E. Molecular Mechanisms and Biological Functions of SiRNA. Int J Biomed Sci 2017, 13 (2), 48–57.
17. PDB101: Molecule of the Month: Small Interfering RNA (siRNA). RCSB: PDB-101. http://pdb101.rcsb.org/motm/98 (accessed 2023-05-22).
18. Cross, D.; Burmester, J. K. Gene Therapy for Cancer Treatment: Past, Present and Future. Clinical Medicine & Research 2006, 4 (3), 218–227. https://doi.org/10.3121/cmr.4.3.218.
19. Vattemi, E.; Claudio, P. P. Gene Therapy for Lung Cancer: Practice and Promise. Ann Ital Chir 2004, 75 (3), 279–289.
20. Rébé, C.; Ghiringhelli, F. Cytotoxic Effects of Chemotherapy on Cancer and Immune Cells: How Can It Be Modulated to Generate Novel Therapeutic Strategies? Future Oncology 2015, 11 (19), 2645–2654. https://doi.org/10.2217/fon.15.198.
21. Dancey, J. E.; Bedard, P. L.; Onetto, N.; Hudson, T. J. The Genetic Basis for Cancer Treatment Decisions. Cell 2012, 148 (3), 409–420. https://doi.org/10.1016/j.cell.2012.01.014.
22. Cooper, G. M. Oncogenes. The Cell: A Molecular Approach. 2nd edition 2000.
23. Tokheim, C. J.; Papadopoulos, N.; Kinzler, K. W.; Vogelstein, B.; Karchin, R. Evaluating the Evaluation of Cancer Driver Genes. Proc. Natl. Acad. Sci. U.S.A. 2016, 113 (50), 14330–14335. https://doi.org/10.1073/pnas.1616440113.
24. Moasser, M. M.; Ai, W. Z. Neoplasia. In Pathophysiology of Disease: An Introduction to Clinical Medicine; Hammer, G. D., McPhee, S. J., Eds.; McGraw-Hill Education: New York, NY, 2019.
25. Hu, B.; Zhong, L.; Weng, Y.; Peng, L.; Huang, Y.; Zhao, Y.; Liang, X.-J. Therapeutic SiRNA: State of the Art. Sig Transduct Target Ther 2020, 5 (1), 101. https://doi.org/10.1038/s41392-020-0207-x.
26. Sioud, M.; Furset, G.; Cekaite, L. Suppression of Immunostimulatory SiRNA-Driven Innate Immune Activation by 2′ -Modified RNAs. Biochemical and Biophysical Research Communications 2007, 361 (1), 122–126. https://doi.org/10.1016/j.bbrc.2007.06.177.
27.) Song, X.; Wang, X.; Ma, Y.; Liang, Z.; Yang, Z.; Cao, H. Site-Specific Modification Using the 2′ -Methoxyethyl Group Improves the Specificity and Activity of SiRNAs. Molecular Therapy - Nucleic Acids 2017, 9, 242–250. https://doi.org/10.1016/j.omtn.2017.10.003.
28. Fluiter, K.; Mook, O. R. F.; Baas, F. The Therapeutic Potential of LNA-Modified SiRNAs: Reduction of off-Target Effects by Chemical Modification of the SiRNA Sequence. Methods Mol Biol 2009, 487, 189–203. https://doi.org/10.1007/978-1-60327-547-7_9.
29. Bramsen, J. B.; Pakula, M. M.; Hansen, T. B.; Bus, C.; Langkjær, N.; Odadzic, D.; Smicius, R.; Wengel, S. L.; Chattopadhyaya, J.; Engels, J. W.; Herdewijn, P.; Wengel, J.; Kjems, J. A Screen of Chemical Modifications Identifies Position-Specific Modification by UNA to Most Potently Reduce SiRNA off-Target Effects. Nucleic Acids Research 2010, 38 (17), 5761–5773. https://doi.org/10.1093/nar/gkq341.
30. Janas, M. M.; Schlegel, M. K.; Harbison, C. E.; Yilmaz, V. O.; Jiang, Y.; Parmar, R.; Zlatev, I.; Castoreno, A.; Xu, H.; Shulga-Morskaya, S.; Rajeev, K. G.; Manoharan, M.; Keirstead, N. D.; Maier, M. A.; Jadhav, V. Selection of GalNAc-Conjugated SiRNAs

with Limited off-Target-Driven Rat Hepatotoxicity. Nat Commun 2018, 9 (1), 723. https://doi.org/10.1038/s41467-018-02989-4.
31. Mahmoodi Chalbatani, G.; Dana, H.; Gharagouzloo, E.; Grijalvo, S.; Eritja, R.; Logsdon, C. D.; Memari, F.; Miri, S. R.; Rad, M. R.; Marmari, V. Small Interfering RNAs (SiRNAs) in Cancer Therapy: A Nano-Based Approach. Int J Nanomedicine 2019, 14, 3111–3128. https://doi.org/10.2147/IJN.S200253.
32. Suter, S. R.; Ball-Jones, A.; Mumbleau, M. M.; Valenzuela, R.; Ibarra-Soza, J.; Owens, H.; Fisher, A. J.; Beal, P. A. Controlling MiRNA-like off-Target Effects of an SiRNA with Nucleobase Modifications. Org. Biomol. Chem. 2017, 15 (47), 10029–10036. https://doi.org/10.1039/C7OB02654D.
33. Sparks, J.; Slobodkin, G.; Matar, M.; Congo, R.; Ulkoski, D.; Rea-Ramsey, A.; Pence, C.; Rice, J.; McClure, D.; Polach, K. J.; Brunhoeber, E.; Wilkinson, L.; Wallace, K.; Anwer, K.; Fewell, J. G. Versatile Cationic Lipids for SiRNA Delivery. Journal of Controlled Release 2012, 158 (2), 269–276. https://doi.org/10.1016/j.jconrel.2011.11.006.
34. Bramsen, J. B.; Pakula, M. M.; Hansen, T. B.; Bus, C.; Langkjær, N.; Odadzic, D.; Smicius, R.; Wengel, S. L.; Chattopadhyaya, J.; Engels, J. W.; Herdewijn, P.; Wengel, J.; Kjems, J. A Screen of Chemical Modifications Identifies Position-Specific Modification by UNA to Most Potently Reduce SiRNA off-Target Effects. Nucleic Acids Research 2010, 38 (17), 5761–5773. https://doi.org/10.1093/nar/gkq341.
35. Terrazas, M.; Ocampo, S. M.; Perales, J. C.; Marquez, V. E.; Eritja, R. Effect of North Bicyclo[3.1.0]Hexane 2′ -Deoxy-Pseudosugars on RNA Interference: A Novel Class of SiRNA Modification. ChemBioChem 2011, 12 (7), 1056–1065. https://doi.org/10.1002/cbic.201000791.
36. Alagia, A.; Jorge, A. F.; Aviñó, A.; Cova, T. F. G. G.; Crehuet, R.; Grijalvo, S.; Pais, A. A. C. C.; Eritja, R. Exploring PAZ/3′ -Overhang Interaction to Improve SiRNA Specificity. A Combined Experimental and Modeling Study. Chem. Sci. 2018, 9 (8), 2074–2086. https://doi.org/10.1039/C8SC00010G.
37. Eberle, F.; Gießler, K.; Deck, C.; Heeg, K.; Peter, M.; Richert, C.; Dalpke, A. H. Modifications in Small Interfering RNA That Separate Immunostimulation from RNA Interference. The Journal of Immunology 2008, 180 (5), 3229–3237. https://doi.org/10.4049/jimmunol.180.5.3229.
38. Suter, S. R.; Ball-Jones, A.; Mumbleau, M. M.; Valenzuela, R.; Ibarra-Soza, J.; Owens, H.; Fisher, A. J.; Beal, P. A. Controlling MiRNA-like off-Target Effects of an SiRNA with Nucleobase Modifications. Org. Biomol. Chem. 2017, 15 (47), 10029–10036. https://doi.org/10.1039/C7OB02654D.
39. Wang, J.; Lu, Z.; Wientjes, M. G.; Au, J. L.-S. Delivery of SiRNA Therapeutics: Barriers and Carriers. AAPS J 2010, 12 (4), 492–503. https://doi.org/10.1208/s12248-010-9210-4.
40. Mousavizadeh, A.; Jabbari, A.; Akrami, M.; Bardania, H. Cell Targeting Peptides as Smart Ligands for Targeting of Therapeutic or Diagnostic Agents: A Systematic Review. Colloids and Surfaces B: Biointerfaces 2017, 158, 507–517. https://doi.org/10.1016/j.colsurfb.2017.07.012.
41. Wang, F.; Wang, Y.; Zhang, X.; Zhang, W.; Guo, S.; Jin, F. Recent Progress of Cell-Penetrating Peptides as New Carriers for Intracellular Cargo Delivery. J Control Release 2014, 174, 126–136. https://doi.org/10.1016/j.jconrel.2013.11.020.

42. Bitler, B. G.; Schroeder, J. A. Anti-Cancer Therapies That Utilize Cell Penetrating Peptides. Recent Pat Anticancer Drug Discov 2010, 5 (2), 99–108. https://doi.org/10.2174/157489210790936252.
43. Ren, G.; Roberts, A. I.; Shi, Y. Adhesion Molecules: Key Players in Mesenchymal Stem Cell-Mediated Immunosuppression. Cell Adhesion & Migration 2011, 5 (1), 20–22. https://doi.org/10.4161/cam.5.1.13491.
44. Takeichi, M. The Cadherins: Cell-Cell Adhesion Molecules Controlling Animal Morphogenesis. Development 1988, 102 (4), 639–655. https://doi.org/10.1242/dev.102.4.639.
45. CDH1 gene: MedlinePlus Genetics. https://medlineplus.gov/genetics/gene/cdh1/ (accessed 2023-05-22).
46. Pećina-Šlaus, N. [No Title Found]. Cancer Cell Int 2003, 3 (1), 17. https://doi.org/10.1186/1475-2867-3-17.
47. Vleminckx, K.; Vakaet, L.; Mareel, M.; Fiers, W.; van Roy, F. Genetic Manipulation of E-Cadherin Expression by Epithelial Tumor Cells Reveals an Invasion Suppressor Role. Cell 1991, 66 (1), 107–119. https://doi.org/10.1016/0092-8674(91)90143-m.
48. Mrozik, K. M.; Blaschuk, O. W.; Cheong, C. M.; Zannettino, A. C. W.; Vandyke, K. N-Cadherin in Cancer Metastasis, Its Emerging Role in Haematological Malignancies and Potential as a Therapeutic Target in Cancer. BMC Cancer 2018, 18 (1), 939. https://doi.org/10.1186/s12885-018-4845-0.
49. Radice, G. L.; Rayburn, H.; Matsunami, H.; Knudsen, K. A.; Takeichi, M.; Hynes, R. O. Developmental Defects in Mouse Embryos Lacking N-Cadherin. Dev Biol 1997, 181 (1), 64–78. https://doi.org/10.1006/dbio.1996.8443.
50. Fontana, F.; Hickman-Brecks, C. L.; Salazar, V. S.; Revollo, L.; Abou-Ezzi, G.; Grimston, S. K.; Jeong, S. Y.; Watkins, M.; Fortunato, M.; Alippe, Y.; Link, D. C.; Mbalaviele, G.; Civitelli, R. N-Cadherin Regulation of Bone Growth and Homeostasis Is Osteolineage Stage-Specific. J Bone Miner Res 2017, 32 (6), 1332–1342. https://doi.org/10.1002/jbmr.3112.
51. George-Weinstein, M.; Gerhart, J.; Blitz, J.; Simak, E.; Knudsen, K. A. N-Cadherin Promotes the Commitment and Differentiation of Skeletal Muscle Precursor Cells. Dev Biol 1997, 185 (1), 14–24. https://doi.org/10.1006/dbio.1997.8542.
52. Paik, J.-H.; Skoura, A.; Chae, S.-S.; Cowan, A. E.; Han, D. K.; Proia, R. L.; Hla, T. Sphingosine 1-Phosphate Receptor Regulation of N-Cadherin Mediates Vascular Stabilization. Genes Dev 2004, 18 (19), 2392–2403. https://doi.org/10.1101/gad.1227804.
53. Yap, A. S.; Kovacs, E. M. Direct Cadherin-Activated Cell Signaling: A View from the Plasma Membrane. J Cell Biol 2003, 160 (1), 11–16. https://doi.org/10.1083/jcb.200208156.
54. Kalluri, R.; Weinberg, R. A. The Basics of Epithelial-Mesenchymal Transition. J. Clin. Invest. 2009, 119 (6), 1420–1428. https://doi.org/10.1172/JCI39104.
55. Hazan, R. B.; Phillips, G. R.; Qiao, R. F.; Norton, L.; Aaronson, S. A. Exogenous Expression of N-Cadherin in Breast Cancer Cells Induces Cell Migration, Invasion, and Metastasis. Journal of Cell Biology 2000, 148 (4), 779–790. https://doi.org/10.1083/jcb.148.4.779.
56. Kurtova, A. V.; Balakrishnan, K.; Chen, R.; Ding, W.; Schnabl, S.; Quiroga, M. P.; Sivina, M.; Wierda, W. G.; Estrov, Z.; Keating, M. J.; Shehata, M.; Jäger, U.; Gandhi, V.;

Kay, N. E.; Plunkett, W.; Burger, J. A. Diverse Marrow Stromal Cells Protect CLL Cells from Spontaneous and Drug-Induced Apoptosis: Development of a Reliable and Reproducible System to Assess Stromal Cell Adhesion-Mediated Drug Resistance. Blood 2009, 114 (20), 4441–4450. https://doi.org/10.1182/blood-2009-07-233718.
57. Janiszewska, M.; Primi, M. C.; Izard, T. Cell Adhesion in Cancer: Beyond the Migration of Single Cells. Journal of Biological Chemistry 2020, 295 (8), 2495–2505. https://doi.org/10.1074/jbc.REV119.007759.
58. Zheng, Y.; Zhou, H.; Dunstan, C. R.; Sutherland, R. L.; Seibel, M. J. The Role of the Bone Microenvironment in Skeletal Metastasis. Journal of Bone Oncology 2013, 2 (1), 47–57. https://doi.org/10.1016/j.jbo.2012.11.002.
59. Bou Zerdan, M.; Nasr, L.; Kassab, J.; Saba, L.; Ghossein, M.; Yaghi, M.; Dominguez, B.; Chaulagain, C. P. Adhesion Molecules in Multiple Myeloma Oncogenesis and Targeted Therapy. International Journal of Hematologic Oncology 2022, 11 (2), IJH39. https://doi.org/10.2217/ijh-2021-0017.

Chapter 2: Targeting Osteoblast Cell Surface Receptor Periostin as A Viable Option for Peptide Binding to Bone Tissue

2.1 Abstract

Cell-targeting peptides have shown much promise as therapeutic delivery agents in the treatment of various diseases, particularly cancer. CTPs have shown high selectivity and specificity for their desired targets, diminishing unwanted off-target effects. Previous studies have shown successful treatment of bone diseases, such as osteoporosis using osteoblast-targeting peptides.[1] This prior study has formed the basis of our work. In this chapter, the process of designing osteoblast-targeting peptides, which bind to periostin on the cell surface will be discussed, as well as the various characterization methods employed to determine their purity and yield. Synthesis of OSB-targeting peptides was proven to be successful and their uptake into OSB cell lines was also proven successful, as this study highlights. Furthermore, due to the integral role periostin plays in bone development and function, it is always expressed on the cell surface of bone tissue which makes it a reliable therapeutic target for drug delivery into the BM environment. Here, we report that the osteoblast-targeting peptide was successfully synthesized and taken up into our osteoblast cell line. We have also confirmed the expression of periostin along the cell surface of our cell line as well, confirming periostin as a reliable target for our peptide binding. Many cancers such as breast, prostate, and pancreatic cancers can migrate to bone tissue as a direct result of the EMT transition, which is a hallmark of many cancers. Consequently, caner metastasis within bone and multiple myelomas originating within bone tissue thrive as a direct result of the nature of the BM environment. For this reason, identifying a reliable marker expressed on osteoblast cells will allow anti-cancer therapies to be delivered to bone tissue selectively, and effectively to limit cancer cell spread and metastasis within bone.

2.2 Introduction

Periostin is a cell adhesion protein. This protein was first discovered in a mouse osteoblastic cell line. It is typically expressed in the periosteum, which is a specialized membrane covering the outer layer of bones governing bone growth diameter as well as cortical thickness.[2-4] Periostin is also expressed in the teeth in the periodontal ligament, heart valves, and tendons, and has also been detected in ore-osteoblast cells by *in situ* hybridization.[5-8] Osteoblast cells, as stated previously are a type of bone cell. They are responsible for bone formation mainly during skeletal development and remodeling.[9] Osteoblast cells arise from the differentiation of mesenchymal cells in the periosteum, and these cells form closely packed sheets on the surface of bones.[9,10] During the process of new bone formation osteoblasts release a variety of growth factors and signaling molecules such as hormones, enzymes, alkaline phosphatase, IGFs, TGFβ, collagenase, osteocalcin, and type I collagen.[9,10] Once the process of bone formation has completed, osteoblasts will be subject to two potential fates: they can become flattened and remain a part of the quiescent lining cells of the bone surfaced, or they can undergo apoptosis.[9] The bone matrix is the third most common site for tumor cells to spread and metastasize, and furthermore "the site at which secondary tumors form is not random; for metastases to develop tumor cells must arrive in an environment that is permissive for their colonization and subsequent growth. In the case of bone metastasis, it is hypothesized that tumor cells home to specific niches: The endosteal niche (which is primarily made up of osteoblasts), the hematopoietic stem cell (HSC) niche and the vascular niche."[9] For example, within the endosteal niche "the CXCR4/CXCL12 interaction is thought to be a key component in the homing and adhesion of tumor cells to the metastatic niche in bone. Osteoblasts express the chemokine CXCL12 whereas the majority of metastatic breast and prostate cancer cells express the

corresponding receptor CXCR4. Once tumor cells have colonized the endosteal niche evidence suggests that osteoblasts maintain these tumor cells in a quiescent state, through the interactions of CXCR4/CXCL12, using similar mechanisms to those used by osteoblasts for maintaining quiescence of HSCs."[9] Thus, the importance of finding a bone specific receptor to treat diseases in the BM, such as cancers is an ideal treatment approach, and we have highlighted the success at targeting the periostin receptor for such aims.

2.3 Chapter Objectives

This thesis chapter focuses on the synthesis, characterization, and confirmation of periostin binding of the OSB-targeting peptides. This peptide has previously been identified as selectively binding to osteoblast cells, and this thesis chapter aims to corroborate these findings. Periostin is a cell surfaced adhesion protein which also functions as a receptor for the synthesized peptides. Because these OSB-targeting peptides so efficiently bind to periostin, they can be functionalized easily with simple modifications which serve to deliver siRNAs across the cell membrane. This serves as the hypothesis for our work. In order to confirm this hypothesis, a short, fluorescently labeled peptide sequence which specifically binds to periostin will be synthesized and functionalized with a polycationic tail consisting of various arginine lengths. This peptide will be purified, and its identity will be confirmed using both mass spectroscopy as well as UV-spectroscopy. After confirmation of periostin expression on the surface of the mouse fibroblast cell line, MC3T3.E1 using flow cytometry, the binding of the peptides to the cells will be examined and finally the uptake of the peptide into the cells will again be tested using flow cytometry.

2.4 Results and Discussion

2.4.1 Identification and Synthesis of Osteoblast-targeting Peptide

Each peptide sequence was made following solid-phase peptide synthesis protocols. Peptides consisted of the fluorophore Fluorescein isothiocyanate (FITC). This allowed for simpler visualization and quantification following the completion of synthesis. A linker was also added following the FITC to avoid degradation of the fluorophore. To maintain symmetry on both ends of the peptide, the linker was also added between the periostin binding portion and the arginine tail. The linker used was FMOC protected 6-aminohexanoic acid. The binding portion of the peptide consisted of three serine residues and two aspartic acid residues, in accordance with the previously identified periostin targeting sequence. Following this portion of the peptide and the linker was the polyarginine tail. Tail lengths of both 9 and 12 arginine residues were synthesized. Each peptide was cleaved from solid support by trifluoroacetic acid (TFA) cleavage and then characterized using both mass spectroscopy as well as UV-spectroscopy and reverse phase high-performance liquid chromatography. Mass to charge ratios were calculated and reported up to the highest ionization state observed for the synthesized sequences. UV-spectroscopy was used to calculate the purified amount of each peptide obtained using the beer-lambert law and the extinction coefficient for FITC, as well as its excitation wavelength of 450 nm. Measuring the concentration dependent upon FITC concentration was chosen over measuring based on peptide bonds present because each sequence of completed peptides was fluorescently labeled. Observed retention times characteristic of each sequence were also noted in both MeOH as well as MeCN solvents. Table 2.1 summarizes all data characteristic of each peptide sequence. The following figures 2.1-2.5 are representative HPLC traces characteristic of each peptide sequence synthesized.

Sequence	Crude Purity (%)[1]	Purified Purity (%)[2]	Theoretical MW (g/mol)[3]	Experimental MW (g/mol)[4]	Z[5]	Retention Time (min)[6]	Retention Time (min)[7]
FITC-Ahx-SDSSD	83	100	504.4	504.4	2	10	15
FITC-Ahx-SDSSD-Ahx-R_9	74	89	309.6	309.6	8	7.4	16
FITC-AHX-SDSSD-Ahx-R_{12}	78	100	589.0	589.0	5	13	16
FITC-Ahx-R_9	66	95	312.0	312.0	6	6.3	9.6
FITC-Ahx-R_{12}	92	100	292.8	292.8	8	13	15

[1]Crude purity determined from HPLC trace before purification
[2]Purified purity determined from HPLC after purification
[3]Theoretical MW found using ChemDraw. MW for FITC-Ahx-SDSSD expressed using negative polarity, all others found using positive polarity
[4]Experimental weight found from LCMS, corresponding to charge state of molecule (M+z/H)
[5]Z is the charge state of peptide found using LCMS which corresponds to the MW of the peptide
[6]Retention time using gradient of 20 to 95 MeCN over 27 minutes in H_2O and 0.1% FA. For the FITC-Ahx-SDSSD peptide retention time was noted using a gradient of 2 to 98 over 24 minutes
[7]Retention time using gradient of 20 to 95 MeOH over 26 minutes in H_2O and 0.1% FA

Table 2.1: Peptide characterization table. All reported values correspond to purified peptide samples.

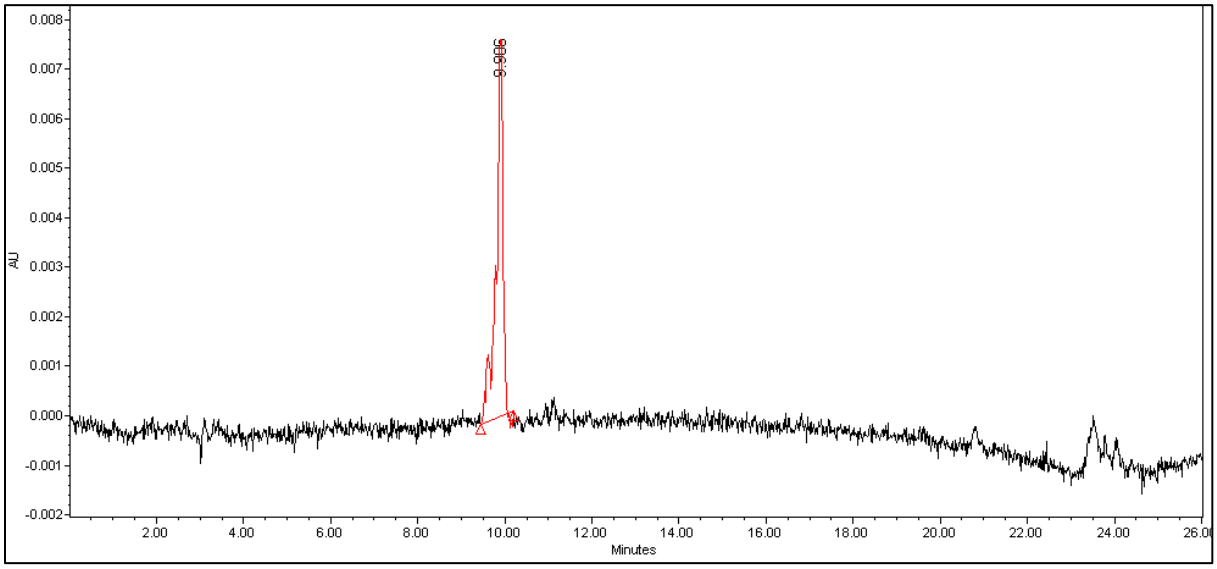

Figure 2.1: Representative HPLC trace of the FITC-Ahx-R_9 peptide shown in the 450 nm channel. Run conditions were 20 to 95 MeOH with an aqueous phase of 0.1% FA/H_2O for 26 minutes.

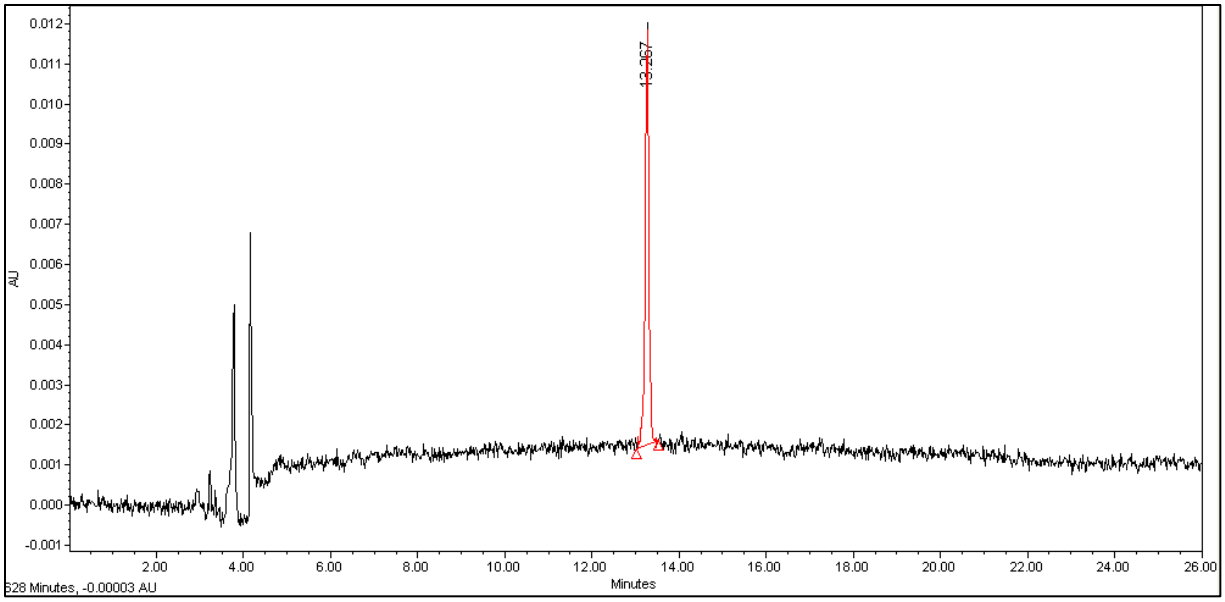

Figure 2.2: Representative HPLC trace of the FITC-Ahx-R_{12} peptide shown in the 450 nm channel. Run conditions were 20 to 95 MeCN with an aqueous phase of 0.1% FA/H_2O for 27 minutes.

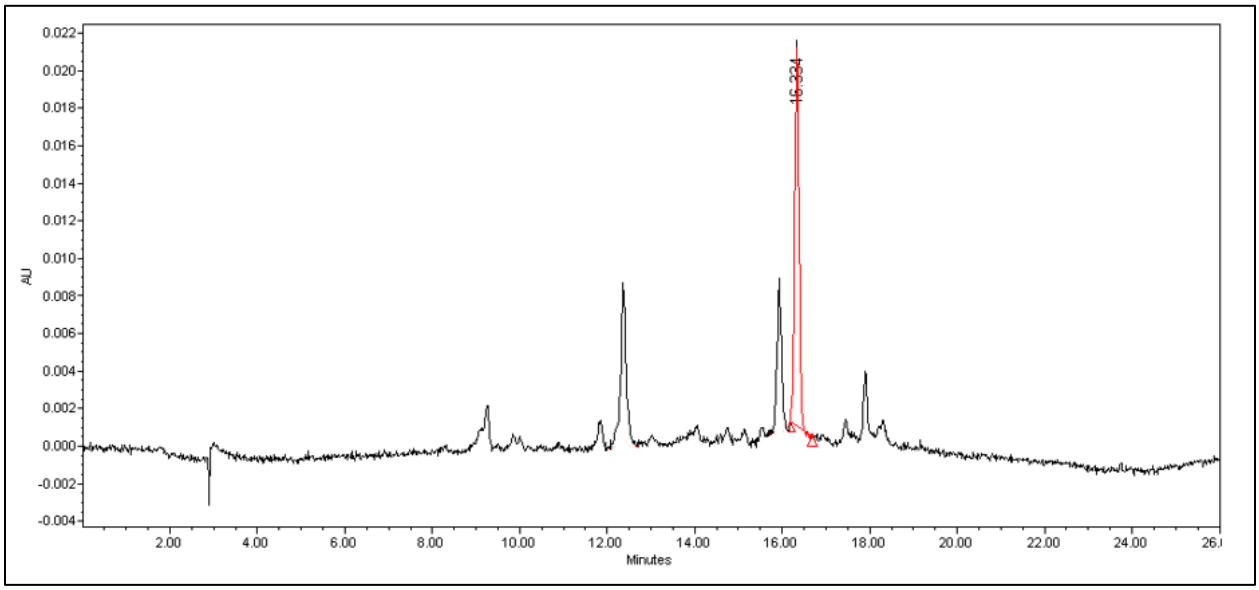

Figure 2.3: Representative HPLC trace of the FITC-Ahx-SDSSD-Ahx-R_9 peptide shown in the 450 nm channel. Run conditions were 20 to 95 MeOH with an aqueous phase of 0.1% FA/H_2O for 26 minutes.

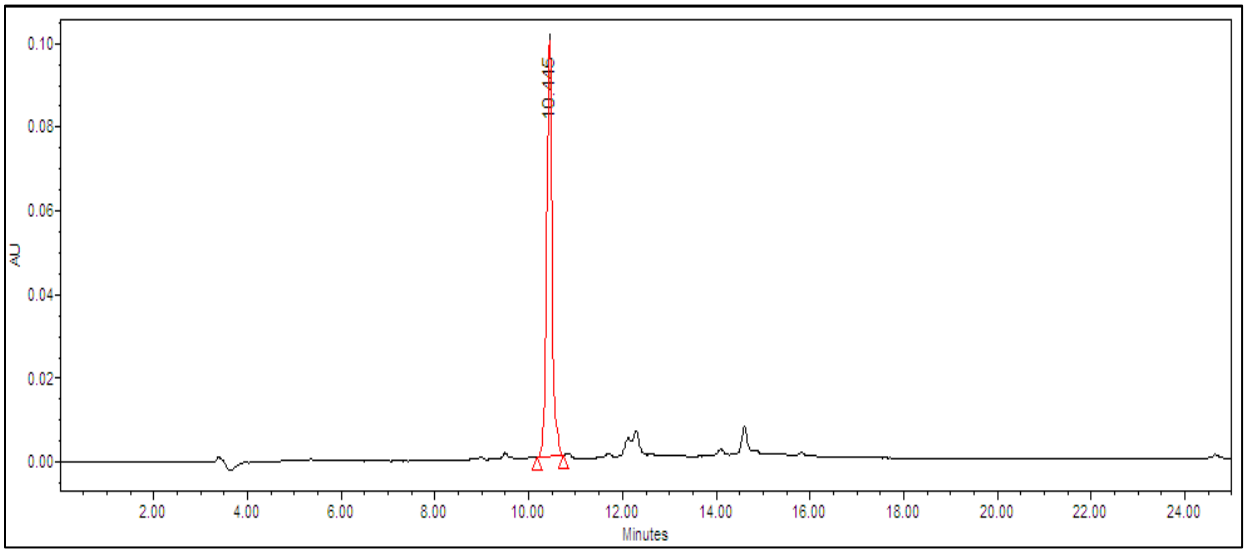

Figure 2.4: Representative HPLC trace of the FITC-Ahx-SDSSD peptide shown in the 450 nm channel. Run conditions were 2 to 98 MeCN with an aqueous phase of 0.1% FA/H_2O for 24 minutes.

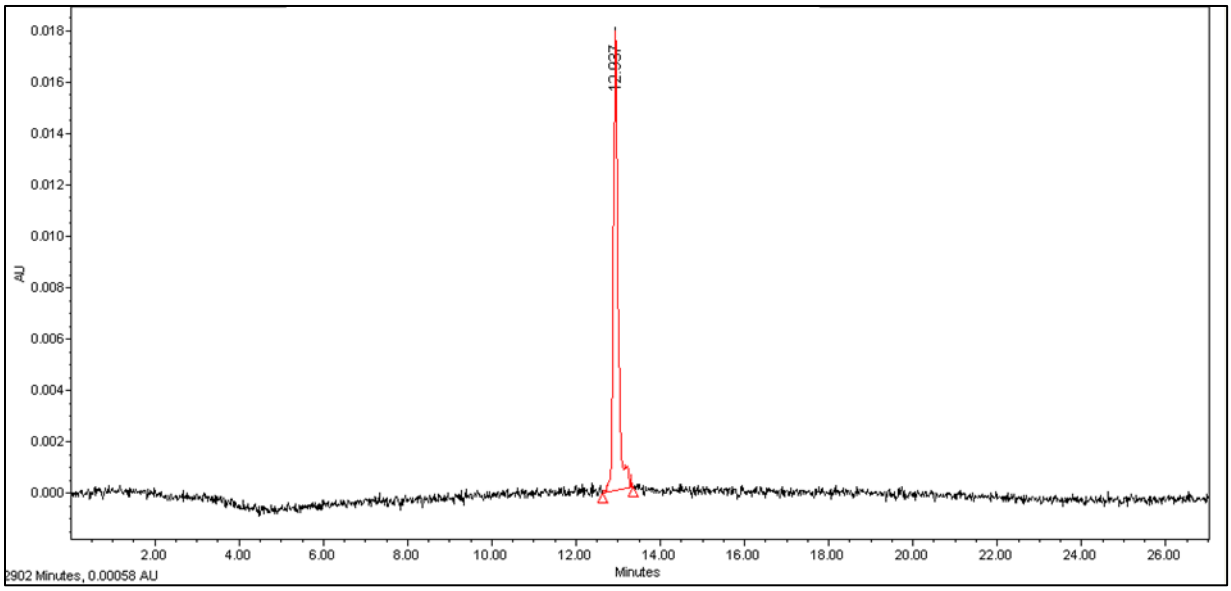

Figure 2.5: Representative HPLC trace of the FITC-Ahx-SDSSD-Ahx-R_{12} peptide shown in the 450 nm channel. Run conditions were 20 to 95 MeCN with an aqueous phase of 0.1% FA/H_2O for 27 minutes.

2.4.2 OSB-targeting Peptide Successfully and Selectively Binds to Osteoblast cells

To determine and confirm whether the synthesized peptide specifically targeted osteoblast cells and bound to periostin, flow cytometry was run using two cell lines aside from the osteoblast cell line, MC3TS.E1. The first test was performed with varying levels of peptide in conjunction with OSB cells. The concentrations of peptide tested were 1 µM, 10 µM and 25 µM peptide. Each peptide was fluorescently labeled using FITC, which allowed for detection using flow cytometry. The control cells used were RPMI cells, and as the results show, peptide selectively bound to the OSB cells and not the RPMI cells (Figure 2.6). As a second confirmation the ATDC5 cell line was also tested for periostin expression using a periostin expressing antibody (Figure 2.7). Two cell populations were tested to determine if the ATDC5 cells expressed periostin, one stained with the periostin-detecting antibody and one without. Both stained and unstained populations were identical and showed no shift, indicating the absence of periostin on the ATDC5 cell line.

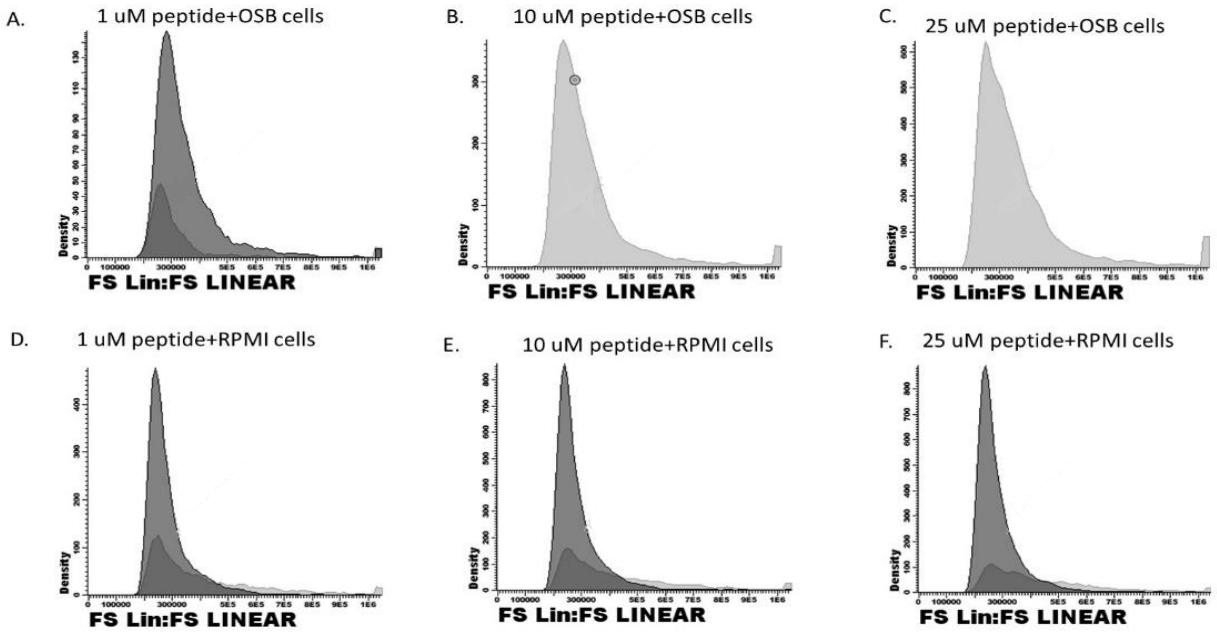

Figure 2.6: Concentration dependent study of peptide binding to osteoblast cells vs peptide incubated with RPMI cells. No change was observed between 1 µM- 25 µM peptide concentration, indicating that at lower concentrations peptide successfully bound to the cells. *Courtesy of Dr. Jenny Zilberberg, The Center for Discovery and Innovation.*

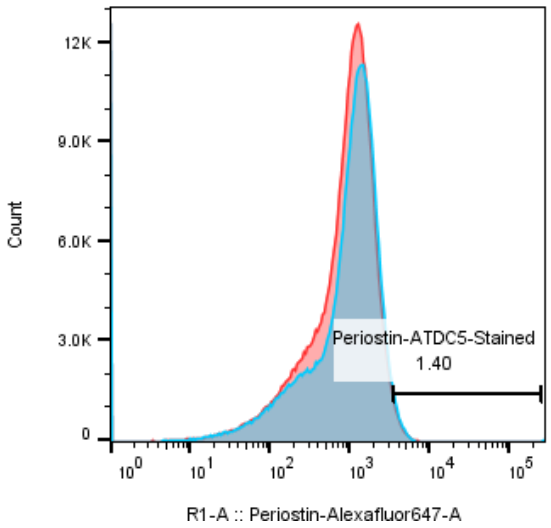

Figure 2.7: Negative control for periostin detection using ATDC5 cell line. Two cell samples run, one stained population using periostin-detecting antibody and an unstained control cell line.

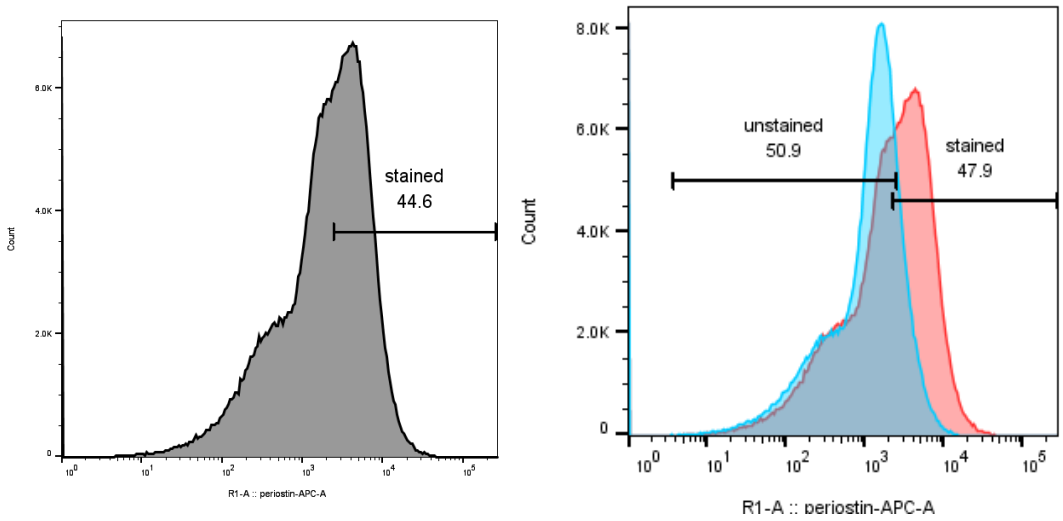

Average # of stained cells= 1.261 x10^5

STDEV= 4.814 x10^4

Mean +/- STDEV= 1.261 x10^5 +/- 4.814 x10^4

Figure 2.8: Representative figure for unstained MC3T3.E1 cell population (left) and stained vs unstained MC3T3.E1 cell populations (right). Image on left includes gating for the percentage of cells which should be positive for periostin.

Following testing and confirmation of negative cell line controls, the osteoblast cell line MC3T3.E1 was tested for periostin expression (Figure 2.8). Once again, two cell populations were tested. One stained using the periostin-detecting antibody and one without. The cells were gated to compare both periostin positive and periostin negative populations, while excluding all dead cells from the gating. There was a consistent shift observed between both the stained and unstained cells run on flow indicating and confirming the presence of periostin on the cell surface of the osteoblast cells.

2.4.3 Uptake of OSB-targeting Peptide via Flow Cytometry

To determine whether each synthesized sequence was taken into the cells, a protocol for the uptake of each peptide via flow cytometry was adapted from and designed using the internalization protocol from the study done by Françoise Illien.[11] Initially, the optimal concentration of peptide was determined by flow cytometry. This was done by testing varying peptide concentrations ranging from 1-6 μM. Because binding was observed at 1 μM and there was not much difference between the varying concentrations, this concentration was used for all tests. Each peptide sequence was incubated with the cells at 37 ˚C for 1 hour to allow for internalization and binding to the membrane, while maintaining cell viability. The peptides were added to the cell media used to culture the MC3T3.E1 cells. Following the incubation step, the cells incubated with peptide were split in half to test one half without quenching and the other half with quenching using a 0.2% Trypan Blue solution. Trypan Blue was chosen because it quenches FITC signals and will not pass the cell membrane of a healthy cell. Because of this, it was expected that the FITC bound to the membrane would no longer fluoresce as strongly or at all following the quenching step. This would indicate that all FITC-labeled peptides had been internalized by the cells and the signals picked up by flow cytometry were from within the cell. The results obtained highlighted this expected trend, as is shown in Figures 2.9-2.10. Representative images were chosen from all flow cytometry runs performed and the average number of quenched cells and unquenched cells was determined. The standard deviation was also determined for each set of cells across the various runs performed and this was reported to account for differences in numbers of cells harvested and counted from each population.

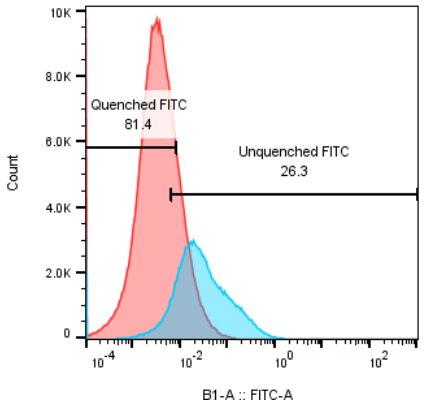

Average # Quenched Cells= 1.198 x 10^7

STDEV= 1.468 x10^7

Mean +/- STDEV= 1.198 x 10^7 +/- 1.468 x10^7

Average # Unquenched Cells= 1.905 x 10^7

STDEV= 2.611 x10^7

Mean +/- STDEV= 1.905 x 10^7 +/- 2.611 x10^7

Figure 2.9: Representative image of MC3T3.E1 cells incubated with 1 uM peptide (FITC-Ahx-SDSSD-Ahx-R12) for 1 hour at 37C. Blue population indicates cells incubated with peptide and non-quenched. Red population indicates cells incubated with peptide for 1 hr and quenched with 0.2% Trypan Blue for 10 minutes following peptide incubation period.

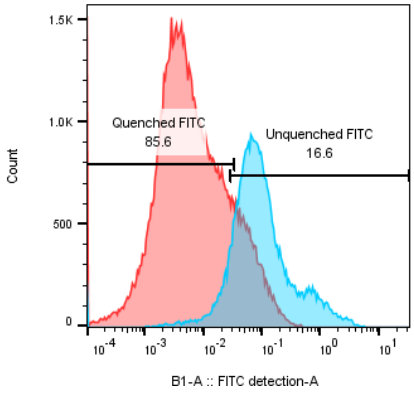

Average # Quenched Cells= 4.527 x 10^6

STDEV= 3.999 x10^6

Mean +/- STDEV= 4.527 x 10^6 +/- 3.999 x10^6

Average # Unquenched Cells= 8.979 x 10^5

STDEV= 1.420 x10^6

Mean +/- STDEV= 8.979 x 10^5 +/- 1.420 x10^6

Figure 2.10: MC3T3 cells incubated with 1 uM peptide (FITC-Ahx-SDSSD-Ahx-R9) for 1 hour at 37C. Blue population indicates cells incubated with peptide and non-quenched. Red population indicates cells incubated with peptide for 1 hr and quenched with 0.2% Trypan Blue for 10 minutes following peptide incubation period.

Finally, to confirm that the results were indicative of the peptide being taken up into the cells, and that the FITC signal was not due to nonspecific binding, an isotype control, CD90-FITC was incubated with cells. One population of cells incubated with the isotype control was quenched using Trypan Blue, while the other was not and these results were compared to cells run by themselves. The cells run by themselves showed no signal in the range where FITC was

detected, and the isotype control quenched and unquenched showed no change. These results indicated that our previous studies showed that the peptide was being internalized by the cells successfully. A representative image for the isotype control run is shown below in Figure 2.11.

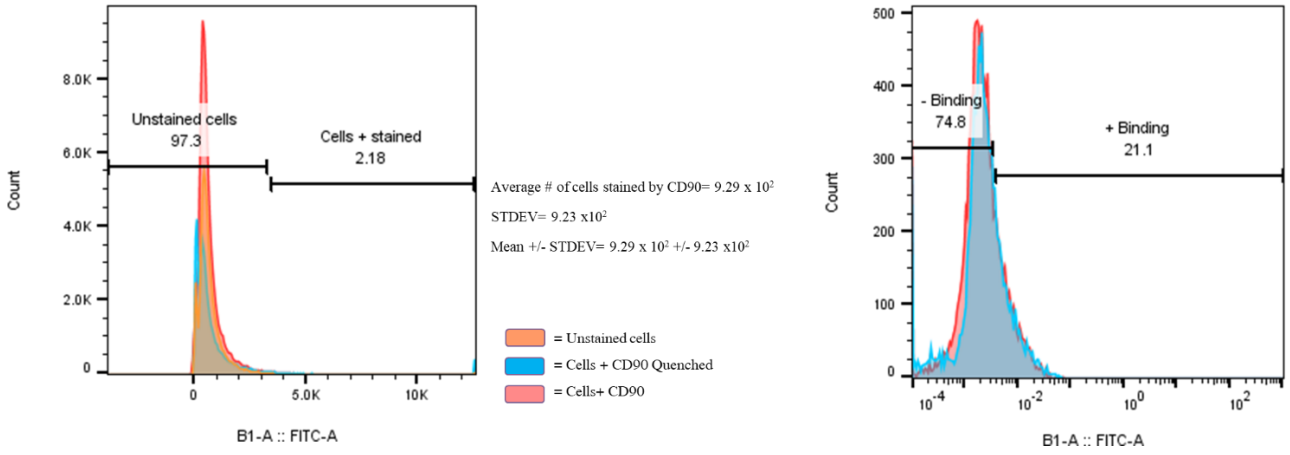

Figure 2.11: Representative image of isotype control tests on MC3T3.E1 cell line. The image on left shows control cells and isotype control + cells both quenched and unquenched. Cells were quenched using 0.2 % Trypan Blue. The image on the right were control cells detected in the range for FITC.

2.5 Conclusions

The successful synthesis and characterization of the periostin binding peptide was performed as highlighted in this chapter. The peptide was then shown to successfully bind to osteoblast cells selectively while not binding to other cell lines. Furthermore, this peptide was also shown to successfully internalize following binding to the cell membrane. In conclusion, these results indicate that periostin-binding peptides can be used to shuttle therapeutic agents across the cell membrane to treat diseases, such as cancer.

2.6 Materials and Methods

2.6.1 Solid-phase Peptide Synthesis

Solid-phase peptide synthesis was performed following traditional methods by hand and by use of microwave synthesizer. Each sequence was synthesized using a ResPrep 6 mL

reservoir with an appropriate ResPrep filter. The resin used to synthesize each peptide was an FMOC protected Rink Amide resin (ApexBio Rink Amide Resin, A6576) and was deprotected using 20% Piperidine in DMF, then swelled using DMF prior to the addition of each amino acid. The synthesis was performed on a 0.1 mmol scale. Amino acids were used in an excess of 3 equivalents to ensure their addition at each coupling step. The first Arginine addition was performed twice when done by hand. Each amino acid was added to a small glass vial along with 113 mg HCTU and dissolved in 4 mL of DMF. Following the solubilization of the amino acid and HCTU, 66 µL of NMM was then added to the vial with vortexing to activate the amino acid for coupling. All amino acid residues were FMOC protected and following each addition step, a deprotection step was preformed using 20% Piperidine in DMF for 20 minutes with shaking to remove the FMOC protecting group. The amino acids used were as follows: Aspartic Acid (CeroSalus Advanced ChemTech, Fmoc-Asp(OBut)-OH), Serine (NovaBiochem, Fmoc-Ser(tBu)-OH), and Arginine (AK Scientific, Fmoc-L-Arg(PBF)-OH). The linker used between the polyarginine tail and prior to the addition of the FITC fluorophore was CHEM-IMPEX InT'L INC. Fmoc-6-aminohexanoic acid. Next a wash step was performed using DMF, MeOH, and DCM in order. Each wash step was performed 3 times. Each peptide was then labeled with FITC (Thermo Scientific, FITC (Fluorescein Isothiocyanate), Prod #46424) following a deprotection step after addition of the Ahx linker, and the FITC mixture was prepared in a total of 4 mL in a mixture composed of 50% Pyridine, 30% DMF, and 20% DCM. FITC was added as a 1.1 mole equivalent and added directly to the mixture of Pyridine/DMF/DCM. This was vortexed and then added directly to the cartridge containing the peptide and resin overnight on the Lab-Line Instruments Title Plate Shaker, covered with foil.

When performing SPPS using the Microwave Synthesizer (CEM Discover BIO) synthesizer and Discover open Vessel software, all steps were the same except for shortened couplings, wash steps and deprotections. Amino acid quantities as well as FITC, NMM, DMF, and HCTU were all used in the same amounts as when synthesizing by hand. Amino acids were weighed out in excess of 3 equivalents and dissolved in a total of 4 mL of DMF. Whether by hand or by microwave synthesizer, synthesis was done on a 0.1 mmol scale. Steps for cleaving and labeling the completed peptide were identical when using the microwave synthesizer as well.

After completing each desired sequence, the desired peptide was cleaved from solid support using a mixture of TFA/H_2O/TES (3.8 mL TFA/100 µL TES/ 100 µL H_20) on the shaker for approximately 4 hours. Once the cleavage was complete the liquid was collected in microcentrifuge tubes and the TFA was evaporated off under nitrogen gas. Following the TFA evaporation, the solid peptide was then washed with ice cold ether, spun down in the centrifuge and the ether was decanted from the solid peptide. This was performed a total of 3 times before storing the completed peptide sequence at -80°C.

2.6.2 Mass Spectroscopy

Mass spectroscopy was used to confirm sequence identity of each completed peptide sequence using the Hewlett Packard Series 1100 MSD mass spectrometer. Each peptide was first dissolved in solvent (ddH_2O for each pure sequence) and tested under positive polarity from the weights 200 to 3000. The formula for mass to charge ratio was employed based on each peptide's specific molecular weight and expected possible charge states. The control peptide (FITC-Ahx-SDSSD) was tested using negative polarity due its negatively charged aspartic acid residues.

2.6.3 UV Spectroscopy

UV-spectroscopy was performed using the Hewlett Packard 8452A Diode Array Spectrophotometer and Agilent Technologies UV-visible ChemStation software at a wavelength of 450 nm to detect the concentration of FITC-labeled peptides. The Beer-lambert law was used to determine purified peptide concentrations using the extinction coefficient for FITC. Each sequence tested was dissolved in ddH_2O and ddH_2O was used as a blank prior to measuring peptide concentration.

2.6.4 High Performance Liquid Chromatography

High performance liquid chromatography (HPLC) was performed using the Waters HPLC with Empower software. Two gradients of 20 to 95 MeOH with and aqueous phase of 0.1% FA over 26 minutes and 20 to 95 MeCN with an aqueous phase of 0.1% FA over 27 minutes were used with each peptide. Retention times were recorded, and each peptide peak was collected and pooled to acquire each pure peptide sample. Each peptide was purified using either a Thermo Scientific BDS HYPERSIL C_8, 250 x 4.6 column or a Waters Symmetry® C_{18}, 4.6 X 250 mm column dependent upon length or presence of the polyarginine tail.

2.6.5 Semi-Prep

Samples run on the Semi-prep were dissolved in roughly 1 mL of ddH_2O and run on the Varian ProStar and Varian PrepStar Semi-Prep, in conjunction with the Varian ProStar 325 UV-Vis Detector and Model SD-1 pumps. Semi-preparatory separations ran at a flow rate of 5 mL/minute, and maximum injection volume for samples was 10 mL. The gradient used was 40-75% Acetonitrile over the course of 50 minutes using a Phenomenex LUNA 10 C18 (2) 250 X 21.20 mm, 10 micron column. Each sample peak observed at both 820 nm and 450 nm and was collected to be tested and ensure presence of pure peptide using small scale HPLC (Waters 2695

Separations Module and Waters 2998 Photodiode Array Detector) as well as MS. Samples were then rotovapped to remove any excess organic solvent and to concentrate them down before determining sample concentration via UV-Vis on the Hewlett Packard 8452A Diode Array Spectrophotometer and Agilent Technologies UV-visible ChemStation software.

2.6.6 Cell Culture

MC3T3.E1 cell lines were cultured in 100 mm tissue culture dishes with Corning® MEM (Minimum Essential Medium) Alpha Medium media containing 1% P/S, 1% Q, and 10% FBS. Cells were plated from frozen stock and grown to a confluency of about 80-90% before harvesting for experimentation. All cells were harvested by removing growth media with aspiration, then washed with 1X PBS which was aspirated off. This was followed by 2-3 mL of Trypsin or TripLE for 3 minutes at 37°C. Cells were removed from the incubator following the incubator following the trypsin treatment and checked using the LeicaDMi1 microscope to ensure optimal cell lifting. Trypsin treatment was neutralized with growth media in an amount up to a total volume of 10 mL, dependent upon trypsin concentration. Cells were then split in a ratio in accordance with density of the original culture plate.

2.6.7 Flow Cytometry

Before performing flow cytometry, all cells were grown to a confluency of 80-90%. The cells were harvested following the protocol for cell culturing, but cells were not split between plates. The cells were collected following the trypsin neutralization with growth media and placed in a 15 mL conical tube, and 12 µL of cells was pipetted out to be counted using the hemocytometer under the LeicaDMi1 microscope. After determining the cell count, the protocol for direct staining of adherent monolayers of cells was followed. Lifting cells using 0.2% EDTA/PBS was substituted for TripLE due to poor lifting in the EDTA/PBS solution. TripLE

also preserves cell surface markers in a higher number than Trypsin which made it an appropriate substitution. After cells had been counted, the cells were placed in conical tubes (number based on number of samples to be tested) and centrifuged at 1000 RPM for 5 minutes. The supernatant was discarded, and the pellet was washed and resuspended in 1X PBS (about 500 µL to 1mL). Cells were then blocked using blocking buffer (2 mL FACS, 40 µL FBS) on ice for 10 minutes. The cells were not rinsed following blocking. The population of cells to be stained was incubated with 1ug of antibody (Cruz Biosciences Periostin Antibody (F-10) Alexa Fluor® 647, sc-398631 AF647) diluted in FACS buffer (2% FBS/PBS) on ice for 15-30 minutes in a covered bucket. Cells were then centrifuged for 5 minutes at 1000 RPM and the supernatant was discarded. They were washed with 1X PBS, centrifuged under the same conditions and the PBS was aspirated from the cells. Finally, cells were resuspended in 500 µL FACS buffer (2% FBS/PBS). Samples were run using the Miltenyi Biotec Flow Cytometer. All results were processed using Flojo software.

For all quenching studies using the flow cytometer, cell cultures were rinsed with 1X PBS and then lifted using about 5 mL of TripLE for about 3 minutes at 37°C until the cells detached. 5 mL of growth media was then used to neutralize the TripLE and the cell suspension was pipetted into a 15 mL conical tube. From this, 12 µL of cells was removed to be counted using the hemocytometer. Following the cell count, the cell suspension was centrifuged for 5 minutes at 1000 RPM and the supernatant was aspirated and discarded. Cells were then separated into microcentrifuge tubes and incubated with 1 µM peptide in 1 mL of growth media for 1 hour at 37°C. Following incubation, cells were washed with cold 1X PBS then centrifuged at 800 G (or higher). The supernatant was discarded, and cell samples were resuspended in 600 µL of FACS buffer (2% FBS/PBS). Samples were then split (300 µL each sample). One sample was

quenched with 0.2% Trypan Blue (1:1 ratio of Trypan Blue solution to volume of cell suspension) from a stock solution of 0.4% Trypan Blue (0.4 g trypan Blue, 80 mL PBS boiled and brought up to 100 mL with PBS). The cells treated with Trypan Blue were incubated at 37°C for 10 minutes, then spun down and washed with 1X PBS and resuspended in 300 µL FACS buffer. Flow was run using the Miltenyi Biotec Flow Cytometer and all results were processed using Flojo.

2.7 References

1. Sun, Y.; Ye, X.; Cai, M.; Liu, X.; Xiao, J.; Zhang, C.; Wang, Y.; Yang, L.; Liu, J.; Li, S.; Kang, C.; Zhang, B.; Zhang, Q.; Wang, Z.; Hong, A.; Wang, X. Osteoblast-Targeting-Peptide Modified Nanoparticle for SiRNA/MicroRNA Delivery. ACS Nano 2016, 10 (6), 5759–5768. https://doi.org/10.1021/acsnano.5b07828.
2. González-González, L.; Alonso, J. Periostin: A Matricellular Protein With Multiple Functions in Cancer Development and Progression. Front. Oncol. 2018, 8, 225. https://doi.org/10.3389/fonc.2018.00225.
3. Merle, B.; Garnero, P. The Multiple Facets of Periostin in Bone Metabolism. Osteoporos Int 2012, 23 (4), 1199–1212. https://doi.org/10.1007/s00198-011-1892-7.
4. Bonnet, N.; Garnero, P.; Ferrari, S. Periostin Action in Bone. Molecular and Cellular Endocrinology 2016, 432, 75–82. https://doi.org/10.1016/j.mce.2015.12.014.
5. Horiuchi, K.; Amizuka, N.; Takeshita, S.; Takamatsu, H.; Katsuura, M.; Ozawa, H.; Toyama, Y.; Bonewald, L. F.; Kudo, A. Identification and Characterization of a Novel Protein, Periostin, with Restricted Expression to Periosteum and Periodontal Ligament and Increased Expression by Transforming Growth Factor β. J of Bone & Mineral Res 1999, 14 (7), 1239–1249. https://doi.org/10.1359/jbmr.1999.14.7.1239.
6. Kruzynska-Frejtag, A.; Machnicki, M.; Rogers, R.; Markwald, R. R.; Conway, S. J. Periostin (an Osteoblast-Specific Factor) Is Expressed within the Embryonic Mouse Heart during Valve Formation. Mechanisms of Development 2001, 103 (1–2), 183–188. https://doi.org/10.1016/S0925-4773(01)00356-2.
7. Yoshiba, N.; Yoshiba, K.; Hosoya, A.; Saito, M.; Yokoi, T.; Okiji, T.; Amizuka, N.; Ozawa, H. Association of TIMP-2 with Extracellular Matrix Exposed to Mechanical Stress and Its Co-Distribution with Periostin during Mouse Mandible Development. Cell Tissue Res 2007, 330 (1), 133–145. https://doi.org/10.1007/s00441-007-0439-x.
8. Litvin, J.; Selim, A.-H.; Montgomery, M. O.; Lehmann, K.; Rico, M. C.; Devlin, H.; Bednarik, D. P.; Safadi, F. F. Expression and Function of Periostin-Isoforms in Bone. J. Cell. Biochem. 2004, 92 (5), 1044–1061. https://doi.org/10.1002/jcb.20115.
9. Ottewell, P. D. The Role of Osteoblasts in Bone Metastasis. Journal of Bone Oncology 2016, 5 (3), 124–127. https://doi.org/10.1016/j.jbo.2016.03.007.
10. Karsenty, G.; Kronenberg, H. M.; Settembre, C. Genetic Control of Bone Formation. Annu Rev Cell Dev Biol 2009, 25, 629–648. https://doi.org/10.1146/annurev.cellbio.042308.113308.
11. Illien, F.; Rodriguez, N.; Amoura, M.; Joliot, A.; Pallerla, M.; Cribier, S.; Burlina, F.; Sagan, S. Quantitative Fluorescence Spectroscopy and Flow Cytometry Analyses of Cell-Penetrating Peptides Internalization Pathways: Optimization, Pitfalls, Comparison with Mass Spectrometry Quantification. Sci Rep 2016, 6 (1), 36938. https://doi.org/10.1038/srep36938.

Chapter 3: Cell Surface Adhesion Proteins: Viable Therapeutic Targets Which Play an Indirect Role in Cancer Cell Migration and Metastasis in Bone Tissue

3.1 Abstract

Cell surface adhesion proteins have been established to play a vital role in EMT transitions facilitating cancer cell spread and metastasis within bone tissue. These proteins are found along the surface of some cancer cells, such as breast cancer and prostate cancers, and these adhesion proteins interact with the adhesion proteins found on the surface of bone cells. Because of the important role they play in cancer progression, we hypothesized that by targeting and decreasing or silencing their expression (specifically N-cadherin) on the cell surface of osteoblast cells cancer migration and metastasis in bone could be prevented. Despite its highly important role and nature in the EMT transition, N-cadherin has not been studied as extensively as E-cadherin, highlighting the reason N-cadherin was chosen as the focus in this research. It was determined that synthesizing siRNAS encoding for cell surface adhesion proteins was successful and that they could be purified using HPLC, although desired concentration was difficult to reach as well as tedious and impractical when done in lab. Furthermore, the synthesized siRNAs and peptides were successfully complexed at low ratios to one another and exhibited good stability in serum. TEM and DLS data indicated that the complexes formed aggregates, although interestingly the FITC-Ahx-R_{12}:siRNA sample as well as the FITC-Ahx-SDSSD-AHx-R_9:siRNA sample showed the least amount of aggregation overall and the N-cadherin duplex exhibited the highest stability of all samples tested, with a zeta potential of -21.3. All samples also had Pdl values below 0.5, indicating their structures were well-defined in size. In addition to these results, the complexes were also stable and resisted denaturation when tested with a denaturing

PAGE gel. Furthermore, after running an FBS stability assay, the complexes exhibited higher stability than the peptide controls, indicating once again that the complexes themselves were highly stable when in the presence of serum. This indicated that the complexes would be able to withstand incubation periods in cell growth media, and bind to osteoblast cells, as intended. Finally, the heparin displacement assay indicated a very strong interaction between the peptide and siRNA. Ideally, for RNAi to take place within the cell, the siRNA must release from the peptide. Because of the strongly bound siRNA to the peptides, the likelihood of this taking place was significantly lowered, indicating that this delivery method would potentially not be the best for inducing RNAi within the osteoblast cells.

3.2 Introduction

Cell surface adhesion proteins have been established to play a vital role in cancer cell spread and metastasis with bone tissue. Many cell surface adhesion proteins have been studied in depth, particularly E-cadherin and its role in cancers has been highlighted extensively. Both E-cadherin and n-cadherin play a synergistic role in enabling cancer cell spread and metastasis and maintaining their normal levels is crucial in ensuring effective cancer treatment as well as increasing survival rates among patients. Specifically, these proteins play a major role in the EMT transition, and "N-cadherin is upregulated while E-cadherin is downregulated during EMT in cancers and this "cadherin switch" is associated with enhanced migratory and invasive traits, which caused inferior patient survival rate."[1-4] Furthermore, of particular interest is n-cadherin for the role it plays in various cancers, as well as the lack of research surrounding this protein when compared to E-cadherin. "N-cadherin promotes tumor cell survival, migration and invasion, and a high level of its expression is often associated with poor prognosis. N-cadherin is

also expressed in endothelial cells and plays an essential role in the maturation and stabilization of normal vessels and tumor-associated angiogenic vessels."[5]

3.3 Chapter Objectives

This thesis chapter aims to highlight the viability of targeting cell-surface adhesion proteins as therapeutic targets in the treatment of cancers. It also aims to investigate the success of synthesizing siRNA in the lab and whether in-lab synthesis yields sufficient siRNA for cell studies. The characterization of siRNA will also be investigated through HPLC and UV-spectroscopy to determine a profile for synthesized siRNA. Cell-targeting peptides have shown promise in being used as drug delivery agents and in this chapter, we show the ability of the SDSSD polyarginine peptide to complex to siRNA encoding for n-cadherin. NATIVE Page, FBS stability assays and heparin displacement assays, and denaturing PAGE gels have shown that the SDSSD polyarginine peptide binds successfully and tightly to siRNA encoding for n-cadherin and exhibits high stability. High-performance liquid chromatography yielded clean traces of each siRNA sequence synthesized as well, highlighting the ease of in-lab synthesis using the gene synthesizer.

3.4 Results and Discussion

3.4.1 Synthesis and Characterization of siRNA For Cell Surface Adhesion Proteins

In order to generate the following siRNA sequences, the gene synthesizer was used. Each sequence encodes for a cell surface adhesion protein. The sequence used for synthesis is shown in Table 3.1 and lists the identity of each adhesion protein's siRNA sense strand sequence from the 5'→3' direction. To make the antisense strands, complementary sequences were made based off the sequences listed below.

siRNA Sequence Name	Sequence (5'→3') Sense Strand
β-catenin	CATGUGUTGGUAAGCUCUA
FN-siRNA	AAC TTC AAA TTA TGA ACA AGA
N-cadherin	CUAACAGGGAGUCAUAUGGUGGAGC-TdT

Table 3.1: siRNA sequences synthesized in the lab by substituting Thymine base pairs for Uracil base pairs. Overhang sequence TdT was kept on N-cadherin using Thymine. All sequences are for various cell surface adhesion proteins. The strand sequence base pairs are shown from the 5'→3' direction. The antisense strand was synthesized complementary to the sense strand.

Sample Name	Dilution Factor[1]	Λ-max (nm)[2]	Absorbance[3]	O.D. (Abs. x Dilution)[4]	Concentration (O.D./Extinction coefficient)[5]
N-cadherin Anti	100	260	0.39	39	1.46×10^{-4}
N-cadherin Sense	100	260	0.30	30	1.12×10^{-4}
β-catenin Anti	10	260	0.49	4.9	2.62×10^{-5}
β-catenin Sense	10	260	0.47	4.7	2.69×10^{-5}
Fibronectin Anti	10	260	0.42	4.2	2.23×10^{-5}
Fibronectin Sense	10	260	0.45	4.5	2.07×10^{-5}

[1]The dilution factors used correspond to the amount of siRNA in ddH_20 tested on the UV-spectrometer. All sample volumes equaled 1 mL
[2]A maximum absorbance at 260 nm was measured, corresponding to the λ_{max} of RNA
[3]Absorbance values listed correspond to the absorbance at 260 nm for each sample
[4]Optical Density values for each sample measured by multiplying the absorbance at 260 nm by the dilution factor value
[5]Final concentrations of pure siRNA samples obtained by dividing the optical density by the extinction coefficient for each siRNA sample synthesized

Table 3.2: RNA Characterization table for all sequences synthesized. Reported values are unique to each sequence.

Following the determination of the correct sense strand sequence for each desired siRNA sequence, the sequences were synthesized using the ABI 3400 DNA synthesizer, and sample specifications were documented in a characterization table. The dilution factor of pure RNA tested in RNase free H_2O was used to determine each sample O.D. value, absorbance, and concentration of collected pure RNA. The yields and O.D. values for synthesized RNA were lower than desirable except for the n-cadherin sequence. Even with low yields, based on the representative HPLC traces as well as the characterization tables, it was determined that

synthesizing siRNA in the lab was a viable option for acquiring siRNAs, but the scale did not allow for a sufficient amount of pure sample to solely rely upon lab made siRNA for testing.

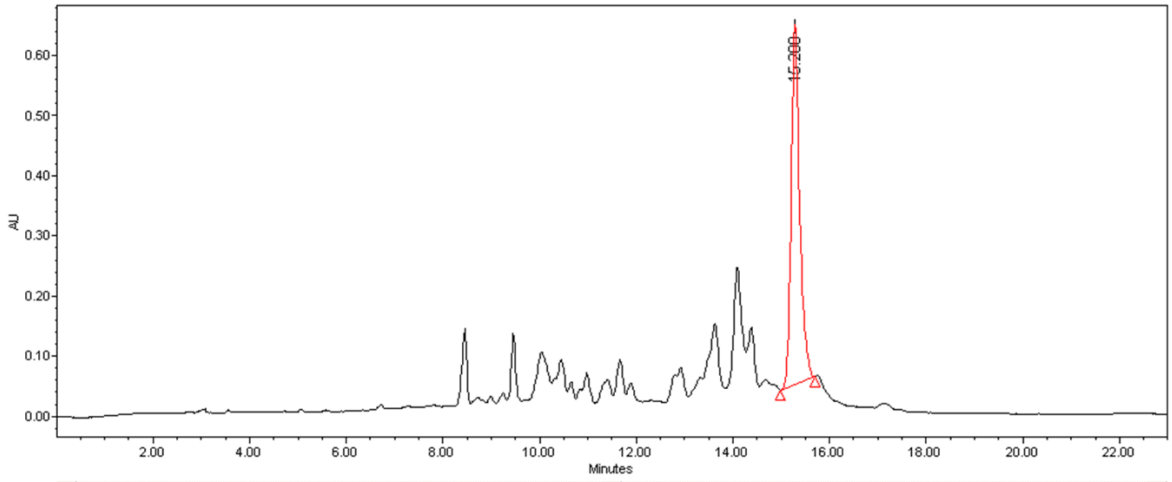

Figure 3.1: Crude HPLC trace for n-cadherin antisense siRNA synthesized using the gene synthesizer. Peaks before the highlighted peak are characteristic failure sequences. Reverse phase chromatography was used on a Symmetry C18 4.6 x 250 mm column with two solvents. Solvent A was 0.1 M TEAA, pH=7 and Solvent B was 0.1 M TEAA/20% Acetonitrile, pH=7. The gradient used was 40 to 60 Acetonitrile over 23 minutes.

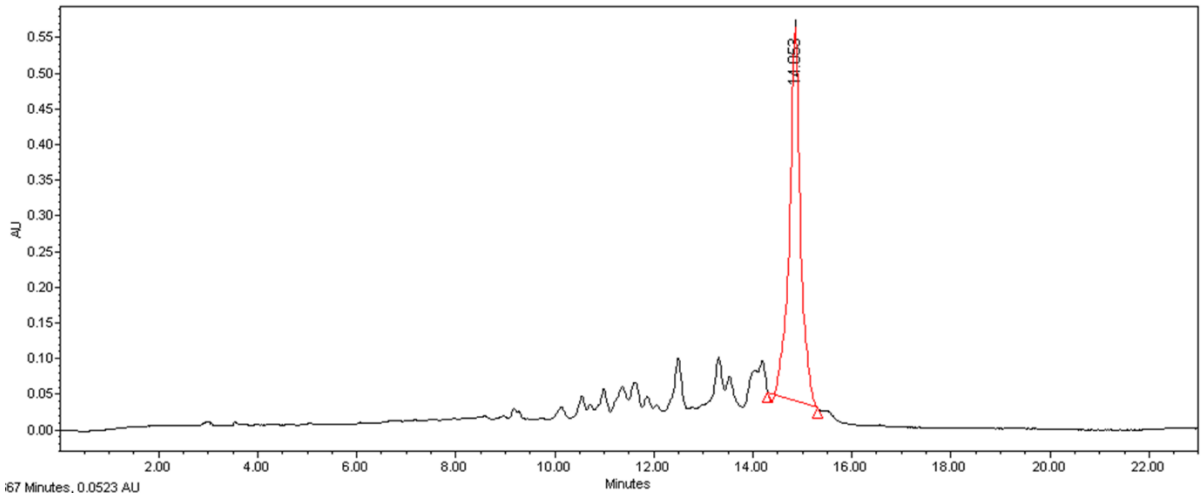

Figure 3.2: Crude HPLC trace of n-cadherin sense strand using the gene synthesizer. Peaks before the highlighted peak are characteristic failure sequences. Reverse phase chromatography was used on a Symmetry C18 4.6 x 250 mm column with two solvents. Solvent A was 0.1 M TEAA, pH=7 and Solvent B was 0.1 M TEAA/20% Acetonitrile, pH=7. The gradient used was 40 to 60 Acetonitrile over 23 minutes.

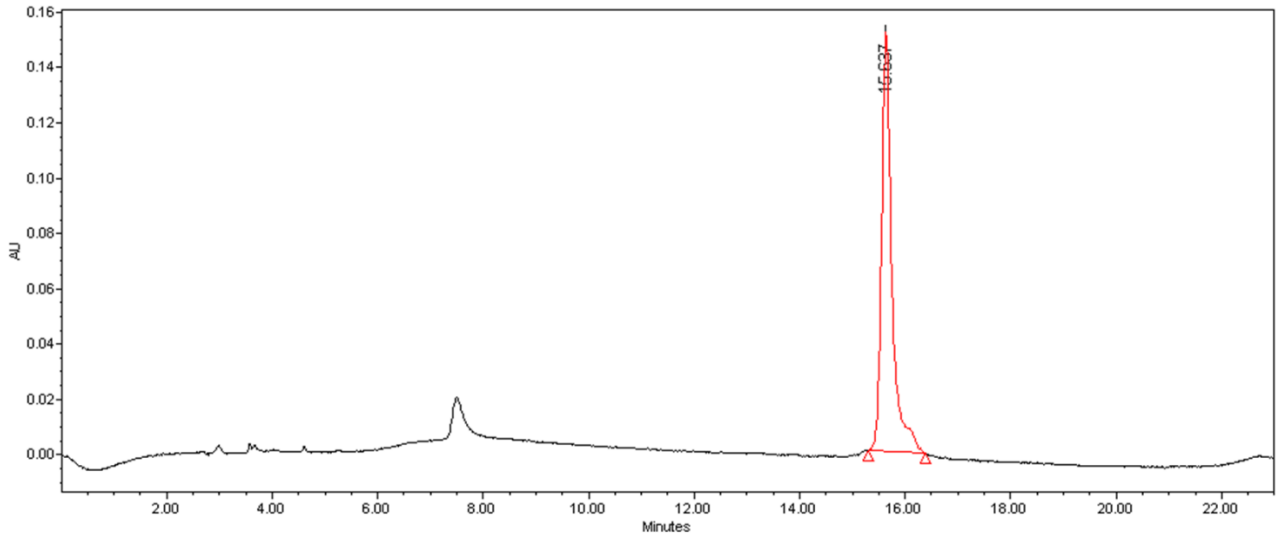

Figure 3.3: Pure HPLC trace of n-cadherin antisense siRNA strand. Highlighted peak indicative of the siRNA. Reverse phase chromatography was used on a Symmetry C18 4.6 x 250 mm column with two solvents. Solvent A was 0.1 M TEAA, pH=7 and Solvent B was 0.1 M TEAA/20% Acetonitrile, pH=7. The gradient used was 40 to 60 Acetonitrile over 23 minutes.

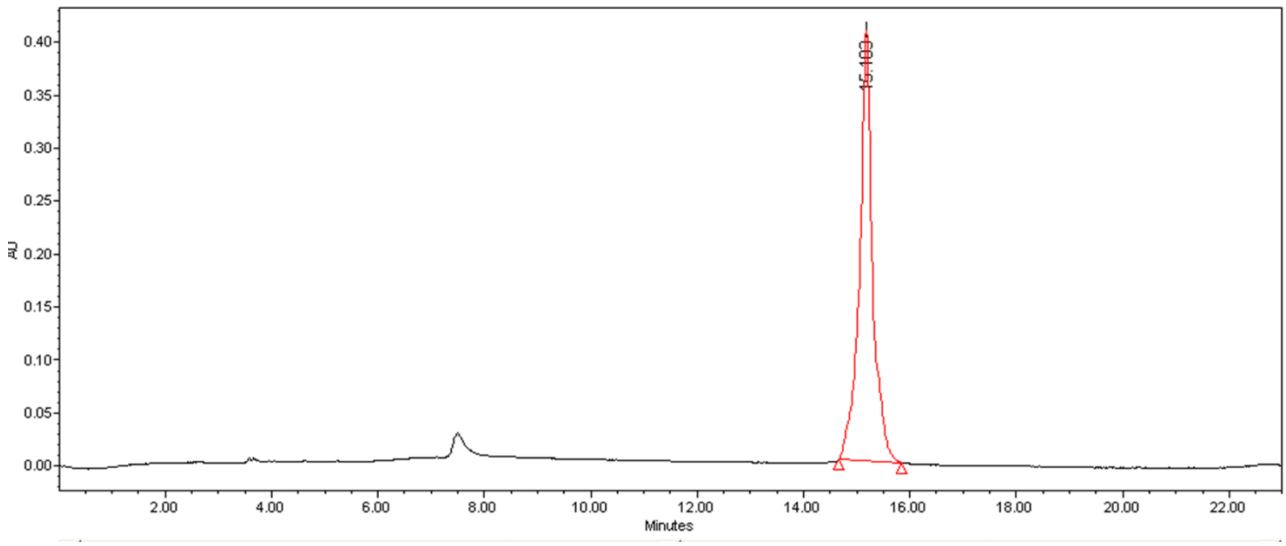

Figure 3.4: Pure HPLC trace of n-cadherin sense strand. Highlighted peak indicative of the siRNA. Reverse phase chromatography was used on a Symmetry C18 4.6 x 250 mm column with two solvents. Solvent A was 0.1 M TEAA, pH=7 and Solvent B was 0.1 M TEAA/20% Acetonitrile, pH=7. The gradient used was 40 to 60 Acetonitrile over 23 minutes.

All synthesized RNA was purified using reverse phase HPLC and C_{18} columns heated to 60°C. Heating of the column during the purification ensured separation of each RNA strand.

Representative HPLC traces for n-cadherin prior to and after purification are shown above in Figures 3.1-3.4 and each HPLC run was done over the course of 23 minutes. Before sample purification, crude samples of the N-cadherin siRNA showed characteristic failure peaks before the elution of the desired sample peak. This was expected and indicative of sequences which failed to form the full n-cadherin sequence during synthesis. After collection of the pure n-cadherin peak, the pure sample was once again run on HPLC to ensure elimination of failure sequences which was successful. Ghost peaks were seen as indicated by the small peak at ~8 minutes after purification most likely from minor sample aggregation or from leftover purifications either in the column itself or within the system, but samples still had sufficient purity for biological applications, indicating the successful collection of the desired sequence.

3.4.2 DLS/TEM Analysis of peptide:siRNA Complexes

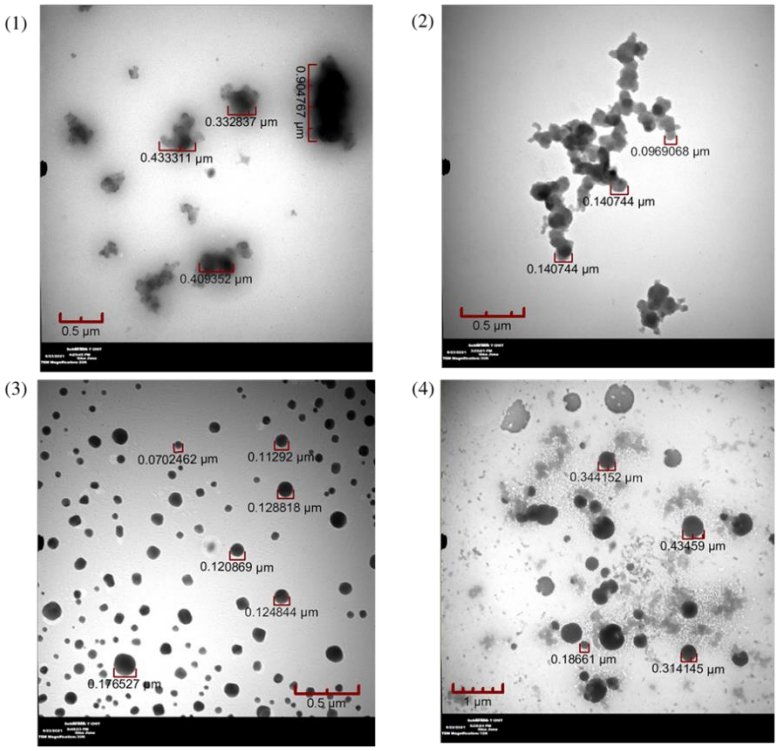

(1): N-cadherin siRNA control
(2): FITC-Ahx-R_9:siRNA
(3): FITC-Ahx-R_{12}:siRNA
(4): FITC-Ahx-SDSSD-Ahx-R_9:siRNA

Sample Name	Average Hydrodynamic Diameter (nm)	Zeta Potential (mV)[1]	Pdl[2]
N-cadherin Control	304	-23.3	0.524
FITC-Ahx-R_9:siRNA	797	-17.4	0.383
FITC-Ahx-R_{12}:siRNA	672	-23.6	0.364
FITC-Ahx-SDSSD-AHx-R_9:siRNA	890	7.33	0.650

[1]The larger the Zeta Potential, the more stable the complex
[2]Pdl is unitless. When Pdl=1, particles have random sizes. When Pdl < 0.5, particles have certain, well-defined sizes

Figure 3.5: TEM images of peptide:siRNA complexes, *courtesy of Jorge Ramos and Uri Samuni, Queens College, CUNY.* Corresponding DLS data pertaining to each sample is shown in Table under TEM images. FITC-Ahx-SDSSD-Ahx-R_{12}:siRNA was not tested to conserve sample, and behavior of FITC-Ahx-SDSSD-Ahx-R_9:siRNA was used a comparison in place of FITC-Ahx-SDSSD-Ahx-R_{12}:siRNA. Size distribution by intensity spectra shown in Appendix.

As shown in Figure 3.5, TEM images of each peptide:siRNA complex were obtained courtesy of Jorge Ramos of Queens College. The images showed aggregation of the complexed particles for both the N-cadherin duplex control sample as well as the FITC-Ahx-R_9:siRNA

sample. Both FITC-Ahx-R_{12}:N-cadherin siRNA and FITC-Ahx-R_9:N-cadherin siRNA showed the least amount of aggregation, and interestingly the FITC-Ahx-R_{12}:N-cadherin siRNA sample showed the smallest observed particle size between the two, despite having a longer polyarginine tail length and not containing the SDSSD peptide portion. Furthermore, the siRNA duplex showed the most aggregation of all four samples and the FITC-Ahx-R_{12}:N-cadherin siRNA showed the least. These two samples also had the most desirable zeta potential values at -23.3 mV and -23.6 mV respectively. Typically, zeta potentials under ±30 mV have tendencies to coagulate or aggregate in solution, and the TEM images confirm this as all zeta potentials were below this threshold. The siRNA control had the highest zeta potential of all four samples indicating it had the highest stability of everything tested and the FITC-Ahx-R_{12}:N-cadherin siRNA sample had the second highest stability. In addition to indicating a particle's stability, the zeta potential also tells us how well or how likely a particle is to interact with a cell membrane. Typically, particles with slightly more positive zeta potentials have a higher likelihood of interacting with cell membranes through electrostatic interactions, as cell membranes have a slight negative charge. As shown by the DLS data table, the zeta potential for the peptide:siRNA formulation was more positive which is favorable as the peptide:siRNA complexes would be interacting with the OSB cell membranes. This aggregation indicates that the complexes could potentially be interacting with one another in solution, and this may serve as a complicating factor when exposing the complexes to osteoblast cell populations. The aggregation observed could hinder the ability of the complexes to be internalized by the osteoblast cells.

3.4.3 siRNA successfully Complexes to synthesized OSB-targeting Peptide

To determine the ability and proper concentration of peptide to siRNA to form a complex, NATIVE PAGE gels were run using varying ratios of peptide to siRNA. The RNA

control was prepared in a ratio of 1:1 for equimolar concentrations of the sense and antisense strand to form an RNA duplex. Each synthesized peptide sequence (FITC-Ahx-SDSSD-Ahx-R_9, FITC-Ahx-SDSSD-Ahx-R_{12}, FITC-Ahx-R_9, and FITC-Ahx-R_{12}) were run in increasing ratios as follows: 0.1:1, 1:1, 5:1, and 10:1. The siRNA concentrations were held constant at a mole ratio of 1. Prior to running the gel, all complexes were annealed using Annealing Buffer (10 mM TRIS, 50 mM NaCl, 1 mM EDTA pH=7). The gel was stained using STAINS-ALL (25 mg Alfa Aesar Stains-All Powder®, 50 mL isopropyl alcohol, 25 mL formamide, 125 mL water) which only binds to free, unbound RNA. This was used to detect any unbound RNA which would indicate unsuccessful complexation to peptide. As was indicated by the gel, the free siRNA was successfully detected by the STAINS-ALL, and at 0.1:1 free siRNA was also detected. At a ratio of 1:1, 5:1, and 10:1 no free RNA was detected indicating that from a ratio of 1:1 and higher, the peptide and siRNA successfully complexed. Using the lowest working concentration of peptide to siRNA (1:1) was used to form and test complexes in the following gels.

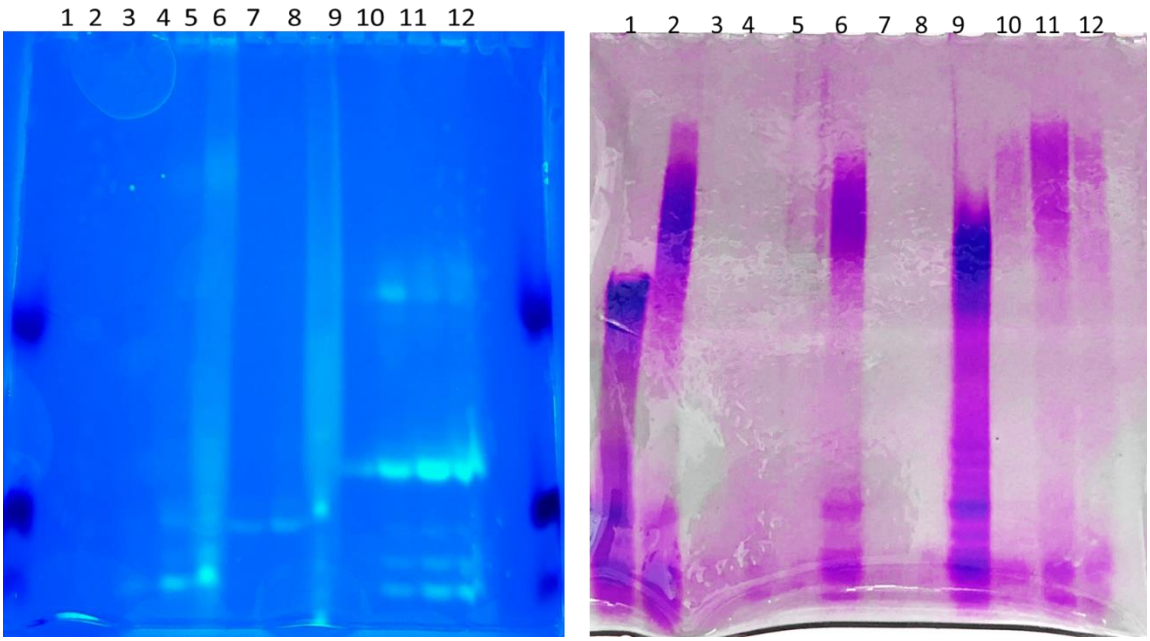

Figure 3.6: Side by side comparison of Native PAGE gel imaged under UV light vs same gel after incubation with STAINS-ALL and photobleaching. STAINS-ALL (25mg Alfa Aesar Stains-All Powder®, 50 mL isopropyl alcohol, 25 mL formamide, 125 mL water) used to stain gel to detect free, unbound siRNA. UV light used to detect presence of FITC labeled peptide.

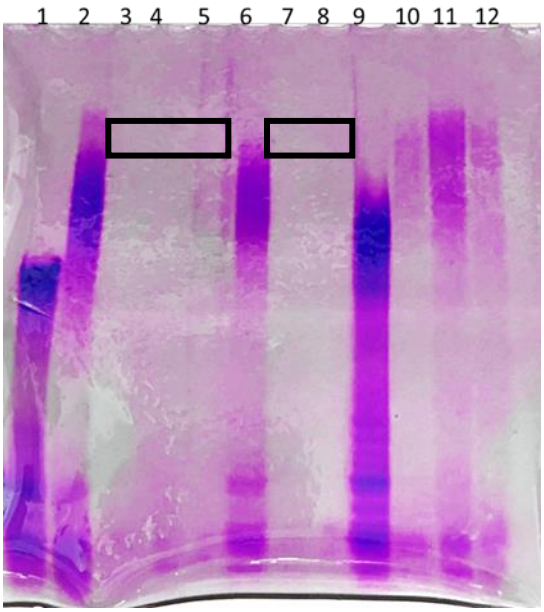

Lane #	Sample	Peptide:siRNA ratio
1	RNA control	1:1
2	FITC-Ahx-SDSSD-Ahx-R_9	0.1:1
3	FITC-Ahx-SDSSD-Ahx-R_9	1:1
4	FITC-Ahx-SDSSD-Ahx-R_9	5:1
5	FITC-Ahx-SDSSD-Ahx-R_9	10:1
6	FITC-Ahx-SDSSD-Ahx-R_{12}	0.1:1
7	FITC-Ahx-SDSSD-Ahx-R_{12}	1:1
8	FITC-Ahx-SDSSD-Ahx-R_{12}	5:1
9	FITC-Ahx-R_9 control	0.1:1
10	FITC-Ahx-R_9 control	1:1
11	FITC-Ahx-R_9 control	5:1
12	FITC-Ahx-R_9 control	10:1

Figure 3.7: Native PAGE gel after photobleaching. Lane numbers and corresponding sample is listed in the table with each peptide to siRNA ratio. Boxed portions of gel show the lack of bands, indicating lack of free siRNA and successful complexation.

3.4.4 Peptide:siRNA complexes Exhibit Desirable Stability

The denaturing PAGE gel was run to test peptide stability as well as RNA stability under denaturing conditions. The gel was prepared by using a 7 M urea concentration to encourage the peptides to denature. Each sample was also incubated with FBS and collected at various time points (0, 2, 6, and 24 hour) over the course of a day. As was shown by the gel (Figure 3.8 and 3.9), the free RNA was picked up by the STAINS-ALL (Lanes 3-6) indicating its in-tact presence over the full course of 24 hours, which was surprising. The absence of bands on the gel for the peptide:siRNA complexes indicated that the complexes interacted strongly and did not disassemble under denaturing conditions, until roughly 6-24 hours later. The peptide controls seemed to slightly less stability than the FITC-Ahx-SDSSD-Ahx-R_9:siRNA sample, indicating that the SDSSD portion may be less susceptible to degradation when exposed to a cellular environment. This would be desirable as the peptide would need to remain intact until taken into the osteoblast cells, and eventual degradation of the peptide once inside the cell would help release siRNA into the cell to induce RNAi and silence expression of N-cadherin. These results indicated that when exposed to denaturing or harsh conditions, the complexes themselves would retain their integrity fairly well and function well in a cellular environment to deliver siRNA to the osteoblast cells, but after about 24 hours, the siRNA should be released within the cells.

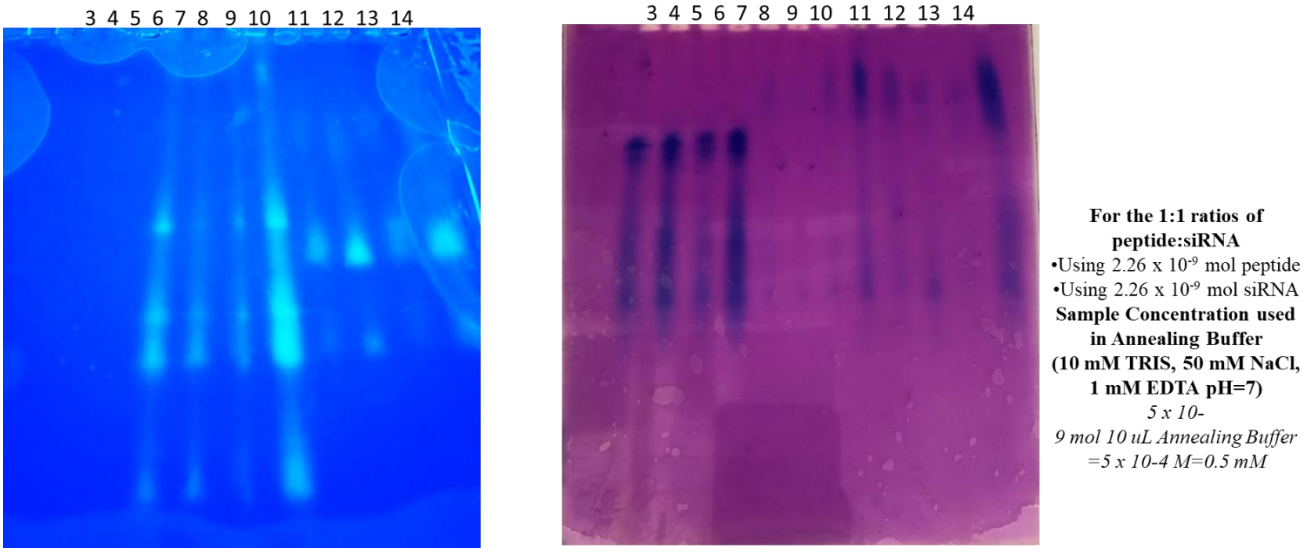

Figure 3.8: Denaturing PAGE gels side by side. Gel image on left represents the gel under UV light, to detect the FITC labeled peptides. Lanes 3-6 show no fluorescence as they are only siRNA samples. The gel image on the right represents the same gel after staining with STAINS-ALL. Conditions listed next to the gels. Each sample was done with 1:1 peptide to siRNA ratios. Sample aggregation likely caused multiple peptide bands when visualized under UV light.

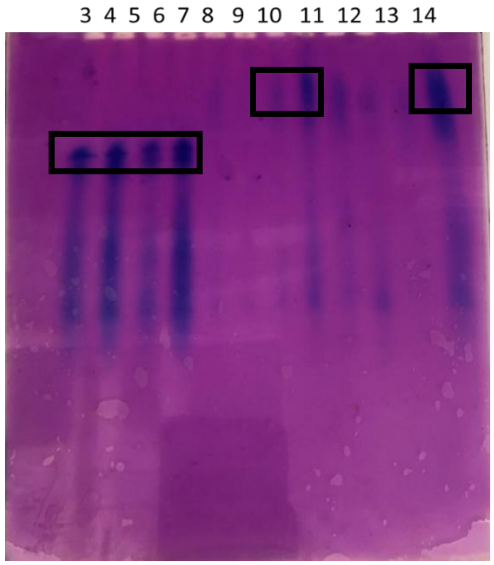

Lane #	Sample	Peptide:siRNA Ratio	Time point collection (hours)
3	RNA control	1:1	0
4	RNA control	1:1	2
5	RNA control	1:1	6
6	RNA control	1:1	24
7	FITC-Ahx-SDSSD-Ahx-R_9	1:1	0
8	FITC-Ahx-SDSSD-Ahx-R_9	1:1	2
9	FITC-Ahx-SDSSD-Ahx-R_9	1:1	6
10	FITC-Ahx-SDSSD-Ahx-R_9	1:1	24
11	FITC-Ahx-R_9	1:1	0
12	FITC-Ahx-R_9	1:1	2
13	FITC-Ahx-R_9	1:1	6
14	FITC-Ahx-R_9	1:1	24

Figure 3.9: Denaturing PAGE gel. Conditions listed next to the gels. Each sample was done with 1:1 peptide to siRNA ratios. Boxed region shows annealed siRNA (sense + antisense strands) detectable at 0, 2, 6 and 24 hours.

To further examine the stability of the complexed samples consisting of a 1:1 ratio of peptide to siRNA were run using a PAGE gel, and incubating samples collected at various time points with FBS (Figures 3.10-3.11). The samples were incubated in FBS and collected at various timepoints of 0 hours, 2 hours, 6 hours, and 24 hours. Following collection, the samples were placed at -80 to stop any further reactions. After samples were collected, they were run on a PAGE gel and stained with STAINS-ALL. Lanes 9 and 10 of the gel (Figure 3.9) indicated that by the 6 hour time point free RNA was beginning to be detected by the STAINS-ALL and by 24 hours, free RNA was detected more strongly, indicating the release of more RNA from the complex. Free RNA was only stable at the 0-hour time point but following that it was no longer detected on the gel. The complexations were also stable at all time points and no bands were detectable on the gel, indicating that the complexes themselves would be stable within serum or a cellular environment, or when exposed to potentially denaturing conditions. The FITC-Ahx-SDSSD-Ahx-R_9 peptide was tested because of excess sample availability, and because its sample identity is so similar to the FITC-Ahx-SDSSD-Ahx-R_{12} peptide, it was assumed that it would behave in a similar way. Furthermore, it was believed that because the FITC-Ahx-SDSSD-Ahx-R_9 peptide has three less arginine residues than the FITC-Ahx-SDSSD-Ahx-R_{12} peptide, it would potentially bind less tightly to the siRNA and exhibit lower stability. Since this was not the observed case, it was determined that the results were satisfactory in regard to the stability profile of the peptide and could be assumed to be the same for the FITC-Ahx-SDSSD-Ahx-R_{12} peptide. UV imaging confirmed sample presence through FITC fluorescence, and as shown by the gel, the free RNA was stable when collected immediately or at 2 hours (indicated by presence of faint band) but degraded past the 2-hour time point. No RNA was detected when complexed to the peptides and showed consistent stability over the 24-hour time period,

indicating that the peptides would be stable when exposed to serum, or in a cellular environment. These results are illustrated in the above and below in Figures 3.9-3.11.

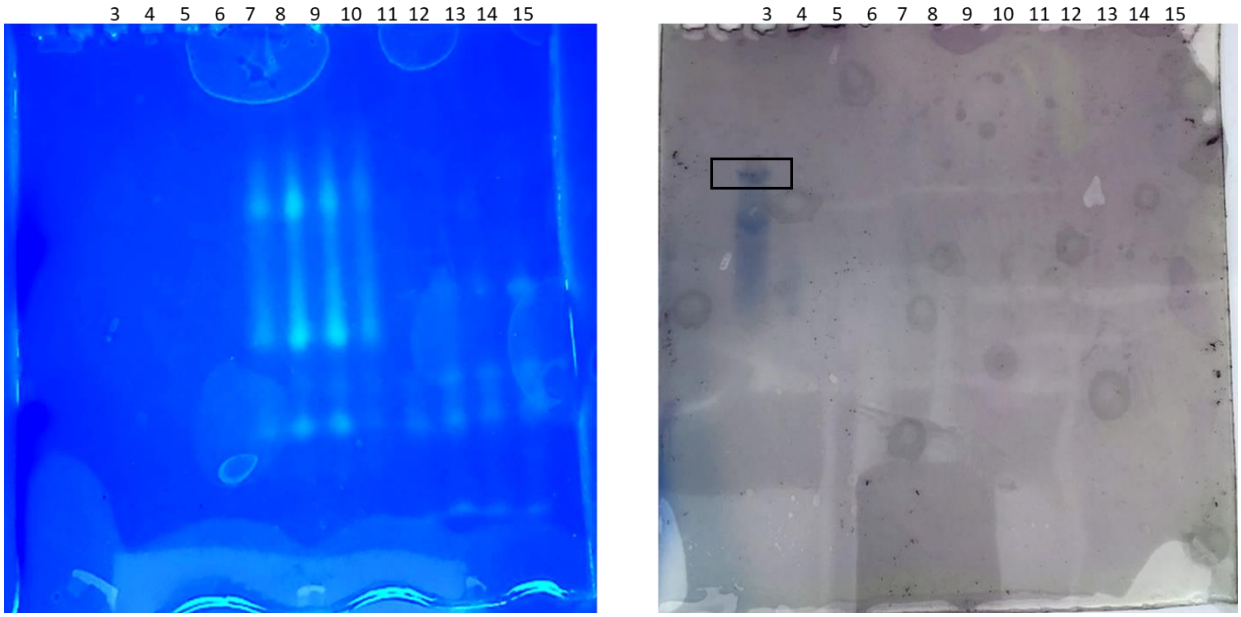

Figure 3.10: FBS Stability assay gels side by side under UV light and after photobleaching. UV light used to image gels to detect FITC labeled peptide presence as a confirmation its presence. FBS stability assay run over 24-hour period with time point collections at 2 hours, 6 hours, and 24 hours. Sample aggregation likely caused multiple peptide bands when visualized under UV light.

Lane #	Sample	Peptide:siRNA	Time Point collection (hr)
3	RNA control (n-cad)	1:1	0
4	RNA control (n-cad)	1:1	2
5	RNA control (n-cad)	1:1	6
6	RNA control (n-cad)	1:1	24
7	FITC-Ahx-R_9	1:1	0
8	FITC-Ahx-R_9	1:1	2
9	FITC-Ahx-R_9	1:1	6
10	FITC-Ahx-R_9	1:1	24
11	FITC-Ahx-SDSSD-Ahx-R_9	1:1	0
12	FITC-Ahx-SDSSD-Ahx-R_9	1:1	2
13	FITC-Ahx-SDSSD-Ahx-R_9	1:1	6
14	FITC-Ahx-SDSSD-Ahx-R_9	1:1	24

Figure 3.11: FBS stability assay run over 24-hour period with time point collections at 2 hours, 6 hours, and 24 hours. Boxed region of the gel indicates the 0-hour time point collection where the duplexed RNA was still stable, indicated by the band on the gel after STAINS-ALL.

As briefly stated above, the FBS stability assay was used to determine how stable the complexations would be when exposed to cell growth media which contains serum, as shown by the gel in Figure 3.11 only free RNA was detectable at the 0-hour time point. Past that at 2, 6 and 24 hours no free RNA was detectable. The peptide controls which consisted of only the polyarginine sequence did not degrade in the presence of serum, and neither did the peptide:siRNA formulations containing the periostin targeting portion (SDSSD). This was expected as the siRNA is interacting with the polyarginine tails and both control and peptide containing the periostin binding region both exhibited high stability in serum, as indicated by the presence of no free RNA bands. These results were significant because this indicated that RNA interference experiments could be carried out to completion successfully, and that the complexes would be stable enough in the cell culture media to bind to the cells and be internalized by them. Figure 3.10 is the FBS stability assay gel under UV light to confirm that each lane without bands

did in fact contain peptide complexes. This confirmed that the lack of bands was not due to poor sample loading or loss of sample from the wells in the gel, but rather positive results.

Finally, the heparin displacement assay was performed to test how easily the siRNA would be released from the polyarginine tail of the peptide within a cellular environment. Heparin was incubated with the complexes at various ratios of heparin to peptide, ranging from 0.1 to 10. The RNA control was not incubated with heparin as it was used to test for successful free RNA presence. Bands of free RNA were detected for the peptide controls beginning at a heparin:peptide ratios of 0.1:1 and 1:1. In addition, faint bands for the peptide complexes with RNA were also seen at a ratio of 5:1 and 10:1 for heparin to peptide:siRNA complex (as seen on gel prior to photobleaching and after photobleaching), indicating that higher concentrations of heparin were more successful at releasing bound RNA than lower concentrations. These results indicated that the RNA bound quite tightly to the peptide but could still be released. This showed that the potential for release of the RNA could occur. These results are summarized in Figure 3.12-3.13.

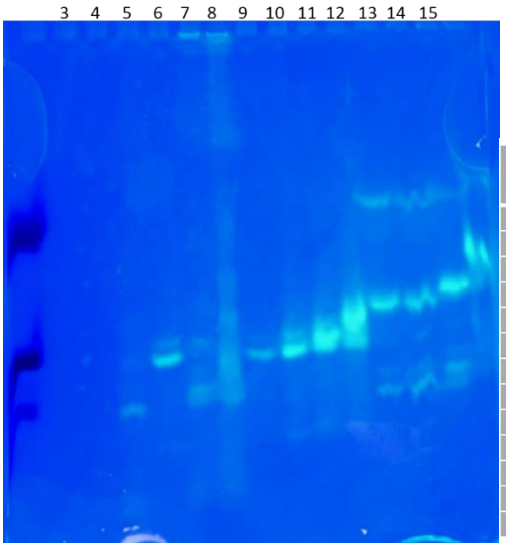

Lane #	Sample	Peptide:siRNA ratio	Heparin Ratio
3	RNA control	1:1	N/A
4	FITC-Ahx-SDSSD-Ahx-R_9	1:1	0.1
5	FITC-Ahx-SDSSD-Ahx-R_9	1:1	1
6	FITC-Ahx-SDSSD-Ahx-R_9	1:1	5
7	FITC-Ahx-SDSSD-Ahx-R_9	1:1	10
8	FITC-Ahx-SDSSD-Ahx-R_{12}	1:1	0.1
9	FITC-Ahx-SDSSD-Ahx-R_{12}	1:1	1
10	FITC-Ahx-SDSSD-Ahx-R_{12}	1:1	5
11	FITC-Ahx-R_9 control	1:1	10
12	FITC-Ahx-R_9 control	1:1	0.1
13	FITC-Ahx-R_9 control	1:1	1
14	FITC-Ahx-R_9 control	1:1	5
15	FITC-Ahx-R_9 control	1:1	10

Figure 3.12: Heparin Displacement Assay imaged under UV light to confirm presence of fluorescently labeled peptide. This ensured peptide:siRNA complex was successfully loaded into each well. Fluorescent bands indicate the presence of peptide on the gel and in each sample, except for lane 3, which only contained siRNA, and no FITC tagged peptide. Sample aggregation likely caused multiple peptide bands when visualized under UV light.

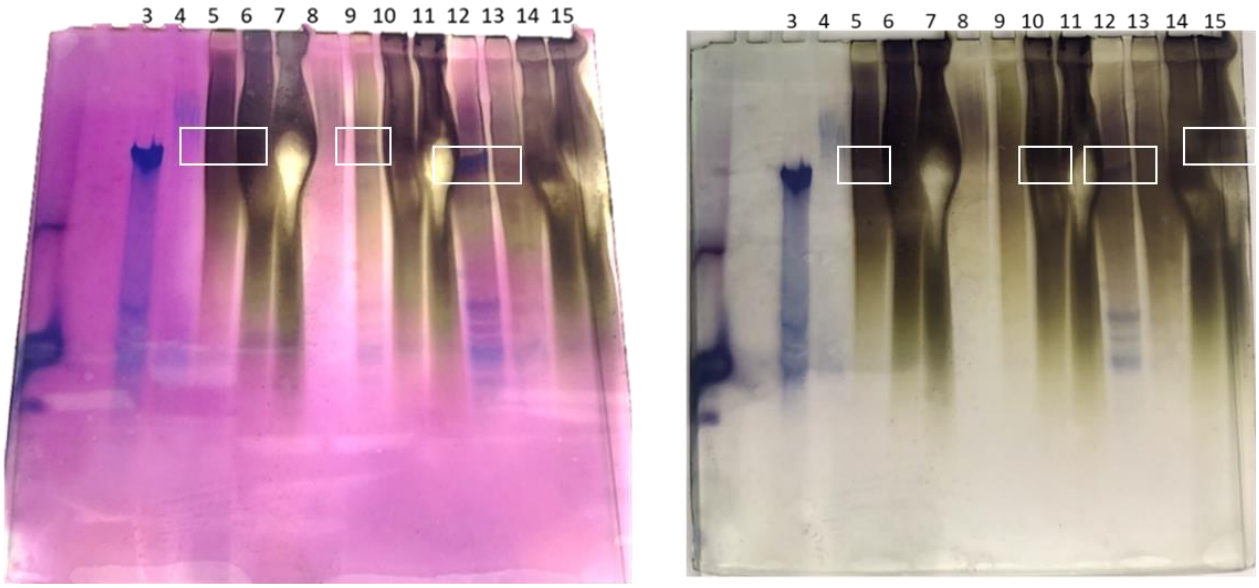

Lane #	Sample	Peptide:siRNA ratio	Heparin Ratio
3	RNA control	1:1	N/A
4	FITC-Ahx-SDSSD-Ahx-R_9	1:1	0.1
5	FITC-Ahx-SDSSD-Ahx-R_9	1:1	1
6	FITC-Ahx-SDSSD-Ahx-R_9	1:1	5
7	FITC-Ahx-SDSSD-Ahx-R_9	1:1	10
8	FITC-Ahx-SDSSD-Ahx-R_{12}	1:1	0.1
9	FITC-Ahx-SDSSD-Ahx-R_{12}	1:1	1
10	FITC-Ahx-SDSSD-Ahx-R_{12}	1:1	5
11	FITC-Ahx-R_9 control	1:1	10
12	FITC-Ahx-R_9 control	1:1	0.1
13	FITC-Ahx-R_9 control	1:1	1
14	FITC-Ahx-R_9 control	1:1	5
15	FITC-Ahx-R_9 control	1:1	10

Figure 3.13: Heparin Displacement assay gels. Leftmost gel is imaged immediately after STAINS-ALL and rightmost gel is the same gel after photobleaching. Boxed regions of the gel indicate bands showing presence of free RNA.

3.5 Conclusions

Based on the previous results, it was concluded that the complexation of the peptides to siRNA could be achieved at low stoichiometric ratios to one another. Equimolar concentrations of each were required to form a complex, and the complexes exhibited desirable and surprising stability. When the peptide:siRNA complexes were tested on a denaturing gel the complexes

remained stable at all time points tested. The control peptide used was the FITC-Ahx-R_9 as a basis for the behavior of both the FITC-Ahx-R_9 and the FITC-Ahx-R_{12} peptides, since the difference in quantity of arginine only differed by 3 residues. The control peptide which consisted of only arginine and a linker exhibited less stability, indicating that the osteoblast-targeting portion of the peptide (SDSSD) seemed to impart higher stability to the complex. Furthermore, based on the FBS stability assay, indicated that when exposed to serum, the peptide:siRNA complexes showed high stability. This led us to believe that these complexes would retain their integrity when used in cell culture assays, and when exposed to a cellular environment as well as growth serum, which would be necessary to successfully carry out RNA interference experiments. Finally, the heparin displacement assay indicated that the RNA could be displaced from the peptide. At higher concentrations of heparin (5:1 and 10:1) for example, heparin was more successful at displacing the bound RNA, but some faint bands were detected in some cases at low concentrations, such as 0.1:1 (heparin:peptide) indicating successful release of the RNA. The successful release of the RNA from the peptide through Heparin and its stability within serum both indicated that the complexes had the potential to be successful when used in RNA interference experiments to decrease expression of N-cadherin. In addition to the information provided by the gels, the TEM results showed the aggregation of the peptide:siRNA complexes as well as larger than desired particle size. Ideally, in order for particles to penetrate cell membranes readily they should be around 27-30 nm in size, or 0.027-0.03 μm.[6] Larger particles on the scale of 70-240 nm in size exhibit less efficient cell uptake, than their smaller counterparts.[7] Smaller nanoparticles or small molecules ranging from 30-50 nm interact best with cell membrane receptors and are taken into the cell typically through receptor-mediated endocytosis.[7] According to the TEM images, the complexes exceed the desired size for cell

entry. This coupled with the results of the gels indicate that in addition to the strongly bound siRNA to the Arginine tails and difficulty dissociating the complexes that the peptides may not be taken into the cells successfully and as a result may not be able to deliver the siRNA to induce n-cadherin silencing within the osteoblast cells.

3.6 Materials and Methods

3.6.1 Automated RNA Synthesis

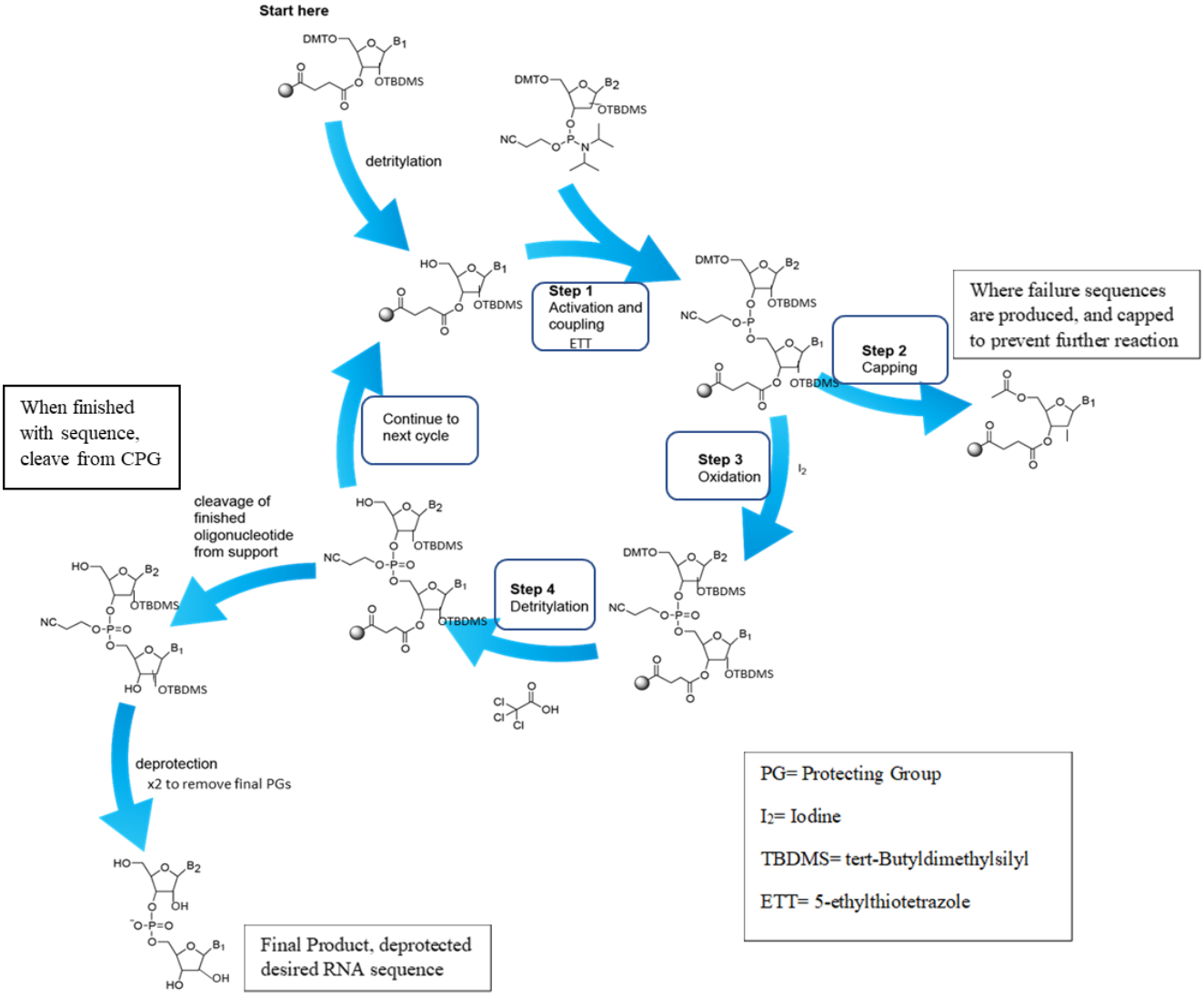

Scheme 3.1: Oligonucleotide Synthesis, adapted from https://www.atdbio.com/content/17/Solid-phase-oligonucleotide-synthesis

Solid-phase automated oligonucleotide synthesis was performed using the ABI 3400 DNA synthesizer, using the ChemGenes 2000 Å, UnyLinker Molecule long alkyl-chain alkyl amine-controlled pore glass (CPG) support on a 1 μmol scale. All phosphonamidites used were from ChemGenes and performed on a 0.15 mol/L scale. To account for loss of phosphonamidites during the synthesis cycle, an extra 6-8 bases for each phosphonamidite were included in calculations. Each base was dissolved in acetonitrile. Each coupling lasted for 5 minutes with 0.25 M 5-ethylthiotetrazole (ETT) as the activating agent in acetonitrile. Each detritylation step lasted for 2 minutes and performed with 3% dichloroacetic acid in dichloromethane. Capping was performed using acetic anhydride/N-methyl imidazole in acetonitrile. Oxidation steps were performed using a 0.01 M iodine in pyridine/THF/H_2O solution. After completion of the synthesis, samples were cleaved from the solid support using NH_4OH:EtOH (3:1 v/v) at 56°C overnight. Following the cleavage step, samples were centrifuged and dried on the Speedvac for roughly 5 hours, until dry. Then samples were stored in the freezer at -80°C. RNA samples were then quantified using UV Spectroscopy by adding 1 mL of autoclaved RNase-free H_2O, centrifuging down the solid support, and extracting the H_2O to test. Finally, to perform the detritylation step, each sample was dried down and the pellet was dissolved in 100 μL of DMSO + 125 μL of triethylamine trihydrofluoride and this was mixed by pipetting. Samples were placed on the heat block at 65°C for 2 hours, then removed, spun down and 25 μL of 3 M sodium acetate in H2O was added with 1 mL of n-butanol. From here, the RNA precipitate was vortexed and stored on dry ice for 15-20 minutes. Samples were once again spun down, the supernatant was removed and the RNA pellet was re-dissolved in 1 mL of RNase-free H2O. Once again, samples were quantified using UV spectroscopy. All samples were purified and analyzed using a Waters symmetry RP C18 reverse-phase column (4.6 x 250 mm, 5.0 μm particle size) heated at

60 °C. HPLC on all RNA samples used two solvents: solvent A was 0.1 M TEAA, pH=7 and Solvent B was 0.1 M TEAA/20% Acetonitrile, pH=7. The gradient used was 40 to 60 Acetonitrile over 23 minutes. The flow rate was 1 mL/min and samples were detected at an absorbance of 260 nm.

3.6.2 UV Spectroscopy

To perform UV-spectroscopy the CARY 3E UV-Vis spectrophotometer was used at a wavelength of 260 nm. Absorption measurements were recorded over a range of 190-300 nm. The maximum wavelength was noted at this value and the dilution factor for each tested sample was multiplied but the absorbance to obtain the optical density (O.D.) value for each sample. This value was then used to calculate the number of moles of each RNA strand, and this was used to obtain equimolar quantities of peptide when creating the complex.

3.6.3 High Performance Liquid Chromatography

Reverse Phase High Performance Liquid Chromatography was used to purify crude stocks of RNA samples using a Waters Symmetry C18 4.6 x 250 mm column heated to 60°C with two solvents. Solvent A was 0.1 M TEAA, pH=7 and Solvent B was 0.1 M TEAA/20% Acetonitrile, pH=7. The gradient used was 40 to 60 Acetonitrile over 23 minutes. All purifications were performed on a Waters 2695 Separations Module using a Waters 2998 Photodiode Array Detector at a wavelength of 260 nm.

3.6.4 Annealing of siRNA:peptide Particles

When annealing the complexes, equimolar quantities of both peptide and RNA were combined in a sterile Eppendorf tube. These tubes were then placed to dry on the Savant Automated Environmental SpeedVac® System AES2010 SpeedVac until dry. Once dried, 50 µL of Annealing Buffer (10 mM TRIS, 50 mM NaCl, 1 mM EDTA, pH=7) was added to each

sample and the samples were then incubated on the heat block (VWR Scientific Standard Heatblock) at 37°C for 30 minutes. Samples were removed from heat and centrifuged for about 1 minute then stored at -80°C until used.

3.6.5 DLS/TEM

Dynamic Light Scattering was performed on complexes after annealing equimolar quantities of peptide and siRNA, following the procedure for complex annealing using Annealing Buffer (10 mM TRIS, 50 mM NaCl, 1 mM EDTA, pH=7). These were then dissolved in RNAse-free water and sent for image analysis on ice. To determine particle size of the complexes, zeta potentials and size distributions, a Malvern Zetasizer, Nano-ZS (Malvern Instruments, UK) was used with a 173° scattering angle and a 4 mW incident He-Ne laser at 633 nm. Samples were measured at 25°C onto folded capillary cells which were equipped with electrodes on both sides. TEM analysis of the complexations was performed using a JEOL 1200EX Transmission Electron Microscope (JEOL Ltd., Japan) at an accelerating voltage of 80 kV. A TEM carbon-film-coated copper grid of 300 mesh was loaded with 10µL of a 1:1 volume ratio of desired sample (complex) and 1% uranyl acetate. Samples sat for 5 minutes on the grid, then excess moisture was wicked off of them. They were then stored for 1 week to allow for sufficient drying before imaging with a Scientific Instruments and Applications Inc. SIA-L3C CCD camera, using the Maxim DL5 software from Diffraction Limited, Ottawa, Canada.

3.6.6 Native PAGE Gel

The Native PAGE gel was used to determine the optimal stoichiometric values of peptide to siRNA for complex formation. Equimolar quantities of both the sense and antisense strands were used on a scale of 0.2 O.D. depending on the ratio of RNA to peptide, the total moles of RNA were multiplied by the ratio value being tested to peptide. Peptide values were held

constant at stoichiometric values of 1, while the RNA value sequentially increased. Samples were prepared by adding the desired amount of peptide and RNA were combined in sterile Eppendorf tubes, dried on the Savant Automated Environmental SpeedVac® System AES2010 SpeedVac and dissolved in 10 µL of Annealing Buffer (10 mM TRIS, 50 mM NaCl, 1 mM EDTA, pH=7) and incubated at 37°C on the heat block for 30 minutes. Then 10 µL of gel loading buffer (30% Sucrose/1X TBE) was added to each sample. To prepare the gel, a 20% Native PAGE gel was made and 10X TBE running buffer was used and run at 300 V, 100 mAmps, and 12 Watts for 2-3 hours. Gel was stained using STAINS-ALL (25mg Alfa Aesar Stains-All Powder®, 50 mL isopropyl alcohol, 25 mL formamide, 125 mL water) and allowed to photo bleach to visualize bands.

3.6.7 Denaturing PAGE Gel

To prepare the 24% PAGE Denaturing Gel 7M urea, 40% acrylamide and 10X TBE was diluted to 50 mL with ddH_2O. The gel was polymerized using 30 mg of ammonium persulfate in 300 mL of DIH_2O and 15 µL of TEMED. The gel was run using the AA Hoefer SE 600 standard Vertical Electrophoresis Unit with the ISCO Electrophoresis Power Supply, Model 493 from Instrumentation Specialties Company as well as the VWR Scientific Model 1160 cooling system. The Gel was run at 350 V for 3 hours. Samples were annealed in 10 µL of Annealing buffer, incubated on the heat block at 37°C for 30 minutes, and then allowed to cool to room temperature and dried down on the SpeedVac. They were then resuspended in Annealing Buffer containing 1X PBS instead of EDTA to prepare for the sample collection and preparation, since the FBS solution contained 1X PBS. Following the addition of 10 µL of the Annealing Buffer with 1X PBS, 10 µL of FBS solution (100 µL of 10% FBS + 900 µL 1X PBS) was added to each sample, and samples were placed back on the heat block at 37°C. Each aliquot collected at 0, 2,

6, and 24 hours was a total of 5 µL, and to these aliquots 10 µL of gel loading buffer (20% formamide in 10X TBE) was added. The 0-hour time point collection was not placed on the heat block but placed at -80°C to prevent any further reaction from taking place. The following samples were collected at 2 hours, 6 hours, and 24 hours and each was placed at -80°C following collection. Each The gel was stained with STAINS-ALL and allowed to photo bleach.

3.6.8 Heparin Displacement Assay

A Native PAGE gel was used to run the heparin displacement assay. Equimolar quantities of both sensed and antisense strands were used to create RNA duplexes. Sample preparation was done on a scale of 0.3 O.D. calculations were similar to varying RNA ratios at different stoichiometric values for sample preparation. The total moles desired of RNA and peptide used were equimolar, and this total value was then multiplied by the stoichiometric ratio of heparin desired. This value was then multiplied by the molecular weight of heparin to obtain the mass value of heparin to be added to each sample. To prepare the gel, a 20% Native PAGE gel was made and 10X TBE running buffer was used and run at 300 V, 100 mAmps, and 12 Watts for 2-3 hours. Gel was stained using STAINS-ALL (25mg Alfa Aesar Stains-All Powder®, 50 mL isopropyl alcohol, 25 mL formamide, 125 mL water) and allowed to photo bleach to visualize bands.

3.6.9 FBS Stability Assay

The FBS stability assay was performed using 1:1 molar ratio of peptide to RNA. Samples were annealed using 10 µL of Annealing Buffer and after samples were annealed and cooled to room temperature, 10 µL of FBS solution (10% FBS, 900 µL 1X PBS) was added to each sample. Samples were incubated at 37°C and aliquots of 5 µL were taken at time points of 0 hours, 2 hours, 6 hours, and 24 hours were collected, and to these 10 µL of gel loading buffer

(20% formamide in 10X TBE) was added. Aliquots were kept in the -80°C to cease any further reactions. To prepare the denaturing gel 7 M urea, 40% acrylamide and 10X TBE, diluted to 50 mL with ddH_2O were used. The gel was polymerized using ammonium persulfate, TEMED and ddH_2O. The gel was stained with STAINS-ALL (25mg Alfa Aesar Stains-All Powder®, 50 mL isopropyl alcohol, 25 mL formamide, 125 mL water) and allowed to photo bleach.

3.7 References

1. Loh, C.-Y.; Chai, J.; Tang, T.; Wong, W.; Sethi, G.; Shanmugam, M.; Chong, P.; Looi, C. The E-Cadherin and N-Cadherin Switch in Epithelial-to-Mesenchymal Transition: Signaling, Therapeutic Implications, and Challenges. Cells 2019, 8 (10), 1118. https://doi.org/10.3390/cells8101118.
2. Mrozik, K. M.; Blaschuk, O. W.; Cheong, C. M.; Zannettino, A. C. W.; Vandyke, K. N-Cadherin in Cancer Metastasis, Its Emerging Role in Haematological Malignancies and Potential as a Therapeutic Target in Cancer. BMC Cancer 2018, 18 (1), 939. https://doi.org/10.1186/s12885-018-4845-0.
3. Araki, K.; Shimura, T.; Suzuki, H.; Tsutsumi, S.; Wada, W.; Yajima, T.; Kobayahi, T.; Kubo, N.; Kuwano, H. E/N-Cadherin Switch Mediates Cancer Progression via TGF-β-Induced Epithelial-to-Mesenchymal Transition in Extrahepatic Cholangiocarcinoma. Br J Cancer 2011, 105 (12), 1885–1893. https://doi.org/10.1038/bjc.2011.452.
4. Aleskandarany, M. A.; Negm, O. H.; Green, A. R.; Ahmed, M. A. H.; Nolan, C. C.; Tighe, P. J.; Ellis, I. O.; Rakha, E. A. Epithelial Mesenchymal Transition in Early Invasive Breast Cancer: An Immunohistochemical and Reverse Phase Protein Array Study. Breast Cancer Res Treat 2014, 145 (2), 339–348. https://doi.org/10.1007/s10549-014-2927-5.
5. Mariotti, A.; Perotti, A.; Sessa, C.; Rüegg, C. N-Cadherin as a Therapeutic Target in Cancer. Expert Opinion on Investigational Drugs 2007, 16 (4), 451–465. https://doi.org/10.1517/13543784.16.4.451.
6. 04-149 (Particle Size and Cell Entry). https://www.brown.edu/Administration/News_Bureau/2004-05/04-149.html#:~:text=Particle%20size%20plays%20a%20key,that%20are%20larger%20or%20smaller (accessed 2023-05-22).
7. Foroozandeh, P.; Aziz, A. A. Insight into Cellular Uptake and Intracellular Trafficking of Nanoparticles. Nanoscale Res Lett 2018, 13 (1), 339. https://doi.org/10.1186/s11671-018-2728-6.

Chapter 4: Osteoblast Cells Expression of Adhesion Proteins Makes Them Viable Therapeutic Targets to Help Potentially Prevent Cancer Spread and Metastasis

4.1 Abstract

The expression of adhesion proteins on the surface of osteoblast cells makes them viable therapeutic targets in the treatment of many diseases, especially cancers which migrate and metastasize within the bone. Because adhesion proteins play an integral role in the EMT transition, we hypothesized that targeting them could mitigate the effects of the EMT transition, reverse it, and decrease drug resistance imparted by adhesion proteins. Although the osteoblast cell line MC3T3.E1 exhibited good viability in the presence of the peptide:siRNA complexes, the complexes themselves did not function as the most efficient siRNA delivery method to the osteoblast cells. Following incubation of the cells with the peptide:siRNA complexes, knockdown of N-cadherin was measured by rT-PCR as well as Western Blot. The only complex which exhibited a very faint decreased in N-cadherin was the FITC-Ahx-SDSSD-Ahx-R_{12}:siRNA complex, but results showed that the decrease in N-cadherin for this complex was not significant enough to cause a decrease which would produce much change to effect the EMT transitions or the "cadherin switching" which are the hallmarks of many cancers within the bone microenvironment.

4.2 Introduction

RNA interference is a process which takes place within the body as a means of gene regulation. This process takes place to maintain an equilibrium between levels of protein as well as gene expression within cells. In recent years, RNAi has had much focus as an effective potential option in the treatment of many diseases, especially cancers. specifically, RNAi can be used to improve the accuracy, stability, and efficiency of existing treatments as well as genetic

therapies.[1] Treating cancers using RNAi has been of particular interest as RNAi therapies have the potential to eliminate unwanted and harmful side effects which traditional cancer therapies exhibit. Furthermore, existing drugs used to treat cancers are harmful and lack specificity for cancerous cells, often harming healthy cells in the process of treatment. “RNAi treatments elicit their pharmacological effect via non-coding RNAs (ncRNAs), which regulate events of the cell instead of translating into proteins, and with small interfering RNAs (siRNAs) and microRNAs (miRNAs), RNAi acts rapidly. siRNA is a double-stranded ncRNA with a length of 20–25 base pairs that are loaded onto the RNA-induced silencing complex (RISC), to degrade and cleave the mRNA before translation”.[1-3] This degradation of complementary mRNA is what prevents the expression of proteins which the mRNA would encode for. Because of this, virtually any protein or gene of interest can be targeted using RNAi as a therapy. This aspect makes RNAi therapies wonderful options in the treatments of various diseases, including cancer, but while RNAi holds promise it also has its drawbacks. Specifically, siRNAs are easily degraded due to their inherent instability and structure, and many delivery methods which prove to be effective often exhibit unacceptable toxicity.[1] Because any protein or gene of interest can be targeted using RNAi therapies, cancer is of specific interest, because “Tumors are the result of the accumulation of various types of gene mutations and the regulation of gene networks formed by the interaction of these mutated genes. Thus, gene therapies are the fundamental treatment. The expression of target genes (vulnerable nodes) is knocked down by RNAi, locating these nodes which are indispensable to tumor maintenance, with low side effects and low risk, blocking the inherent immunosuppression and triggering immune attacks on tumors.”[1,4] Specifically, RNAi-based tumor treatments have been shown to exhibit high silencing capabilities, and RNAi in the treatment of cancer has four main goals: study of the tumor signal transduction pathway, effects

on oncogenes, inhibition of tumor-apoptosis genes, inhibition of tumor-angiogenesis related factors, and reduction of tumor drug resistance.[1] Specifically, reducing drug resistance indirectly through RNAi is of particular interest in relation to cell-surface adhesion proteins.

Drug resistance imparted by cell surface adhesion proteins creates a bone microenvironment highly suited to cancer cell metastasis. Adhesion proteins have the ability to create "shields" through their connective interactions, thus reducing effectiveness of cancer drugs and therefore, reducing effectiveness of treatment. This process is illustrated in the below graphic (Figure 4.1). The homeostasis of adhesion molecules in the bone microenvironment is essential to bone tissue health for this reason.

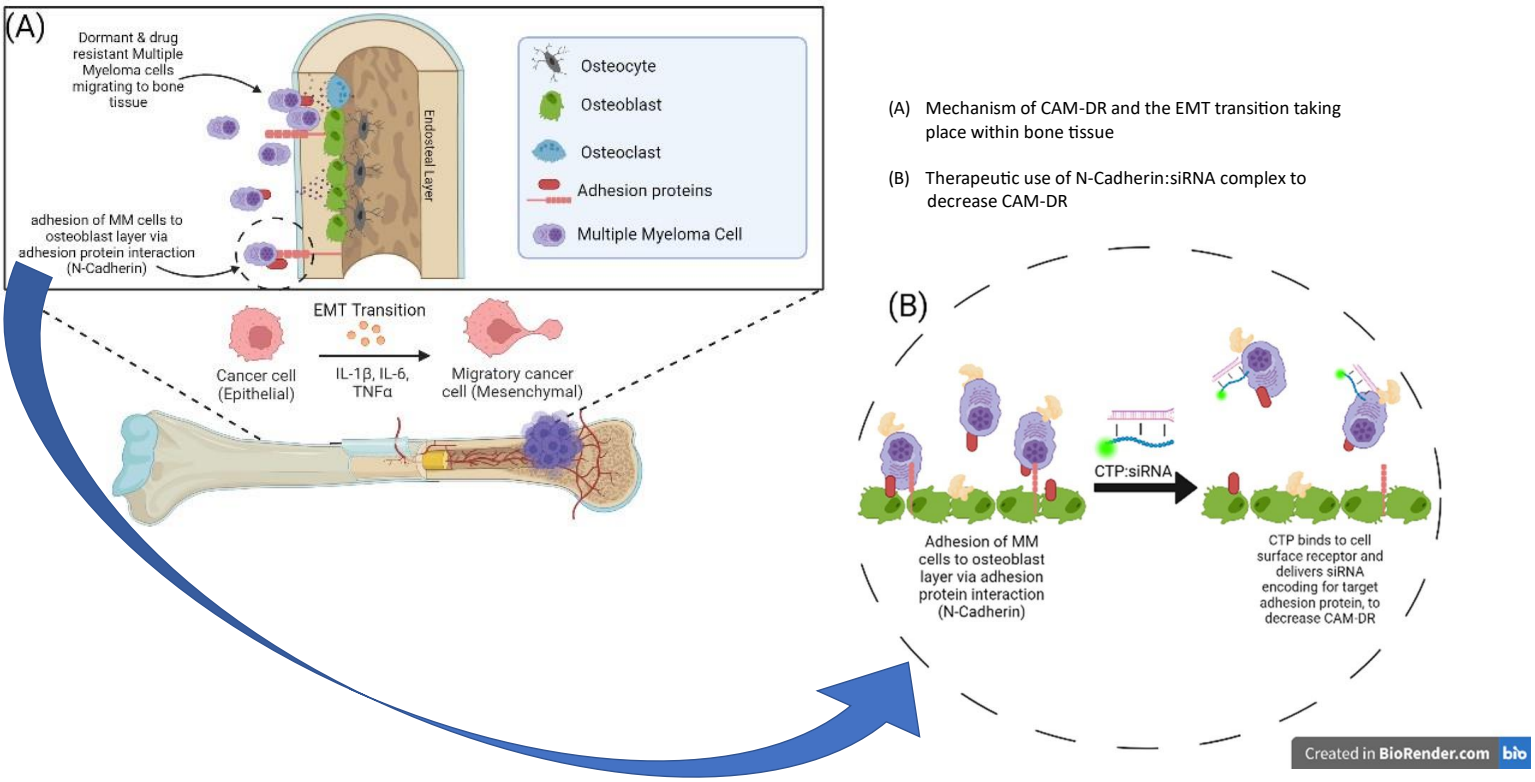

Figure 4.1: Adhesion proteins impart cell adhesion mediated drug resistance to multiple myelomas which migrate to the bone. By using periostin targeting peptides, siRNA encoding for adhesion proteins may help reduce drug resistance imparted by adhesion proteins by silencing or reducing their expression within osteoblasts.

Furthermore, adhesion molecules regulate signaling between the extracellular environment as well as other cells.[5] "These signals include biochemical cues, as adhesion proteins can both act as ligand-activated receptors and activate mechanotransduction triggered by changes in the physical environment. Molecular mechanisms related to cell adhesion signaling have been extensively studied, especially because mutations and changes in expression of these proteins, particularly cadherins and integrins, are frequently associated with diseases ranging from developmental intellectual disability to cancer. In fact, two major hallmarks of cancer, loss of cell-to-cell adhesion and anchorage-independent growth, are both dependent on cell adhesion molecules."[5] Some cadherins mediate adhesive interactions, such as N- and E-cadherin, which form adhesive dimer interfaces through the swapping of paired extracellular cadherin 1 N-terminal domains.[5] This swap generates a two-fold symmetric interaction, preferentially between two apposed cells in the presence of calcium, forming densely and tightly packed junctional structures.[5-7] Another hallmark of cancer cell migration and metastasis within the bone is the Epithelial to Mesenchymal Transition (EMT transition) which cadherins also play a major role in. This process is a reversible transcriptional event which ultimately drives tumor cells to metastasize.[5,8] When cells gain more mesenchymal properties, as opposed to epithelial properties, they are more prone to migration.[5] One of the identifying characteristics of the EMT transition is known as "cadherin switching" which is marked by the loss of E-cadherin and the increase in N-cadherin.[5,9] "This promotes a shift from tight cell-to-cell and cell-basement membrane connections, mediated by E-cadherin and α6β4 integrins, to N-cadherin-dependent adhesions, mediated by β1 and β3 integrins. Thus, EMT allows cells to adhere readily to collagen, a component of the extracellular matrix, rather than the basement membrane. N-cadherin also activates the Rho-family GTPase signaling pathway, enhances fibroblast growth

factor signaling, and modulates the Wnt signaling pathway. All of these pathways contribute to the aggressive tumor phenotype with the capacity to escape from the primary tumor location to secondary sites."[5,10] "Moreover, EMT induced by silencing of E-cadherin has also been shown to protect cells from apoptotic, cell death triggered by disrupted anchorage to basement membrane. However, E-cadherin was also recently shown to act as a survival factor in metastatic invasion of breast cancer by limiting reactive oxygen species-mediated apoptosis. Thus, context-dependent adhesion molecule switching not only contributes to cancer cell motility, but also promotes their proliferation and survival ability in the bloodstream, thereby increasing the probability of distant metastases forming."[5,11,12] Furthermore, collective migration of cancer cells requires changes to the extracellular matrix which facilitate this migration. This remodeling can be driven by cancer cells, and cancer associated fibroblasts (CAFs) can remodel the extracellular matrix to create tracks which can be used by other migrating cancer cells.[5,13] These tracks facilitate the spread and migration to sites other than their origin. "Moreover, by generating heterotypic junctions between N-cadherin on the CAF membranes and E-cadherin on the cancer cell membrane, CAFs can generate intercellular physical force and drive collective invasion of cancer cells."[5, 14] Finally, N-cadherin has been found to be an integral part of leukemic stem cell self-renewal.[5,15] This has been found to cause chemotherapy evasion, and it has also been found that N-cadherin-mediated cell adhesion is functionally essential for the regulation of hematopoietic stem and progenitor cell activity in the bone marrow.[5,14] For these reasons, adhesion molecules, especially N-cadherin, serve as invaluable potential therapeutic targets in the treatment of cancers using RNAi.

4.3 Chapter Objectives

This chapter aims to highlight the effectiveness of the peptide:siRNA complexes at silencing n-cadherin expression. First, RNA interference will be performed on the MC3T3.E1 cells and its success will be examined by performing RT-PCR and qPCR following RNA isolation. Protein isolation will also be performed to perform a Western Blot to examine if protein levels are downregulated following a 24-hour incubation period with the peptide:siRNA complexes. Finally, this chapter will investigate the toxicity of the periostin-targeting peptide (FITC-Ahx-SDSSD-Ahx-R_9 and FITC-Ahx-SDSSD-AHx-R_{12}) to osteoblast cells using flow cytometry and Annexin/7-AAD viability dyes.

4.4 rT-PCR and qPCR Following RNAi on MC3T3.E1 Cells

Reverse transcription-polymerase chain reaction (rT-PCR) was used to transcribe mRNA in the MC3T3.E1 cells into cDNA as a means to detect low levels of N-cadherin mRNA within the cell lines. To further check the results, qPCR was used to double check whether the RNAi experiment was successful or not. The results showed that there was a slight decrease in levels of N-cadherin for the peptide:siRNA complexes indicating that there was some success to the experimental design.

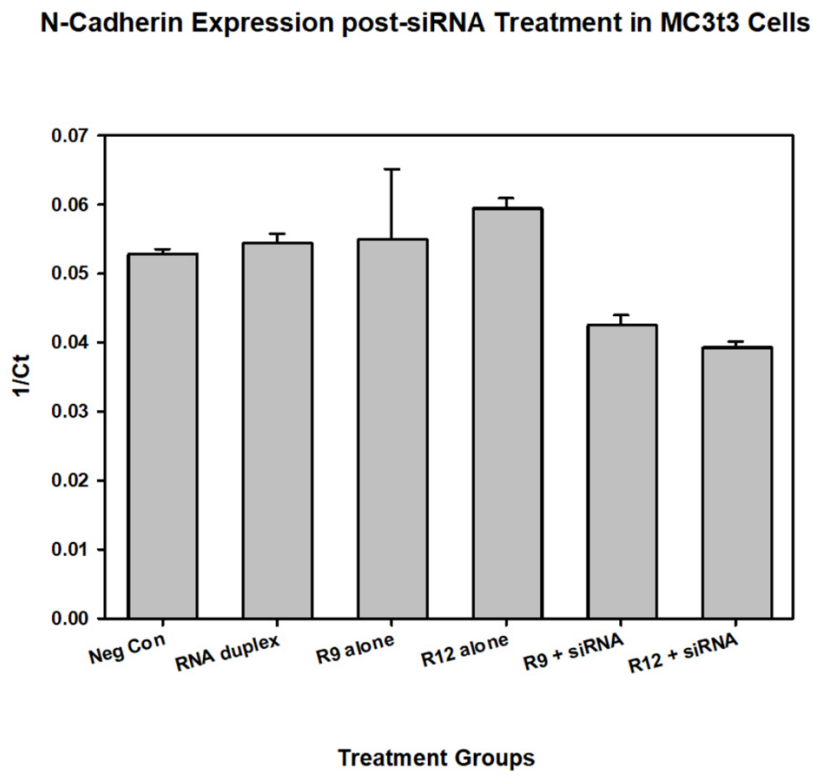

Figure 4.2: Analysis of qPCR results post siRNA treatment in MC3T3.E1 cells. Decrease in N-cadherin levels was statistically significant within the two peptide:siRNA treatment groups. The negative control was cells alone, the RNA duplex was cells + RNA duplex, R_9 alone was the FITC-Ahx-SDSSD-Ahx-R_9 peptide + cells, the R_{12} alone was the FITC-Ahx-SDSSD-Ahx-R_{12} peptide alone and both the R_9 + siRNA and R_{12} + siRNA treatment groups were the FITC-Ahx-SDSSD-Ahx-R_9 peptide:siRNA and FITC-Ahx-SDSSD-Ahx-R_{12}:siRNA respectively.

qPCR data typically examines the change in a gene of interest in relation to a "housekeeping gene". The housekeeping gene is a gene which should be expressed in all cell lines, and should also be unaffected by the treatment conditions. Data is then analyzed by looking at the fold change of the gene of interest in relation to the control or housekeeping gene, as well as a control population. The fold change (C_t) indicates how much of a target gene was expressed relative to the control. In this case, about 40% gene expression was seen for N-cadherin levels as compared to the controls, which expressed 100% levels of N-cadherin.

4.5 Agarose Gel on cDNA following RNAi on MC3T3.E1 Cells

Following reverse transcription-polymerase chain reaction (rT-PCR), agarose gels were run to check for a visual decrease in levels of N-cadherin within the cells after the RNAi experiment. Representative agarose gels are shown below in Figure 4.3.

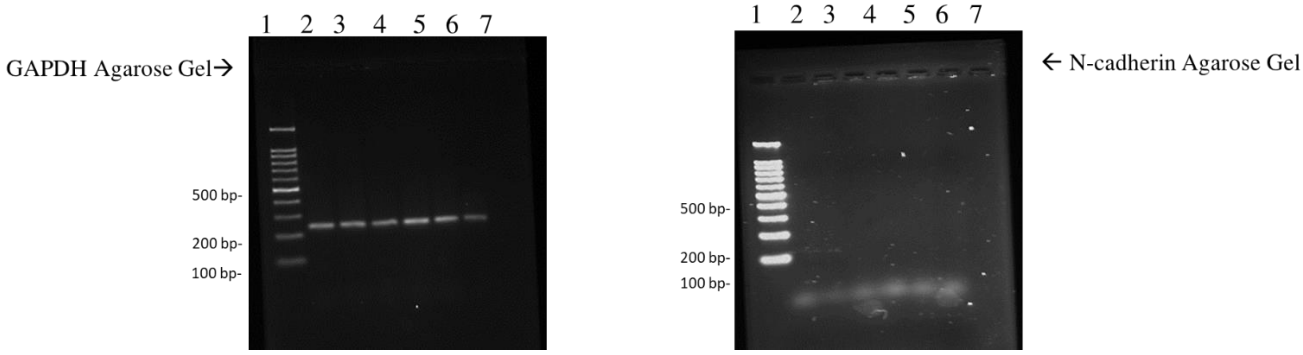

GAPDH Agarose Gel							
Lane #	1	2	3	4	5	6	7
Sample Identity	Ladder	Control lane→ cells only	N-cadherin duplex	R_9 peptide only (FITC-Ahx-SDSSD-Ahx-R_9)	R_{12} peptide only (FITC-Ahx-SDSSD-Ahx-R_{12})	R_9:siRNA (FITC-Ahx-SDSSD-Ahx-R_9:N-cadherin duplex)	R_{12}:siRNA (FITC-Ahx-SDSSD-Ahx-R_{12}:N-cadherin duplex)

N-cadherin Agarose Gel							
Lane #	1	2	3	4	5	6	7
Sample Identity	Ladder	Control lane→ cells only	N-cadherin duplex	R_9 peptide only (FITC-Ahx-SDSSD-Ahx-R_9)	R_{12} peptide only (FITC-Ahx-SDSSD-Ahx-R_{12})	R_9:siRNA (FITC-Ahx-SDSSD-Ahx-R_9:N-cadherin duplex)	R_{12}:siRNA (FITC-Ahx-SDSSD-Ahx-R_{12}:N-cadherin duplex)

Figure 4.3: Representative Agarose Gel of cDNA from rT-PCR for both GAPDH and N-cadherin run using the TAQ_NEB PCR cycle. RNAi performed on cells by incubating complexes, siRNA duplex or peptides in 1mL of media in 6-well culture plates with MC3T3.E1 cells for a 24 hr period. All complexes or siRNA duplexes made in 50 µL of Annealing Buffer (10 mM Tris, 50 mM NaCl,1 mM EDTA) then diluted with 200 µL of serum-free media. 55.5 µL of each sample was added directly to the culture dishes with 1 mL of fresh media. The cultures were swirled to mix and incubated at 37°C for 24 hr. Following the incubation period RNA was isolated using the Zymo Direct-zol™ RNA MicroPrep kit, then frozen at -80°C for further use.

Agarose gels showing the results of rT-PCR on the N-cadherin silenced samples showed little to no decrease in N-cadherin in the cells exposed to the peptide:siRNA complex. The results from all PCR and agarose gel runs remained inconsistent, or appeared to show no change

between the peptides with cells (FITC-Ahx-R_9 and FITC-Ahx-R_{12}) or the peptide:siRNA complexes (FITC-Ahx-SDSSD-Ahx-R_9 and FITC-Ahx-SDSSD-Ahx-R_{12}). This was once again unexpected, as the lanes containing the cells which were incubated with the peptide:siRNA complex should have theoretically shown a decrease in the amount of N-cadherin present. Furthermore, the inconsistency while running agarose gels also rendered traditional rT-PCR and agarose gel on the cDNA products to be an undesirable method for N-cadherin detection in this case.

4.6 BCA Assay Following Protein Isolation

After RNAi and RNA isolation was performed, protein isolation was performed in tandem. To test the success of the protein isolation, a BCA assay was used to confirm the presence of protein in all the unknown samples. Each unknown's concentration was then determined using the equation of the line, where $y = mx + b$. From this, the 'x' value is equivalent to the slope of the line and both 'a' and 'b' are given values from the linear equation. Using this equation and solving for 'y' gave the unknown protein concentrations in each sample. Because the BCA assay is unable to detect specific proteins of interest, this test was only used as a confirmation of protein in each sample to test for the success of isolation. In conjunction with the BCA assay, rT-PCR and qPCR along with agarose gels and a Western blot were used to further confirm or deny whether RNAi took place.

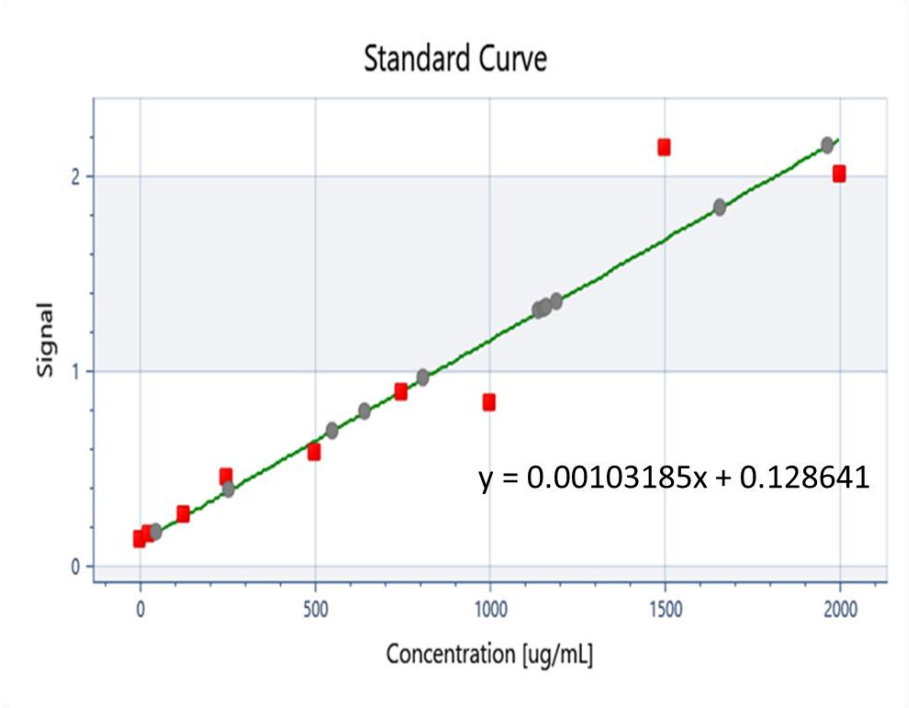

Figure 4.4: Representative BCA assay curve following protein isolation on cells incubated with peptide alone (FITC-Ahx-R_9, FITC-Ahx-R_{12}) and peptide:siRNA complexes (FITC-Ahx-SDSSD-Ahx-R_9:siRNA and FITC-Ahx-SDSSD-Ahx-R_{12}:siRNA) as well as control group cells which were not incubated with either peptide or complexes. Equation of the line shown on graph. Gray points are all standards which fell perfectly on the line of best fit, while red points fell slightly outside of the line. All samples read at 562 nm.

4.7 Western Blot Analysis following RNAi and Protein Isolation on MC3T3.E1 cells

Western Blot results following RNAi repeatedly appeared to indicate a failed experiment, with no visual bands present for N-cadherin. This seemed to consistently occur, or blot results were unreliable and unreproducible, much like the agarose gels following PCR. An example of this is shown below in Figure 4.5.

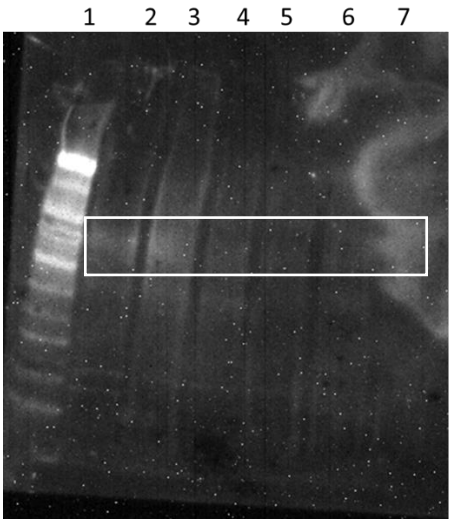

Lane #	Sample Identity
1	Protein Ladder
2	Control (cells only)
3	RNA duplex
4	FITC-Ahx-R_9
5	FITC-Ahx-R_{12}
6	FITC-Ahx-SDSSD-Ahx-R_9:siRNA
7	FITC-Ahx-SDSSD-R_{12}:siRNA

Figure 4.5: Representative Western Blot for the detection of N-cadherin following RNA interference on MC3T3.E1 cell line. Boxed region shows where expected N-cadherin bands would be seen.

Western Blots consistently showed fluorescence of the ladder, but not enough detectable fluorescence of N-cadherin bands. The boxed portion of the blot shows the expected position of N-cadherin bands. As can be seen within the boxed portion, there is very faint fluorescence, but not enough to confirm the success of the blot. Fresh antibodies were used to ensure their viability, and account for the possibility of lack of bands due to antibody degradation. Additionally, the very faint band for N-cadherin in the control cell group indicated that the cells themselves may have been expressing N-cadherin in levels too low for typical Western Blot detection. the sample size of cells may also have been too small to produce enough protein for detection (6-well culture plate, at confluency). This was likely due to not having a high enough concentration of N-cadherin in the protein isolates, making the blot a less successful method for detection of N-cadherin changes following RNAi. Additionally, the absence of bands in the lanes where cells were only incubated with peptide (FITC-Ahx-R_9 and FITC-Ahx-R_{12}) was unexpected, as there was no siRNA present in those samples. The control samples also had a lack of bands, or very faint and undefined bands present for N-cadherin indicating that the

MC3T.3.E1 cells were already expressing lower levels of N-cadherin to begin with. This would explain the difficulty in detecting changes in N-cadherin levels following RNAi, by agarose gel and Western Blot.

4.8 Cell Cytotoxicity Assays via Flow Cytometry

To test for cytotoxicity of the peptides when incubated with the MC3T3.E1 cells, an Annexin V eFluor 450/7-AAD viability dye was used to measure cell death following a 1-hour incubation of the cells with the peptides at 37°C. Annexin V binds to phosphatidylserine when expressed on the outside of the cell membrane in apoptotic cells.[16] Phosphatidylserine is a lipid expressed on the inner portion of the plasma membrane in healthy cells, but once apoptosis begins to take place, lipid asymmetry is lost and it begins to be expressed on the outside of the plasma membrane.[16] For this reason, Annexin V can detect cells in the early stages of cell death. Annexin V can also access the inner portion of the plasma membrane after the cell membrane has begun to rupture and can also be used to detect necrotic cells, but cannot differentiate between early stage cell death and late stage cell death. For this reason, co-staining with another viability dye is often performed. In this case, 7-AAD was chosen as to not interact with the fluorescent signal of FITC, which was bound to the peptides incubated with the cells. 7-AAD viability dye (7-amino-actinomycin D) has a high DNA binding constant and is excluded by intact, healthy cells.[17] Viability dyes only stain dead cells, and specifically 7-AAD is an intercalating dye, which inserts itself in G-C rich regions of double stranded DNA.[18]

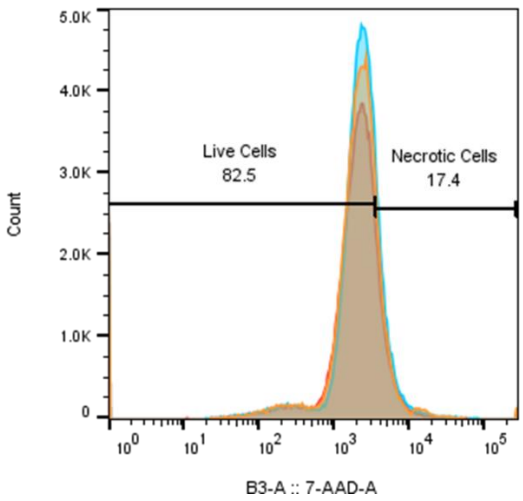

Average # Necrotic Cells following R_9 peptide incubation= 3.10 x 10^4

STDEV= 3.94 x10^3

Mean +/- STDEV= 3.10 x 10^4 +/- 3.94 x10^3

Average # Necrotic Cells following R_{12} peptide incubation= 2.40 x 10^4

STDEV= 2.23 x10^3

Mean +/- STDEV= 2.40 x 10^4

+/- 2.23 x10^3

Figure 4.6: Representative image of flow cytometry data with viability dye 7-AAD to stain for necrotic cells after 1 hour incubation with both peptides (FITC-Ahx-SDSSD-AHx-R_9 and FITC-Ahx-SDSSD-AHx-R_{12}). Image shows control cells and both treated groups overlayed.

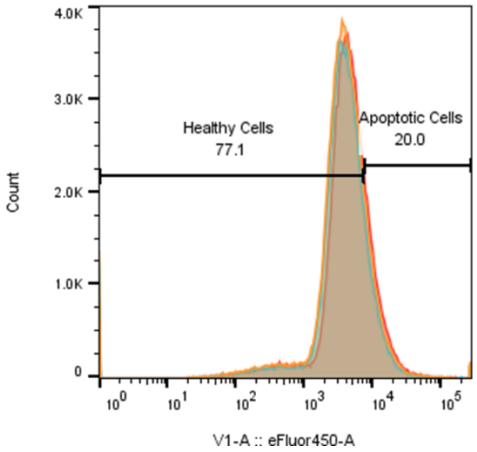

Average # Apoptotic Cells following R_9 peptide incubation= 1.89 x 10^4

STDEV= 1.57 x10^3

Mean +/- STDEV= 1.89 x 10^4 +/- 1.57 x10^3

Average # Apoptotic Cells following R_{12} peptide incubation= 2.09 x10^4

STDEV= 4.11 x10^2

Mean +/- STDEV= 2.09 x10^4 +/- 4.11 x10^2

Figure 4.7: Representative image of flow cytometry data with Annexin V eFluor450 to stain for cells undergoing apoptosis after 1 hour incubation with both peptides (FITC-Ahx-SDSSD-AHx-R_9 and FITC-Ahx-SDSSD-AHx-R_{12}). Image shows control cells and both treated groups overlayed.

Both Figure 4.6 and 4.7 are representative flow cytometry histograms obtained following cell treatment with both peptides, then staining with both Annexin V eFluor450 and 7-AAD. Results showed no changes between control cell populations or between incubation with either peptide. The low numbers of either dead cells or cells undergoing apoptosis were most likely the

result of lifting the cells by trypsin as opposed to exposure to the peptides themselves. If the peptides exhibited high cytotoxicity, there would have been more cells undergoing apoptosis seen following the incubation period. This confirmed the peptide formulations were safe for use with the cells and would not cause cell death prior to RNAi taking place.

4.9 Results and Discussion

Although the periostin binding peptides successfully bind to osteoblast cells, their efficiency as siRNA delivery agents must be improved. Based on the heparin displacement assays shown in Chapter 3, the complexes with peptide and siRNA interacted quite strongly, but could still be released at Heparin:complex ratios of 1:1, 5:1 and 10:1 and some faint bands were even seen for some samples at the lowest heparin ratio of 0.1:1. This led us to believe that siRNA could release after internalization of the peptides into the cells. Prior flow cytometry data from quenching studies also indicated that the peptide:siRNA complexes were being internalized by the MC3T3.E1 cells. In addition, the FBS Stability assay also showed exceptional stability of the peptide:siRNA complexes when in the presence of serum which indicated that the complexes would be stable in the growth media for roughly 6 hours. This was sufficient to allow for complex internalization, as all internalizations occurred within 1 hour. RNAi within the osteoblast cell line seemed to take place after 24 hours, but perhaps not as efficiently as could have been, since this was the incubation period of the complexes with the cells. If RNAi could have been performed for a longer time period, perhaps a more drastic decrease in N-cadherin would have been observed at 48 hours or 72 hours as opposed to 24 hours. Limitations to the length of incubation period impacted how long the experiment could be performed. The MC3T3.E1 cell line has a doubling rate of approximately 36 hours, and all RNAi experiments were performed at ~80-90% confluency. Past 24 hours, the cells would have begun to die rapidly

once at confluency without changes to the culture media as well as passaging the cells to create more surface area for further cell proliferation. This would not have been possible to achieve to measure RNAi over a longer period of time as the new cells would have not been exposed to the complexes so an accurate measure of RNAi over time would be difficult to measure if complexes were repeatedly introduced to the cultures as they grow. Although the peptide:siRNA complexes exceeded the typical acceptable size for cell uptake (TEM images), some form of RNAi did seem to take place. In media, after the peptide was diluted and incubated with the MC3T3.E1 cells, it may have been diluted enough to not form such large aggregates which could have allowed for the internalization of the peptide. Agaorse gels were run to confirm or deny the presence of both GAPDH (housekeeping gene) and N-cadherin following the RNAi experiment. Bands for all samples in the GAPDH gel indicated that the actual PCR reaction was successful, even though bands were not visible in the N-cadherin gel. This indicated that the Master Mix used contained all necessary enzymes, dNTPs and primers and that the cycle for PCR was appropriate for the enzymes as well as primers. Because the agarose gels did not indicate whether RNAi took place successfully, it was also examined by Western Blot. Generally, the results mirrored that of the PCR reaction. As a result, qPCR was run as a final confirmation since it was assumed that there was not a high enough concentration of either cDNA for N-cadherin or N-cadherin protein within the cells to be detectable by these methods. The qPCR results indicated that through some mechanism, N-cadherin is being slightly downregulated in the FITC-Ahx-SDSSD-Ahx-R_{12}:siRNA and FITC-Ahx-SDSSD-Ahx-R_9:siRNA samples. This was concluded after calculating the fold changes for each sample. Most populations tested showed either normal expression of N-cadherin in the control samples, or slightly less than normal expression.

4.10 Materials and Methods

4.10.1 Cell culture

All cells cultured as stated in section 2.6.2. The MC3T3.E1 osteoblast cell line was used for all RNAi and protein isolation experiments.

4.10.2 RNAi

RNA interference was conducted on MC3T3.E1 cell line once cell cultures reached 80-90% confluency. Peptides and siRNA duplex for n-cadherin were combined in equimolar quantities and dried on the Savant Automatic Environmental Speedvac System AES2010 prior to annealing each complex in 50 mL of Annealing Buffer (10 mM Tris, 50 mM NaCl,1 mM EDTA). A total of five samples were tested. The samples were as follows: FITC-Ahx-SDSSD-Ahx-R_9 incubated with MC3T3.E1 cells, FITC-Ahx-SDSSD-Ahx-R_{12} incubated with MC3T3.E1 cells, n-cadherin siRNA duplex incubated with MC3T3.E1 cells, FITC-Ahx-SDSSD-Ahx-R_9:siRNA complex incubated with MC3T3.E1 cells, and FITC-Ahx-SDSSD-Ahx-R_{12}:siRNA complex incubated with MC3T3.E1 cells.

After complexation of the peptide:siRNA complexes were complete and cells had reached 80-90% confluency, the growth media was aspirated from the cultures and 2.5 mL of fresh media was added to each culture dish along with 250 µL of the peptide:siRNA complexes (50 µL of sample in Annealing Buffer + 200 µL in serum-free media). The culture plates were rocked back and forth briefly and incubated at 37°C for 24 hours until harvested and RNA was collected.

When using 6 well plate, 55.5 µL of complexed samples added to each well of 1 mL growth media. Complexed samples were diluted in a total of 200 µL of serum-free growth media and had been annealed with 50 µL of annealing Buffer, for a total volume of 250 µL of

complexed sample. Samples were added to each well and incubated for 24 hours at 37°C before isolation.

4.10.3 RNA Isolation

After incubating the MC3T3.E1 cell line for 24 hours with the peptide:siRNA complexes, RNA from the cells was isolated following the protocol for the Zymo Research Direct-zol RNA MicroPrep Kit. All reagents were added directly to the cell culture dishes, and cell membranes were disrupted and lysed by mechanical disruption via scraping and pipetting. Collected samples were stored at -80°C.

RNA samples were isolated by adding TRI Reagent directly to each culture well or dish and volume was dependent upon culture dish surface area, as indicated by the protocol provided by the Zymo Research Direct-zol RNA MicroPrep Kit. An equal volume of 95%-100% Ethanol to volume of TRI Reagent was added directly to each culture dish/well and lysis was encouraged through either scraping or pipetting. This was then added to a Zymo-Spin™ IC Column in a Collection Tube and centrifuged for 30 seconds at 10,000 x g. The flow through was discarded unless protein isolation was being performed in tandem. Following this, 400 µl of the Direct-zol™ RNA PreWash was added to each sample's column and columns were centrifuged for 30 seconds at 10,000 x g. the flow through was discarded and this step was repeated once more. Then, 700 µl of the RNA Wash Buffer was added to each column and they were centrifuged for 1 minute at 10,000 x g. Columns were then carefully transferred in new RNase-free tubes and 15 µL of RNase-free H_2O was added to the column and then this was centrifuged for 30 seconds at 10,000 x g to elute the purified RNA.

4.10.4 rT-PCR and qPCR

Reverse Transcriptase was run on the isolated RNA after performing RNAi on the MC3T3.E1 cell line. Following the 24 hour incubation period with the peptide:siRNA complexes, the RNA was isolated and stored in the -80 °C**.** Before use, the RNA samples were thawed on ice while all reagents were prepared. The Master Mix I (MMI) was prepared as follows: 2 µL of 5mM dNTPs + 2 µL of oligo dTs in a separate microcentrifuge tube from the RNA samples. These were mixed in a sterile Eppendorf tube and centrifuged down. A total of 4 µL of MMI was added to new sterile Eppendorf tubes corresponding to the number of samples present. To each of these, 100 ng of RNA + RNase-free water to a total volume of 12 µL was added. Each sample was mixed by pipetting and centrifuged, then placed in the Benchmark MyBlock hot bath at 65°C for 3 minutes, then returned to ice. Following the heat bath, Master Mix II (MMII) was prepared by combining (2 µL of 10X RT Buffer) x # of samples, and (1 µL of RNAOUT) x # of samples. This solution was mixed by pipetting and then centrifuged down. From this, 3 µL of the MMII was added to each sample tube, and 1 µL of MM-LVRT enzyme was then added to each tube after the addition of MMII. The samples were then placed in a water bath at 42°C for 1 hour using the Fischer Scientific Isotemp. Following the water bath, samples were spun down and placed in the hot bath for 10 minutes at 95°C, and the tops of the tubes were secured with fasteners. Finally, samples were removed from the hot bath and allowed to cool to room temperature before determining cDNA concentration using the Biodrop Duo from Biodrop at 260 nm.

Following the reverse transcriptase protocol, polymerase chain reaction (PCR) was performed. Primers used were designed based on the primer design from *Epigenetic silencing of E- and N-cadherins in the stroma of mouse thymic lymphomas, Carcinogenesis.* Table 4.1

specifies the forward and reverse sequences for the n-cadherin primers for mouse cell n-cadherin amplification. Before beginning PCR a working primer solution was prepared as follows from 100 µM primer stocks: 10µL of forward n-cadherin primer + 10 µL of reverse n-cadherin primer + 80 µL of RNase free H_2O. After preparing the working primer solution, the Master Mix (MM) was made as follows: 2.5 µL Taq Buffer x (# of samples), 1 µL of 10 µM dNTPs x (# of samples), 1 µL working primer solution x (# of samples), 17.85 µL H_2O x (# of samples), and 0.125 µL of Taq Polymerase Enzyme x (# of samples). Each reagent as well as the MM was vortexed and spun down.

Protein Name	**Forward Primer Sequence**	**Reverse Primer Sequence**
n-cadherin[1]	5'-GTGGAGGCTTCTGGTGAAAT-3'	5'-CTGCTGGCTCGCTGCTT-3'

Table 4.1: Primer design/sequence used for rt-PCR.[19]

The above primer designs for N-cadherin were also used when performing qPCR. Prior to beginning qPCR, the protocol for Reverse Transcriptase was followed as stated above. Once cDNA was generated, the Biodrop Duo from Biodrop was used to confirm presence of cDNA at 260 nm. Prior to beginning qPCR, each cDNA sample was diluted at a 1:20 ratio (5 µL cDNA + 95 µL nuclease-free H_2O) in sterile microcentrifuge tubes. Following the sample dilution, the working primer solution was prepared by taking 10 µL each of the 100 µM stock solutions of both the forward and reverse primers and adding them to 80 µL of nuclease-free H_2O. a working primer solution was made for both GAPDH (housekeeping gene) and N-cadherin (target sequence). Next the qPCR MasterMix was made as follows: (10 µL of BioRad SsoAdvanced Universal SYBR Green Supermix x # samples) + (1 µL working primer solution x # samples) + (6.5 µL nuclease-free H_2O x # samples) + 2.5 µL of diluted cDNA samples added last to each corresponding well in a 384 well plate (clear). Each well contained 17.5 µL of the qPCR

MasterMix + 2.5 µL of cDNA. Two separate sets of MasterMix were made, one for GAPDH and one for N-cadherin. After samples were setup, qPCR was run using the AppliedBiosystems 7900HT Fast Real-Time PCR System and results were analyzed using the SDS 2.4 Software.

4.10.5 Agarose Gel

Upon completion of the rt-PCR samples were analyzed by running an agarose gel. To confirm success of the PCR, GAPDH was also tested on a separate gel. Agarose gels were 2% Agarose in 1X TAE. The agarose and 1X TAE were combined in Erlenmeyer flasks and heated for 20 second intervals, swirling in between in a microwave until the solution was clear. This was then poured into the Life Technologies™ GIBCO BRL Horizontal Gel Electrophoresis Apparatus, Horizon® 58 gel box, and allowed to set and cool for 20 minutes. Following this, 1X TAE was then used as running buffer (enough to cover the gel). The ladder (Denville Scientific DNA Marker 100 bp ladder (11 fragments)) was loaded into well 1. Before loading samples, 10 µL of each sample was combined with 5 µL of DNA loading dye and this full 15 µL of sample was then loaded into the remaining wells. The gel was run for 1 hour at 90V and 120 mA. After 1 hour, the gel was placed in a small box containing enough DI H_2O to cover the gel, then 2 uL of ethidium bromide was added to this and it was placed on the shaker for 10 minutes. Gels were then imaged using the FluoroChem gel imaging system.

4.10.6 Protein Isolation

Protein isolation was performed following the M-PER® Mammalian Protein Extraction Reagent method from Thermo Scientific, or during RNA isolation using TRI Reagent. The first method using M-PER® Mammalian Protein Extraction Reagent was performed following the portion for the lysis of monolayer cultured cells. First, cells were grown to roughly 80-90% confluency, then peptide:siRNA complexes were incubated with the cells following the same

procedure for RNAi. The incubation period lasted for roughly 24 hours and after 24 hours the proteins were isolated from the cells. This was first done by aspirating the growth media from the cells. This was followed by a PBS wash using about 2 mL of the PBS, which was aspirated from the cells. Because 100 mm culture dishes were used, 1000 mLs of M-PER Extraction Reagent were added to the culture dish and they were placed on the Lab-Line Orbit Shaker for 5 minutes. The lysate was then collected and transferred to microcentrifuge tubes and spun down for 5 minutes at ~14,000 x g. The supernatant of each sample was then transferred to new microcentrifuge tubes and stored at

-20°C.

When performing protein isolation using the Zymo Research Direct-zol RNA MicroPrep Kit, the protocol provided by the manufacturer was followed. First, appropriate amount of TRI Reagent was added to the samples, based on the size of the culture dish. To this an equal volume of 95%-100% Ethanol was added, and mixed thoroughly by pipetting. The mixture was then transferred to a a Zymo-Spin™ IC Column2 in a Collection Tube (both provided by the kit) and these were then centrifuged at 10,000 g for 30 seconds. The flow through was then transferred to a larger conical tube, and four volumes of cold acetone was added directly to it. This was mixed by pipetting, and samples were incubated for 30 minutes on ice. Following the 30-minute incubation each sample was centrifuged at maximum speed for 10 minutes. the supernatant was discarded, and 400 µL of 95%-100% Ethanol was added directly to the pellet. This was once again centrifuged at maximum speed for 1 minute, and the supernatant was again discarded. The remaining protein pellet was air dried at room temperature for 10 minutes then resuspended and vortexed in 50 µL of M-PER® Mammalian Protein Extraction Reagent buffer and stored at -20°C for later use.

4.10.7 BCA Assay

The BCA assay was performed to confirm the presence of isolated protein. The protocol followed was the Pierce™ BCA Protein Assay Kit protocol. Before beginning, the volume needed of Working Reagent was determined as follows: (# standards + # unknowns) x (# replicates) x (volume of Working Reagent per sample)= total volume of Working Reagent Required. After the total volume needed was determined, the Working Reagent was made by preparing a 50:1 dilution of Reagent A:B. The microplate portion of the protocol was followed which required 200 µL of Working Reagent per sample when using the microplate. The BSA standards were prepared in varying concentrations and labeled as A-I, according to the protocol. These were prepared in duplicates. Following the preparation of the Working Reagent and the BSA standards, 10 µL of each standard and each unknown was added to its corresponding well on the microplate, and to each of these 10 µL of the Working Reagent was added. The plate was then placed on the plate shaker for 30 seconds, then covered and incubated at 37°C for 30 minutes. The plate was then cooled to room temperature following the 30-minute incubation and absorbance values were read at 562 nm on the VarioSkan LUX, then analyzed using the SkanIT Software.

4.10.8 Western Blot

Western Blot was performed using Nitrocellulose membranes (BioRad Trans-Blot Turbo Transfer Pack). The Wash Buffer used was 1X TBST (100 mL of 10X TBS, 1 mL TWEEN, 900 mL ddH_2O). The 10X TBS (24 g TRIS, 88 g NaCl, 900 mL ddH_2O, pH=7.6) was prepared fresh and used as a stock solution to prepare the 1X TBST from. The protein gel run prior to running the Western Blot was the BioRad Mini-PROTEAN® TGX™ Precast Gels and the running buffer used was 1X MOPS/SDS running buffer with fresh 1X MOPS/SDS within the chamber between

the gels. A stock of 20X MOPS/SDS (209.2 g MOPS, 121.2 g TRIS base, 20 g SDS, 6 g EDTA) was prepared initially. Sample preparation for the SDS gel was as follows: 5 µL of sample + 4.75 µL of NuPage LDS Sample Buffer + 0.25 µL of β-mercaptoethanol. Following the completion of the SDS gel, the gel was then placed between the membrane and filter paper soaked in NuPage Transfer Buffer and transferred using the semi-dry transfer for 3 minutes. Immediately following the transfer, the membrane was washed 4 times, 5minutes with DI H_2O**.** The membrane was then incubated with SuperBlock blocking buffer at room temperature for 30-60 minutes covered on the rocker. The primary antibody (1°ab), N-cadherin (D4R1H) XP (R) Rabbit mAb from Cell Signaling Biotechnology was diluted in 5 mL total of 1X TBST with 0.1% blocking buffer and 5 µL of the 1°ab. The membrane was then incubated protein side-up for 1 hour at room temperature with rocking. Following the incubation, the membrane was washed 3 times for 5 minutes with Wash Buffer. The membrane was then incubated for 1 hour in 2° ab (anti-Rabbit IgG HRP conjugated antibody from R&D Systems) solution protein side-up at room temperature with rocking. Finally, the membrane was washed 6 times, 5 minutes each wash with DI H_2O. Finally, the membrane was incubated with ECL working solution in equal quantities (1mL:1mL) for 1-5 minutes. This was then placed in clear plastic wrap; the bubbles were removed, and it was imaged using the FluoroChem chemiluminescence option.

4.10.9 Annexin V eFluor™ 450/7-AAD staining via Flow Cytometry

Cell viability was tested using the Invitrogen™ eBioscience™ Annexin V Apoptosis Detection Kits, which used Annexin V eFluor™ 450 and 7-AAD Viability Staining Solution. Protocol followed was provided by ThermoFisher. Prior to staining cells, the Binding Buffer was diluted with 1-part 10X Binding Buffer to 9-parts of DI H_2O (1 mL 10X Binding Buffer to 9 mL DI H_2O). Then the media from the MC3T3.E1 cells was aspirated off, the cells were washed

with about 2 mL of 1X PBS and this was once again removed from the cells by aspiration. The cells were lifted from the plate using 2 mL of TripLE and placed in the incubator for 2-3 minutes until lifted. This was then diluted with 7-8 mL of media, for a total volume of 10 mL. The cells were then transferred to a 15 mL conical tube and spun down briefly for 5 minutes at 3000 g. The media was then aspirated, and the cells were once again resuspended in a total of 1 mL of cell growth media with 1 µM total peptide concentration added to each tube. These were then incubated for 1 hour at 37°C to allow for peptide binding to the cells. After 1 hour, the cells were removed from the incubator and spun down. The media was removed from the cell pellets, and they were again washed with 1X PBS, and once again in 1X Binding Buffer. Cell pellets were then resuspended in 1X Binding Buffer (roughly 100 µL or 1-5 x 106 cells/mL), and to each cell suspension 5 µL of Annexin V eFluor™ 450 was added. Each sample was incubated for 10-15 minutes at room temperature, covered with foil. Then, 2 mL of 1X Binding Buffer was added to each suspension and samples were centrifuged at 400-600 x g for 5 minutes at room temperature. The supernatant was then discarded, and each cell pellet was resuspended in 200 µL of 1X Binding Buffer. Then, 5 µL of the 7-AAD Viability Staining Solution was added to this and samples were incubated at room temperature for 5-15 minutes. Cells were not washed prior to analyzing by flow cytometry, since 7-AAD Viability Staining Solution must remain in the buffer during the flow cytometry run.[20]

4.11 References

1. Tian, Z.; Liang, G.; Cui, K.; Liang, Y.; Wang, Q.; Lv, S.; Cheng, X.; Zhang, L. Insight Into the Prospects for RNAi Therapy of Cancer. Front. Pharmacol. 2021, 12, 644718. https://doi.org/10.3389/fphar.2021.644718.
2. Watts, J. K.; Corey, D. R. Silencing Disease Genes in the Laboratory and the Clinic. J. Pathol. 2012, 226 (2), 365–379. https://doi.org/10.1002/path.2993.
3. Ferguson, C. M.; Echeverria, D.; Hassler, M.; Ly, S.; Khvorova, A. Cell Type Impacts Accessibility of MRNA to Silencing by RNA Interference. Molecular Therapy - Nucleic Acids 2020, 21, 384–393. https://doi.org/10.1016/j.omtn.2020.06.006.
4. Mansoori, B.; Sandoghchian Shotorbani, S.; Baradaran, B. RNA Interference and Its Role in Cancer Therapy. Advanced Pharmaceutical Bulletin; eISSN 2251-7308 2014. https://doi.org/10.5681/APB.2014.046.
5. Janiszewska, M.; Primi, M. C.; Izard, T. Cell Adhesion in Cancer: Beyond the Migration of Single Cells. Journal of Biological Chemistry 2020, 295 (8), 2495–2505. https://doi.org/10.1074/jbc.REV119.007759.
6. Patel, S. D.; Ciatto, C.; Chen, C. P.; Bahna, F.; Rajebhosale, M.; Arkus, N.; Schieren, I.; Jessell, T. M.; Honig, B.; Price, S. R.; Shapiro, L. Type II Cadherin Ectodomain Structures: Implications for Classical Cadherin Specificity. Cell 2006, 124 (6), 1255–1268. https://doi.org/10.1016/j.cell.2005.12.046.
7. Geiger, B.; Volk, T.; Volberg, T.; Bendori, R. Molecular Interactions in Adherens-Type Contacts. Journal of Cell Science 1987, 1987 (Supplement_8), 251–272. https://doi.org/10.1242/jcs.1987.Supplement_8.14.
8. Pastushenko, I.; Brisebarre, A.; Sifrim, A.; Fioramonti, M.; Revenco, T.; Boumahdi, S.; Van Keymeulen, A.; Brown, D.; Moers, V.; Lemaire, S.; De Clercq, S.; Minguijón, E.; Balsat, C.; Sokolow, Y.; Dubois, C.; De Cock, F.; Scozzaro, S.; Sopena, F.; Lanas, A.; D'Haene, N.; Salmon, I.; Marine, J.-C.; Voet, T.; Sotiropoulou, P. A.; Blanpain, C. Identification of the Tumour Transition States Occurring during EMT. Nature 2018, 556 (7702), 463–468. https://doi.org/10.1038/s41586-018-0040-3.
9. Wheelock, M. J.; Shintani, Y.; Maeda, M.; Fukumoto, Y.; Johnson, K. R. Cadherin Switching. Journal of Cell Science 2008, 121 (6), 727–735. https://doi.org/10.1242/jcs.000455.
10. Mrozik, K. M.; Blaschuk, O. W.; Cheong, C. M.; Zannettino, A. C. W.; Vandyke, K. N-Cadherin in Cancer Metastasis, Its Emerging Role in Haematological Malignancies and Potential as a Therapeutic Target in Cancer. BMC Cancer 2018, 18 (1), 939. https://doi.org/10.1186/s12885-018-4845-0.
11. Onder, T. T.; Gupta, P. B.; Mani, S. A.; Yang, J.; Lander, E. S.; Weinberg, R. A. Loss of E-Cadherin Promotes Metastasis via Multiple Downstream Transcriptional Pathways. Cancer Research 2008, 68 (10), 3645–3654. https://doi.org/10.1158/0008-5472.CAN-07-2938.
12. Padmanaban, V.; Krol, I.; Suhail, Y.; Szczerba, B. M.; Aceto, N.; Bader, J. S.; Ewald, A. J. E-Cadherin Is Required for Metastasis in Multiple Models of Breast Cancer. Nature 2019, 573 (7774), 439–444. https://doi.org/10.1038/s41586-019-1526-3.

13. Gaggioli, C.; Hooper, S.; Hidalgo-Carcedo, C.; Grosse, R.; Marshall, J. F.; Harrington, K.; Sahai, E. Fibroblast-Led Collective Invasion of Carcinoma Cells with Differing Roles for RhoGTPases in Leading and Following Cells. Nat Cell Biol 2007, 9 (12), 1392–1400. https://doi.org/10.1038/ncb1658.
14. Labernadie, A.; Kato, T.; Brugués, A.; Serra-Picamal, X.; Derzsi, S.; Arwert, E.; Weston, A.; González-Tarragó, V.; Elosegui-Artola, A.; Albertazzi, L.; Alcaraz, J.; Roca-Cusachs, P.; Sahai, E.; Trepat, X. A Mechanically Active Heterotypic E-Cadherin/N-Cadherin Adhesion Enables Fibroblasts to Drive Cancer Cell Invasion. Nat Cell Biol 2017, 19 (3), 224–237. https://doi.org/10.1038/ncb3478.
15. Hosokawa, K.; Arai, F.; Yoshihara, H.; Iwasaki, H.; Hembree, M.; Yin, T.; Nakamura, Y.; Gomei, Y.; Takubo, K.; Shiama, H.; Matsuoka, S.; Li, L.; Suda, T. Cadherin-Based Adhesion Is a Potential Target for Niche Manipulation to Protect Hematopoietic Stem Cells in Adult Bone Marrow. Cell Stem Cell 2010, 6 (3), 194–198. https://doi.org/10.1016/j.stem.2009.04.013.
16. Crowley, L. C.; Marfell, B. J.; Scott, A. P.; Waterhouse, N. J. Quantitation of Apoptosis and Necrosis by Annexin V Binding, Propidium Iodide Uptake, and Flow Cytometry. Cold Spring Harb Protoc 2016, 2016 (11), pdb.prot087288. https://doi.org/10.1101/pdb.prot087288.
17. 7-AAD Viability Staining Solution. https://www.biolegend.com/en-us/products/7-aad-viability-staining-solution-1649?GroupID=BLG13283 (accessed 2023-05-22).
18. Analysis of cell viability using 7-amino actinomycin D (7-AAD): R&D systems. 7-Amino Actinomycin D (7-AAD) Cell Viability Flow Cytometry Protocol. 7-Amino Actinomycin D (7-AAD) Cell Viability Flow Cytometry Protocol. https://www.rndsystems.com/resources/protocols/analysis-cell-viability-using-7-amino-actinomycin-d-7-aad.
19. De Yzaguirre, M. M.; Hernández, J. S.; Navarro, P. F.; Nieva, P. L.; Herranz, M.; Fraga, M. F.; Esteller, M.; Juarranz, A.; Fernández-Piqueras, J. Epigenetic Silencing of E- and N-Cadherins in the Stroma of Mouse Thymic Lymphomas. Carcinogenesis 2006, 27 (5), 1081–1089. https://doi.org/10.1093/carcin/bgi331.
20. EBIOSC Ienceö Annexin V Apopto Sis Detection Kit EFluorö 450. https://assets.fishersci.com/TFS-Assets/LSG/manuals/88-8006.pdf.

Chapter 5: Conclusions, Contributions to Knowledge and Future Work

5.1 Conclusions and Contributions to Knowledge Made in This Thesis

5.1.1 RNAi As a Therapy for Cancers

RNA interference has been studied in various diseases as a potential replacement therapy to harsher options such as chemotherapy. RNAi is a form of gene therapy, and gene therapies allow for the precise targeting of abnormal or diseased cells, while sparing all healthy cells. As mentioned in this thesis, this is ideal for several reasons: 1) unwanted and often harmful side effects are eliminated during treatment, 2) specificity in treating disease exponentially increases, and 3) gene therapies can be tailored and specified to treat almost any disease which arises due to genetic mutations, or where any specific, targetable marker is present on the cells.

Our work has investigated this approach further by combining established gene therapy approaches with preexisting delivery methods, i.e., cell-targeting peptides. In this thesis we have combined both approaches into one potential treatment strategy by complexing osteoblast-targeting peptides with siRNA encoding for cell surface adhesion proteins. Adhesion proteins were chosen as potential therapeutic targets due to their involvement in cancer metastasis within bone, migration to bone, and finally, the drug resistance which they impart to cancers which have spread to bone tissue. Our contribution to the study of gene therapy has shown that when identifiable and reliable targets are found and consistently expressed on the cell surface, cell targeting peptides are an easy way to transport potential therapeutic agents to cells and across cell membranes, barring that the peptide is stable within a cellular environment as well as serum. Furthermore, once barriers to entering the cell are overcome, the release of the therapeutic agent within the cell is also essential to the success of the treatment. We have demonstrated that periostin is a reliable target in osteoblast cells as it is expressed through various stages of the

osteoblast's lifespan and synthesizing periostin targeting peptides is simple as the peptide is only 5 amino acids in length and exhibits desirable and fast binding to its intended target (within 1 hour at 37°C). In addition, based on the work we have performed, for the successful release of the siRNA within the cell, it can be concluded that polycationic tails on the peptide should be long enough to bind the siRNA through electrostatic interactions, but not so long that release within the cell will not take place. As was shown, 9 and 12 residues of polyarginine tails can sufficiently bind siRNA duplexes. Ideally, other negatively charged particulates within the cell should outcompete the siRNA, thereby causing its release within the cytoplasm. Without this, RNAi will not take place unless the peptide:siRNA complex is digested within the cell, and this would probably not lead to a substantial enough RNAi effect taking place where therapeutic significance and relevance are present. The results from the Heparin displacement gel demonstrated that at Heparin ratios of 1:1, 5 to 1 ratio of peptide:siRNA complex and 10:1, free RNA was beginning to be detectable on the gel. In some cases, even at low ratio of 01:1 there were visible free RNA bands. This indicated that the siRNA could successfully be displaced from the polyarginine tail it was bound to. Furthermore, the osteoblast targeting peptides synthesized did not change cell morphology or survival of the cells when cells were treated with peptide:siRNA complexes. This allowed us to conclude that the periostin binding peptide was not cytotoxic. The RNA interference studies showed that cell populations incubated with the peptide:siRNA complexes (FITC-Ahx-SDSSD-Ahx-R_{12} and FITC-Ahx-SDSSD-Ahx-R_9) had a slight decrease in N-cadherin production as shown by the calculated fold change values.

5.2 Conclusions and Future Work

In conclusion, the synthesis of cell-targeting peptides is simple, and depending on length of the desired sequence, quickly achievable in a lab setting. Functionalizing the peptides with siRNA is also a simple task, but challenges to release the siRNA within the cytoplasm still pose the greatest barrier in creating treatments which possess high enough efficacy to be considered usable. These challenges include passing the cell wall, transport into the cytoplasm and, finally, siRNA release from the synthesized complex. To further build upon this work, future endeavors include testing the sequences with shorter length polyarginine tails as well as testing the complexes with 3D bone tissue models to examine their effects, if any. Finally, if these experiments are successful, experimental testing in co-culture with multiple myeloma cells would be indicated to further investigate the effects of adhesion protein down-regulation and reducing cell adhesion mediated drug resistance when cancer cells are exposed to these drugs.

Appendix

Supplemental Size Distribution by Intensity spectra from DLS Analysis

Table of Contents

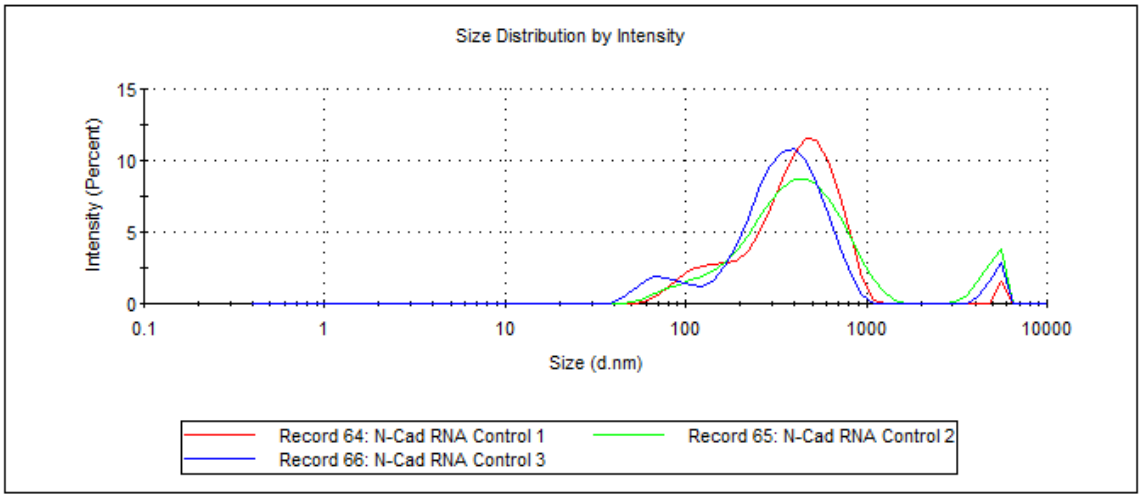

Figure A1: Size distribution intensity spectra of N-cadherin duplex

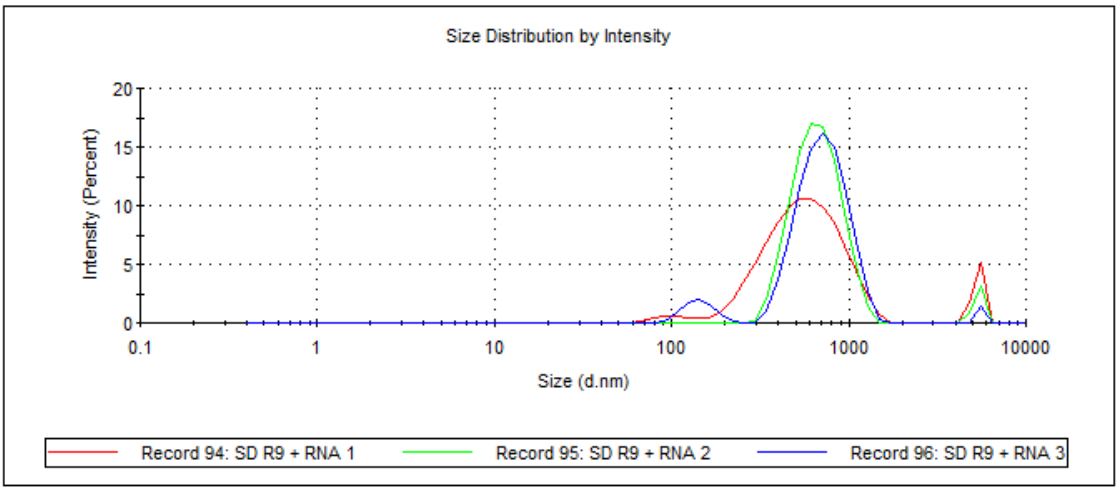

Figure A2: Size distribution intensity spectra of FITC-Ahx-SDSSD-Ahx-R_9:siRNA

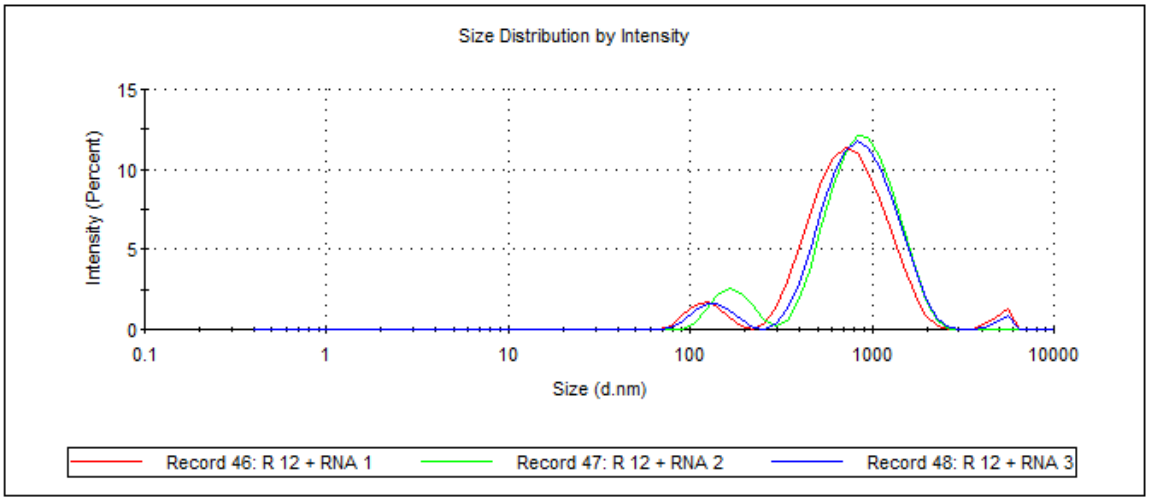

Figure A3: Size distribution intensity spectra of FITC-Ahx -R_{12}:siRNA

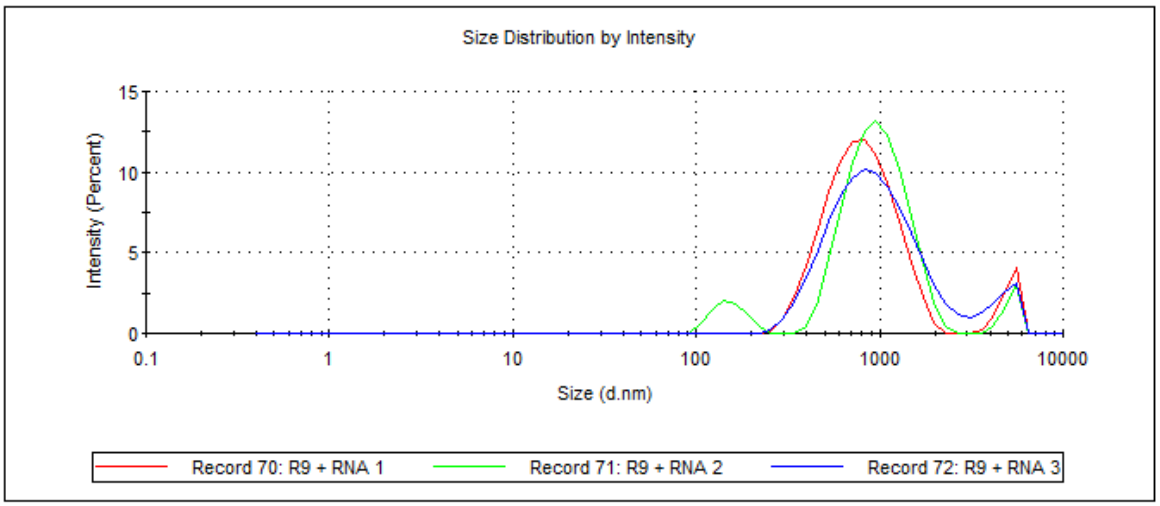

Figure A4: Size distribution intensity spectra of FITC-Ahx-R_9:siRNA